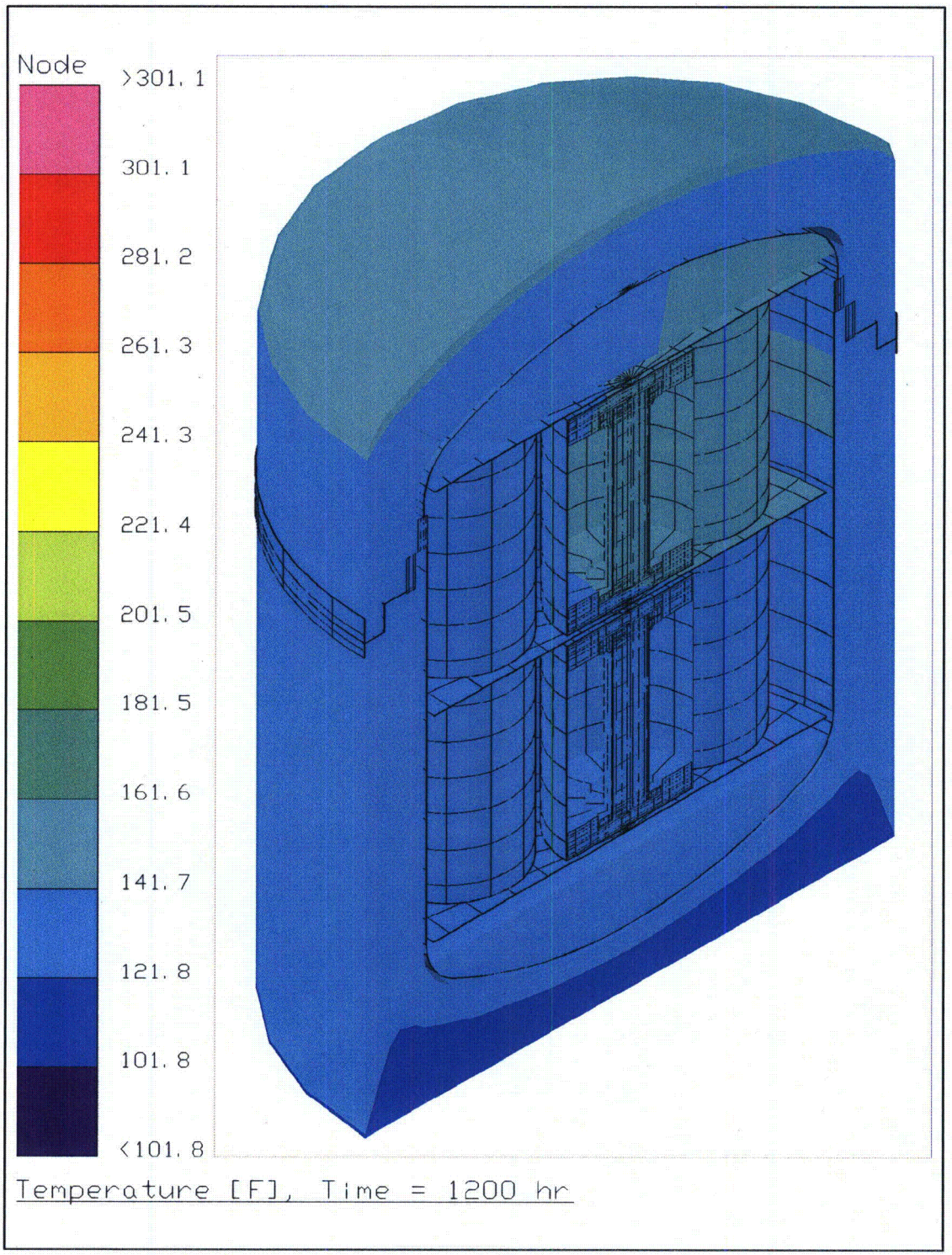

Figure 4-52 – TRUPACT-II Case 4 Package Temperatures with Insolation

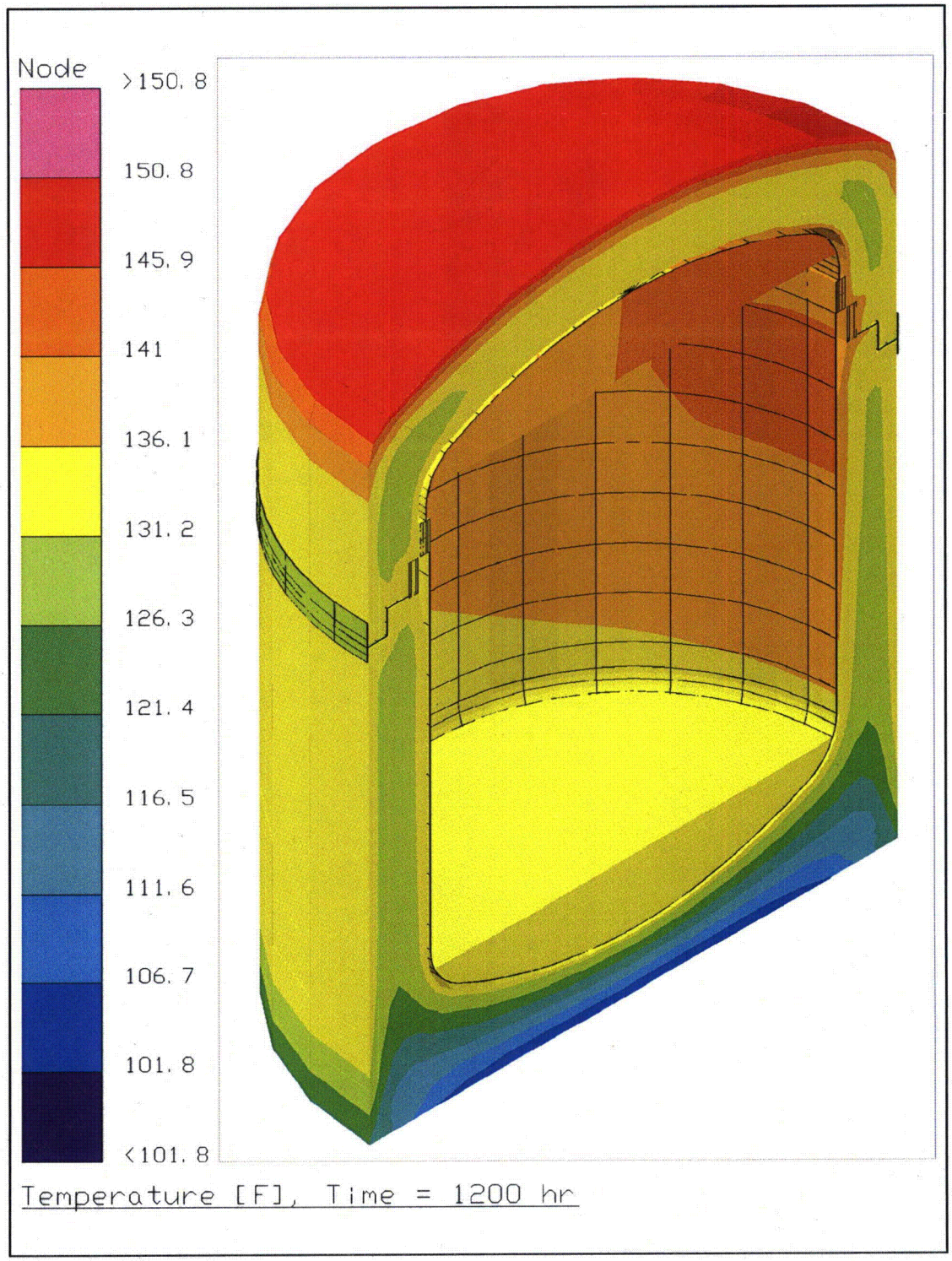

Figure 4-53 – TRUPACT-II Case 4 Packaging Temperatures with Insolation

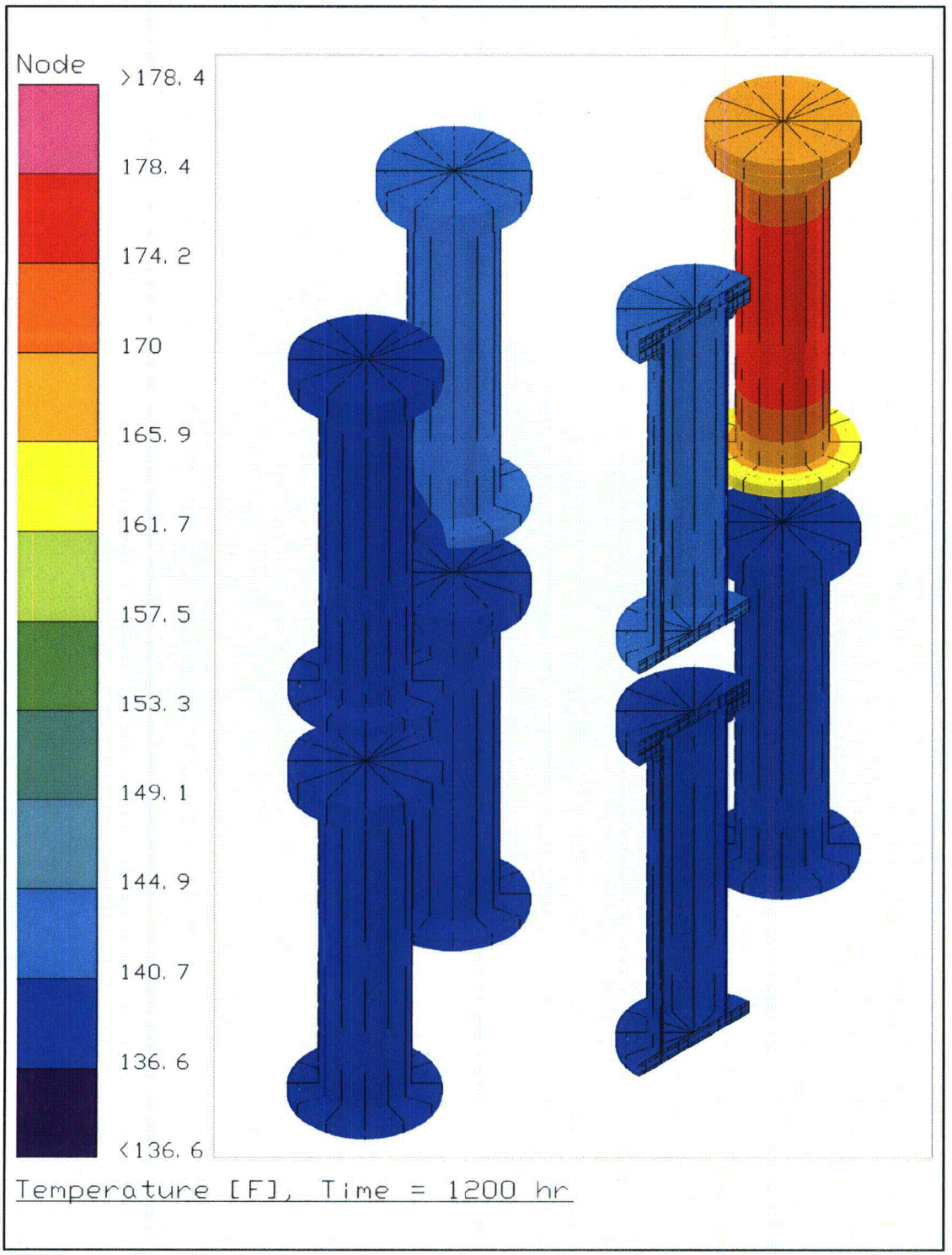

Figure 4-54 – TRUPACT-II Case 4 CCO Temperatures with Insolation

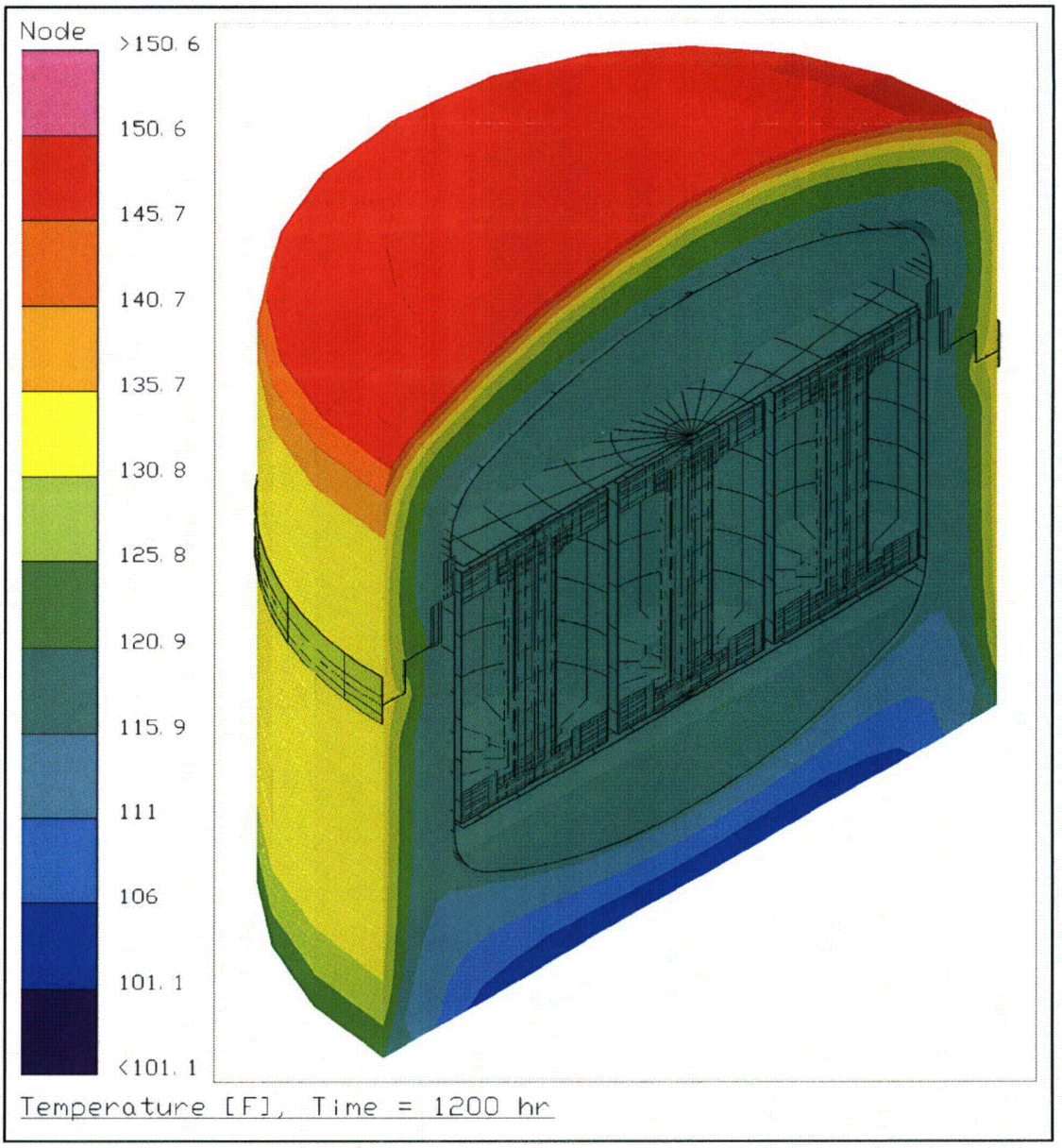

Figure 4-55 – HalfPACT Case 0 Package Temperatures with Insolation

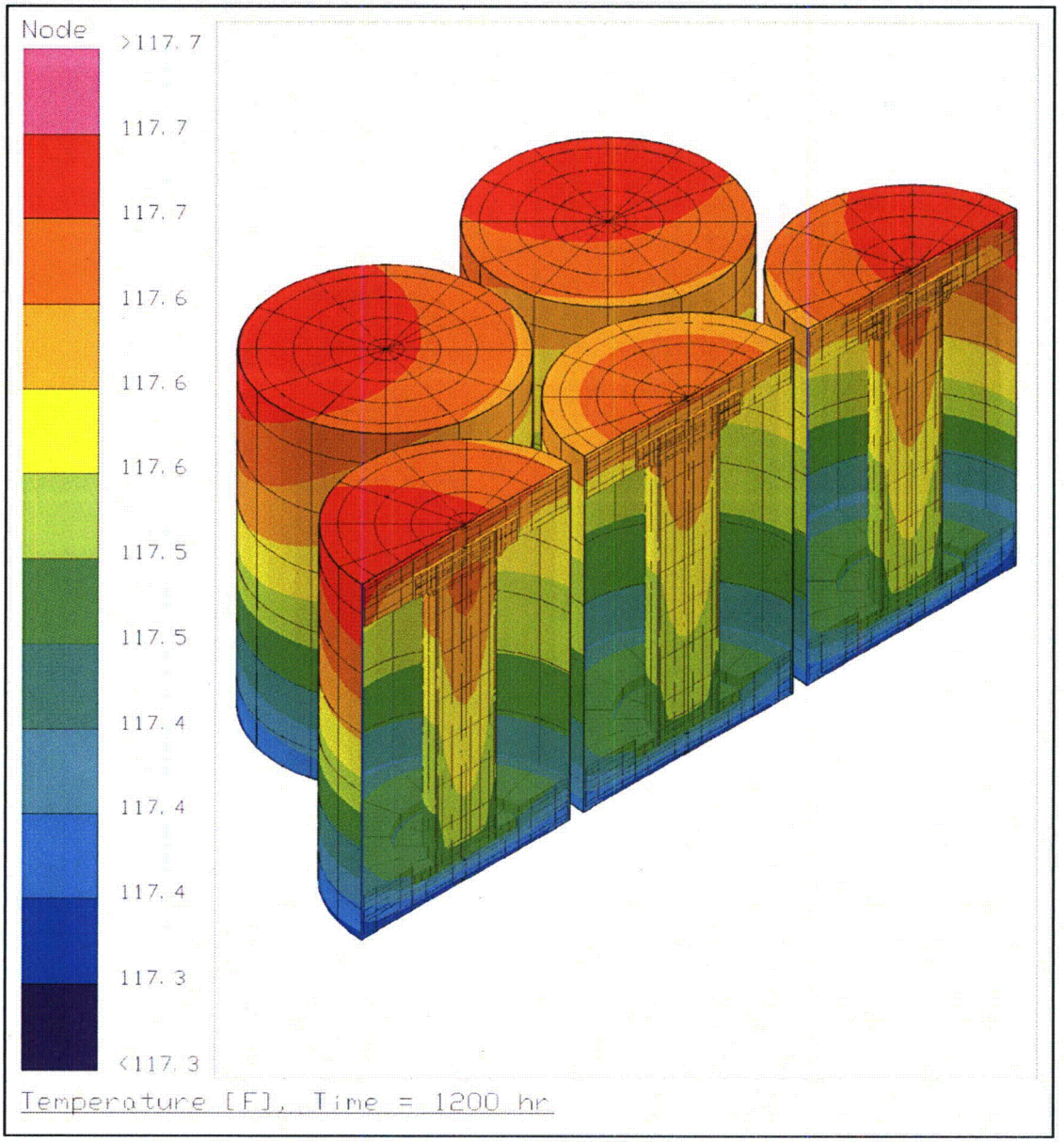

Figure 4-56 – HalfPACT Case 0 Payload Temperatures with Insolation

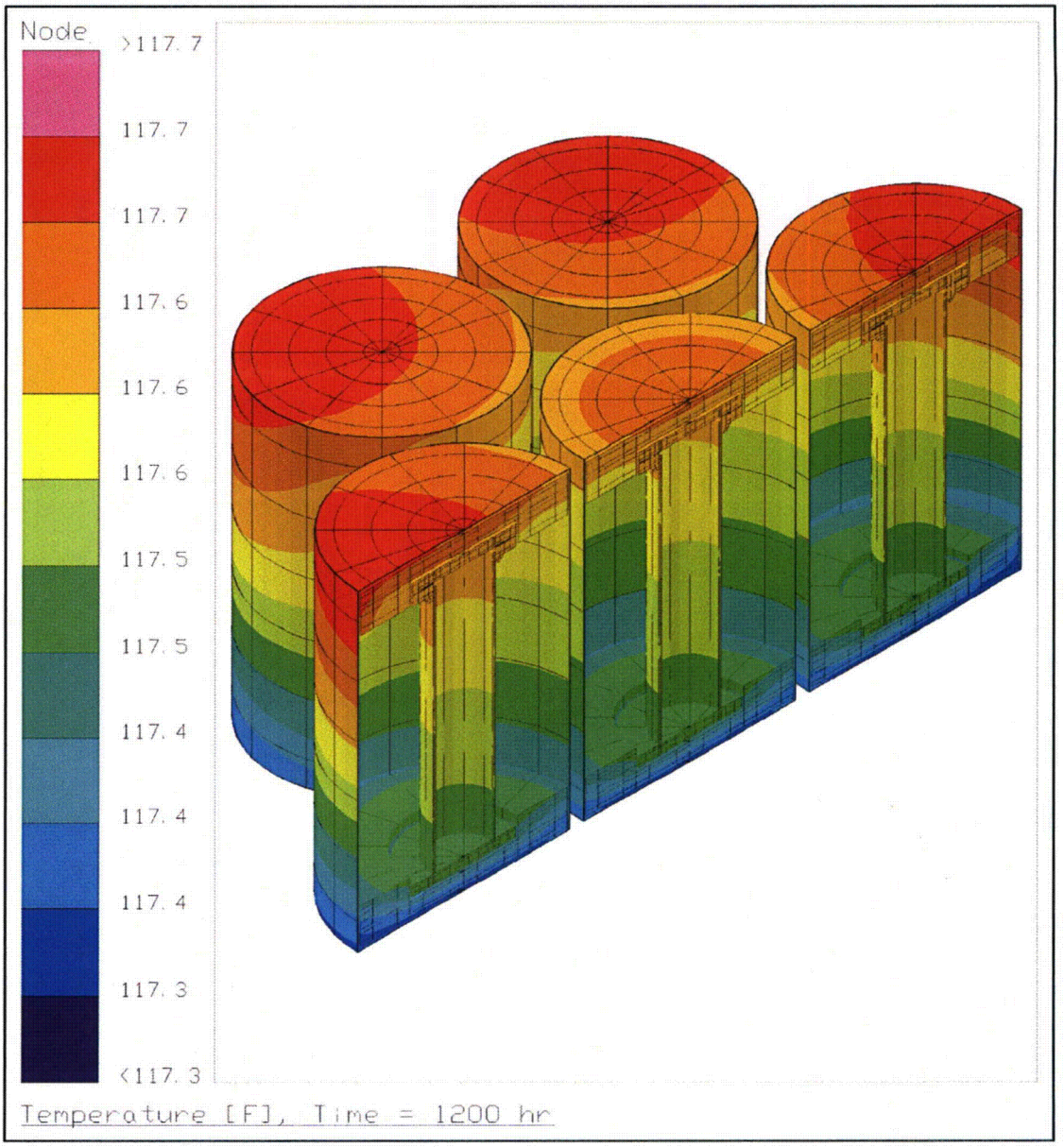

Figure 4-57 – HalfPACT Case 0 CCO Temperatures with Insolation

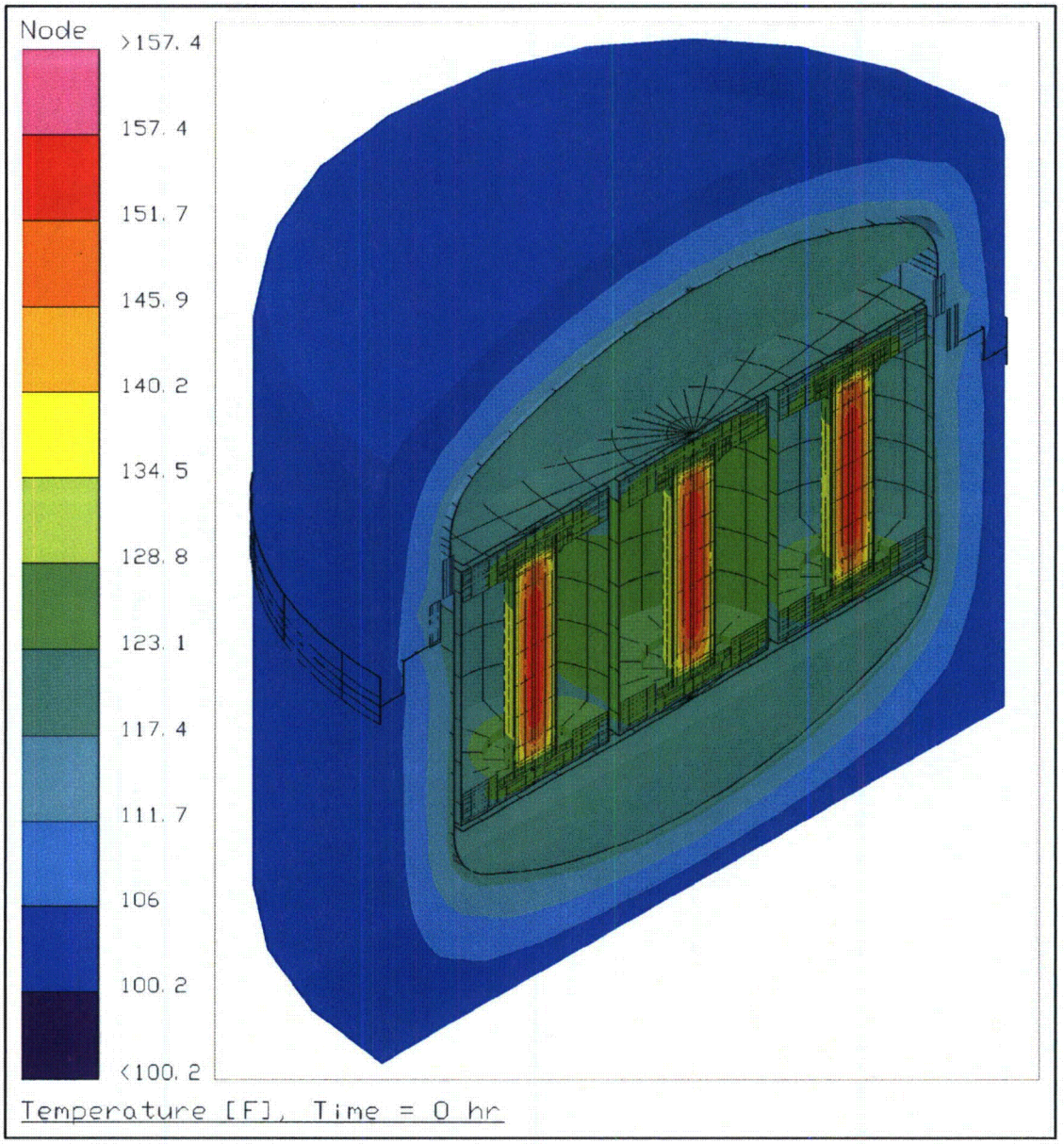

Figure 4-58 – HalfPACT Case 1 Package Temperatures without Insolation

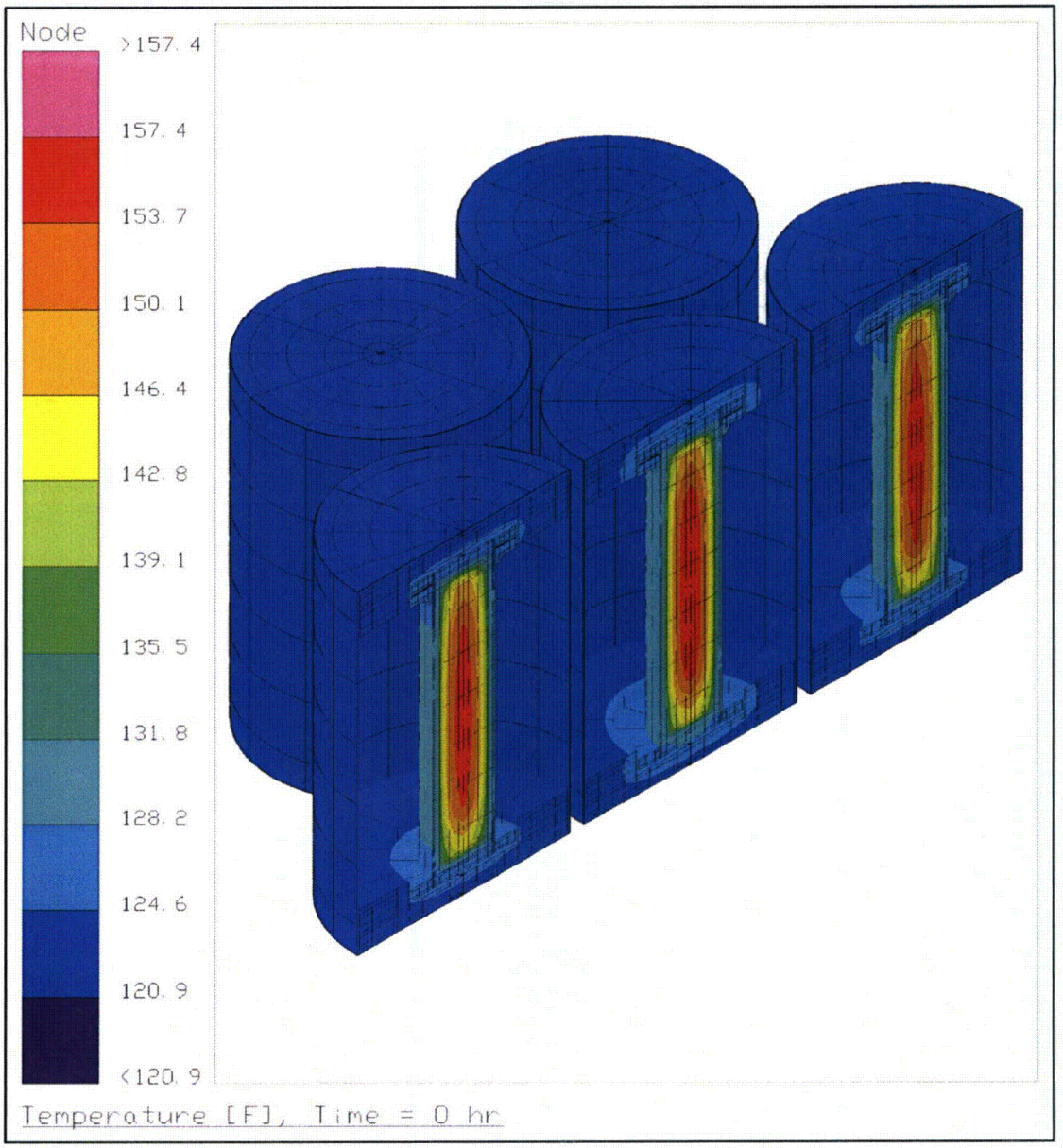

Figure 4-59 – HalfPACT Case 1 Payload Temperatures without Insolation

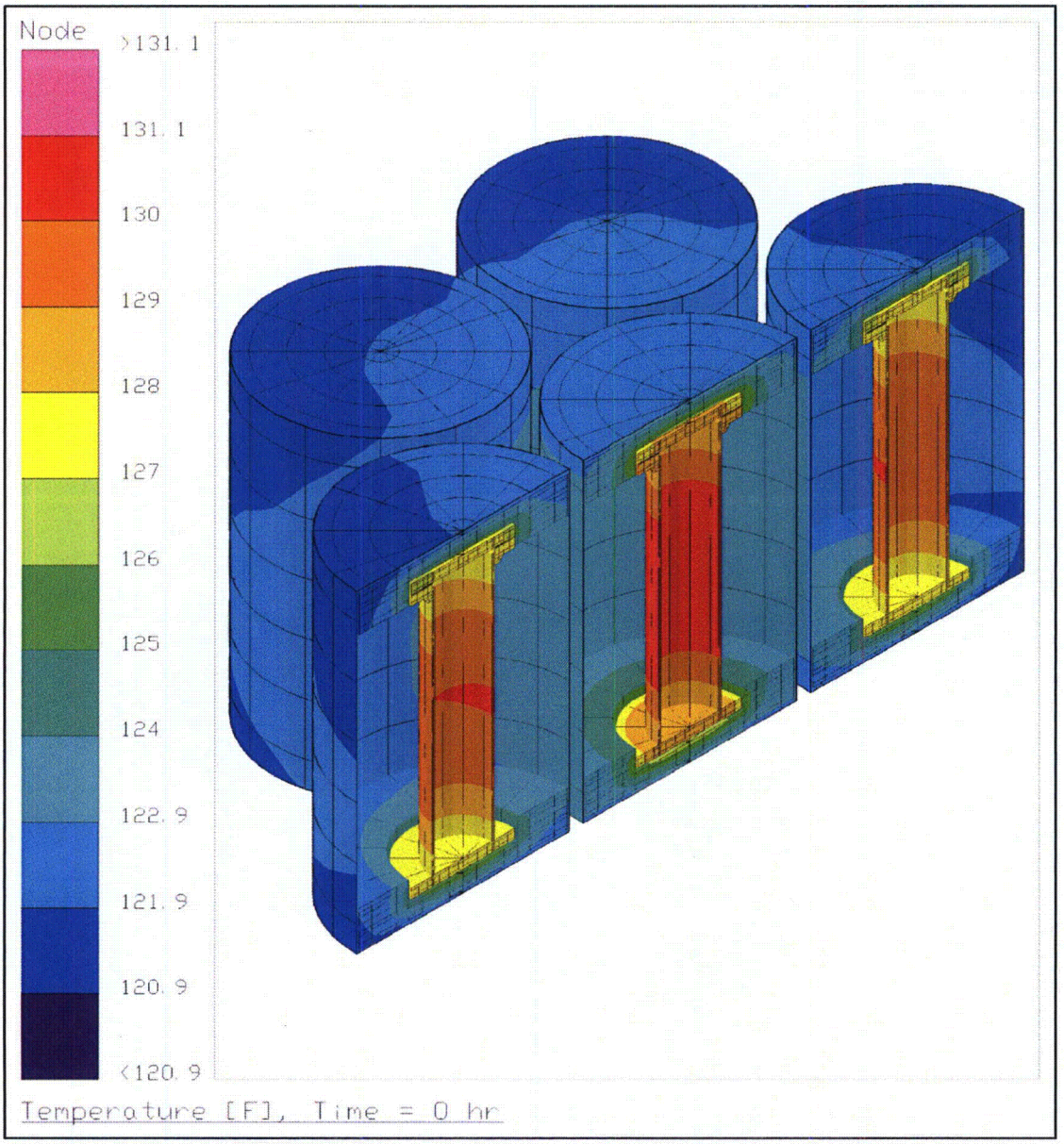

Figure 4-60 – HalfPACT Case 1 CCO Temperatures without Insolation

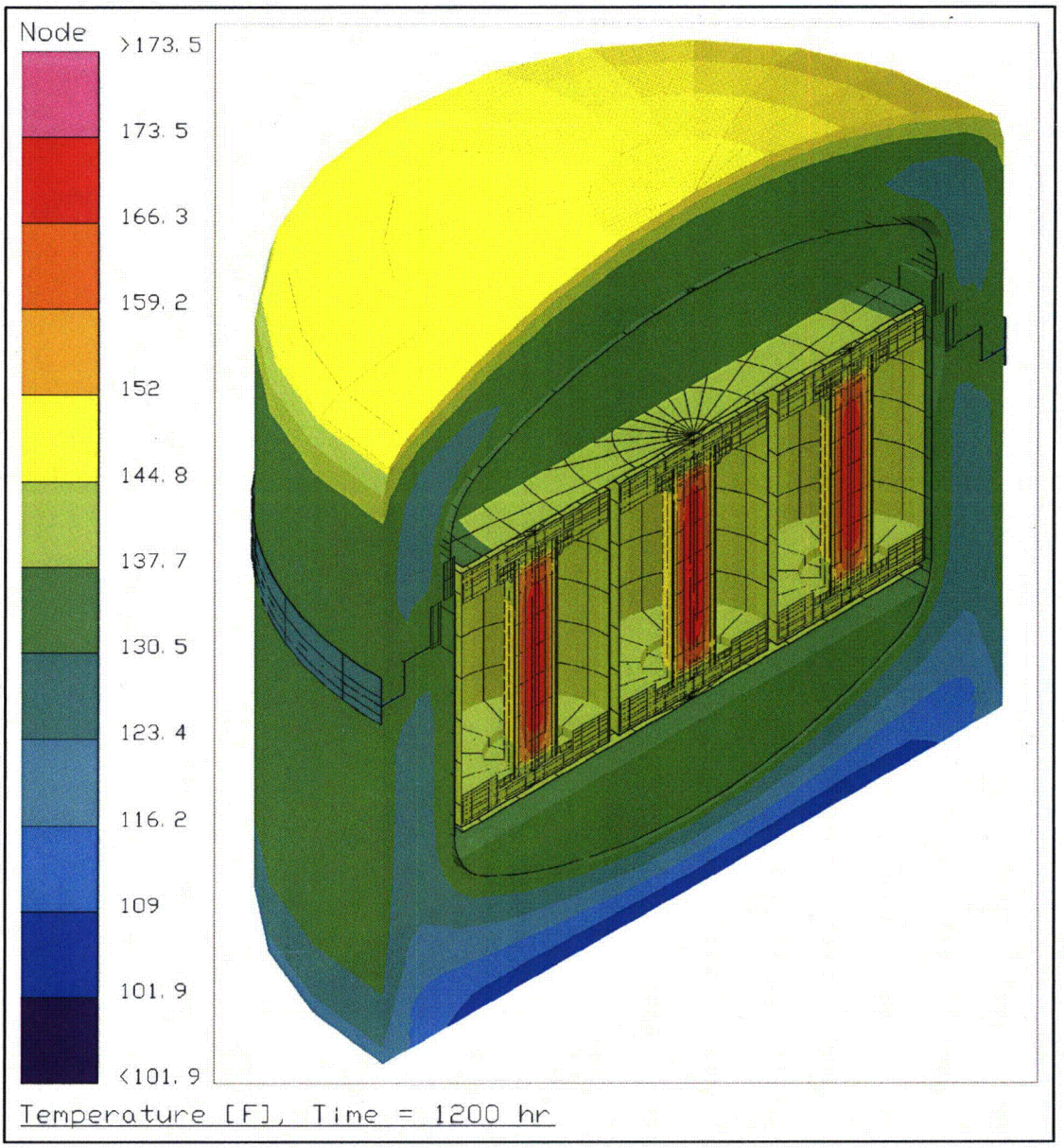

Figure 4-61 – HalfPACT Case 1 Package Temperatures with Insolation

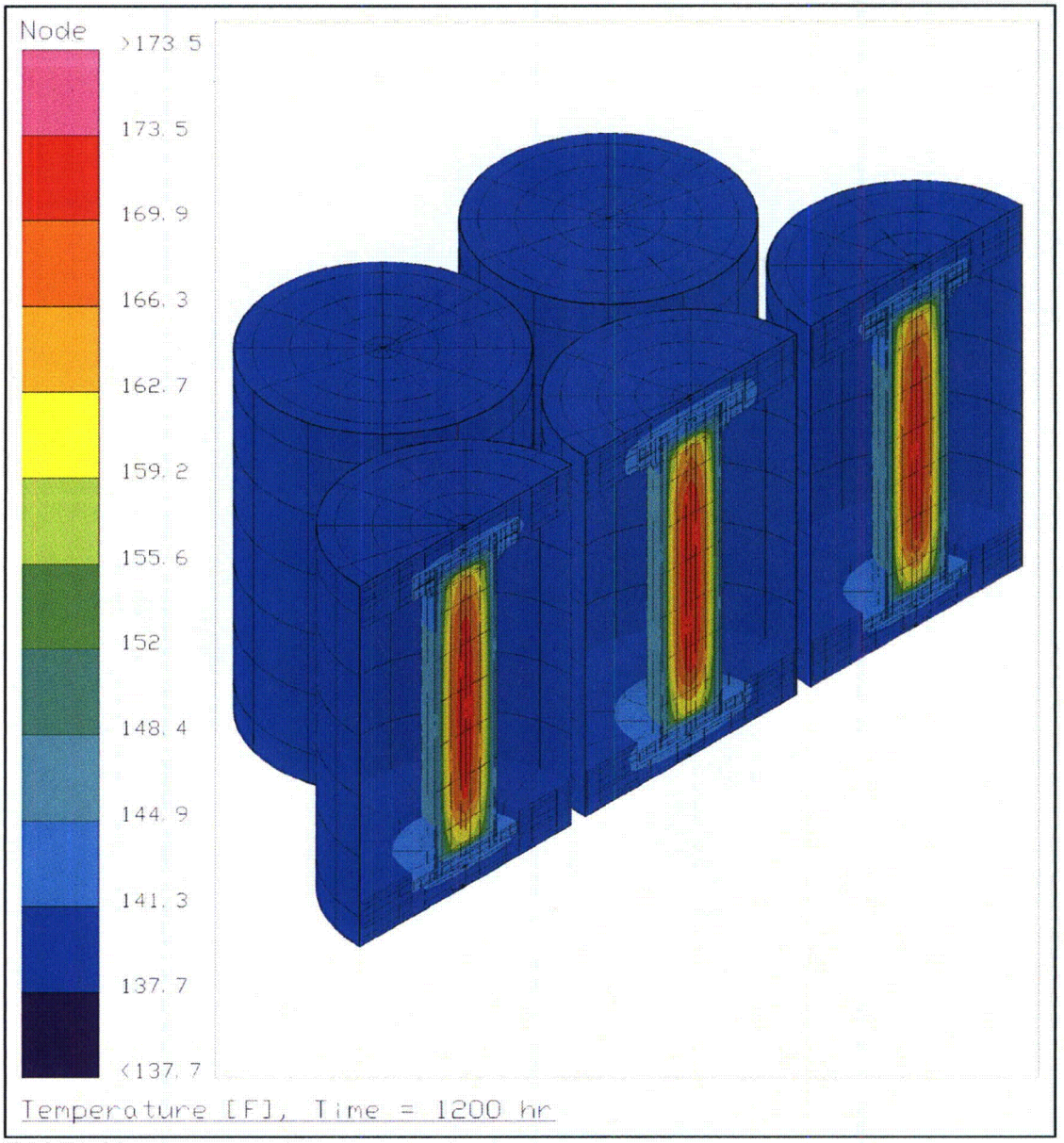

Figure 4-62 – HalfPACT Case 1 Payload Temperatures with Insolation

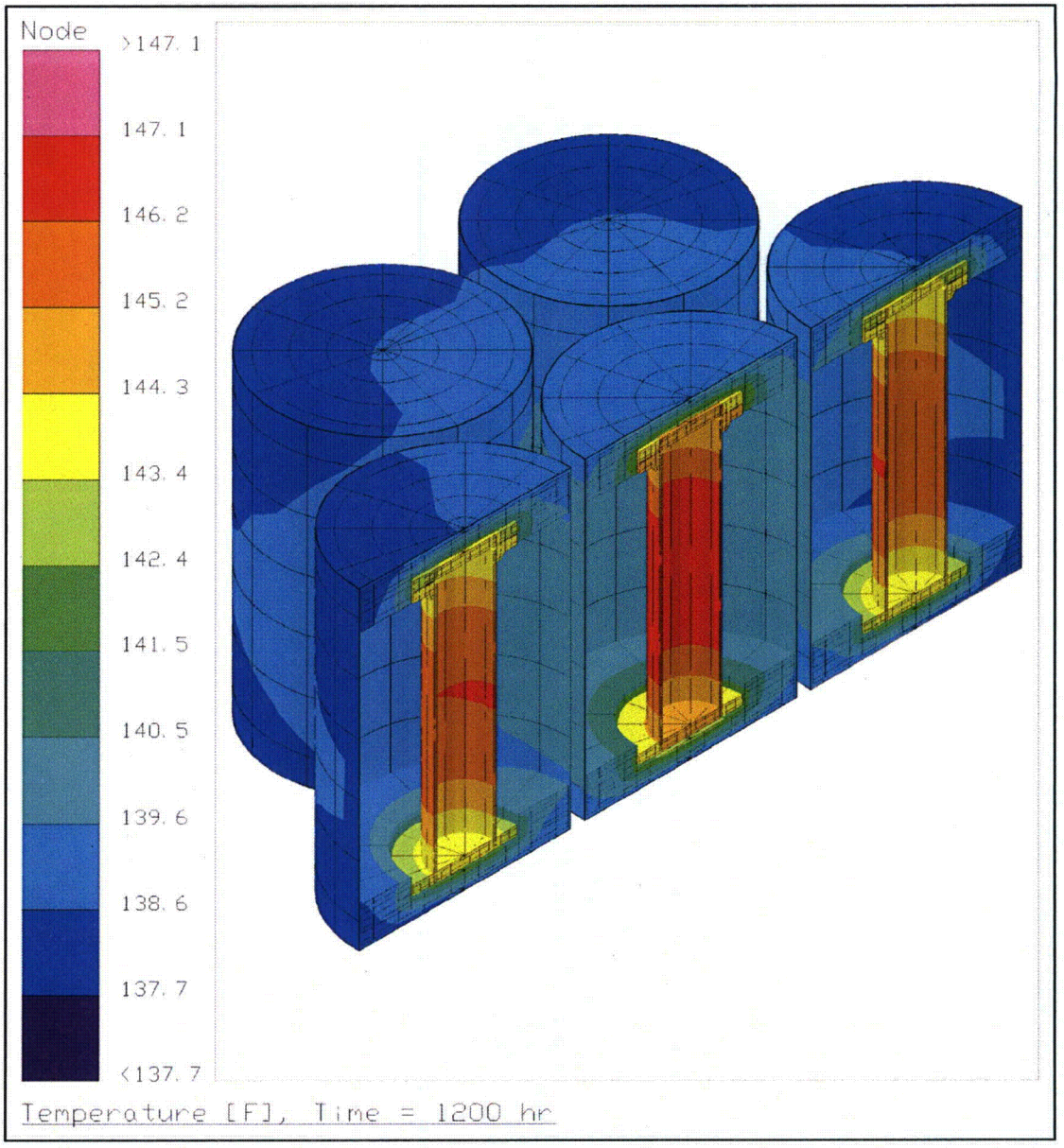

Figure 4-63 – HalfPACT Case 1 CCO Temperatures with Insolation

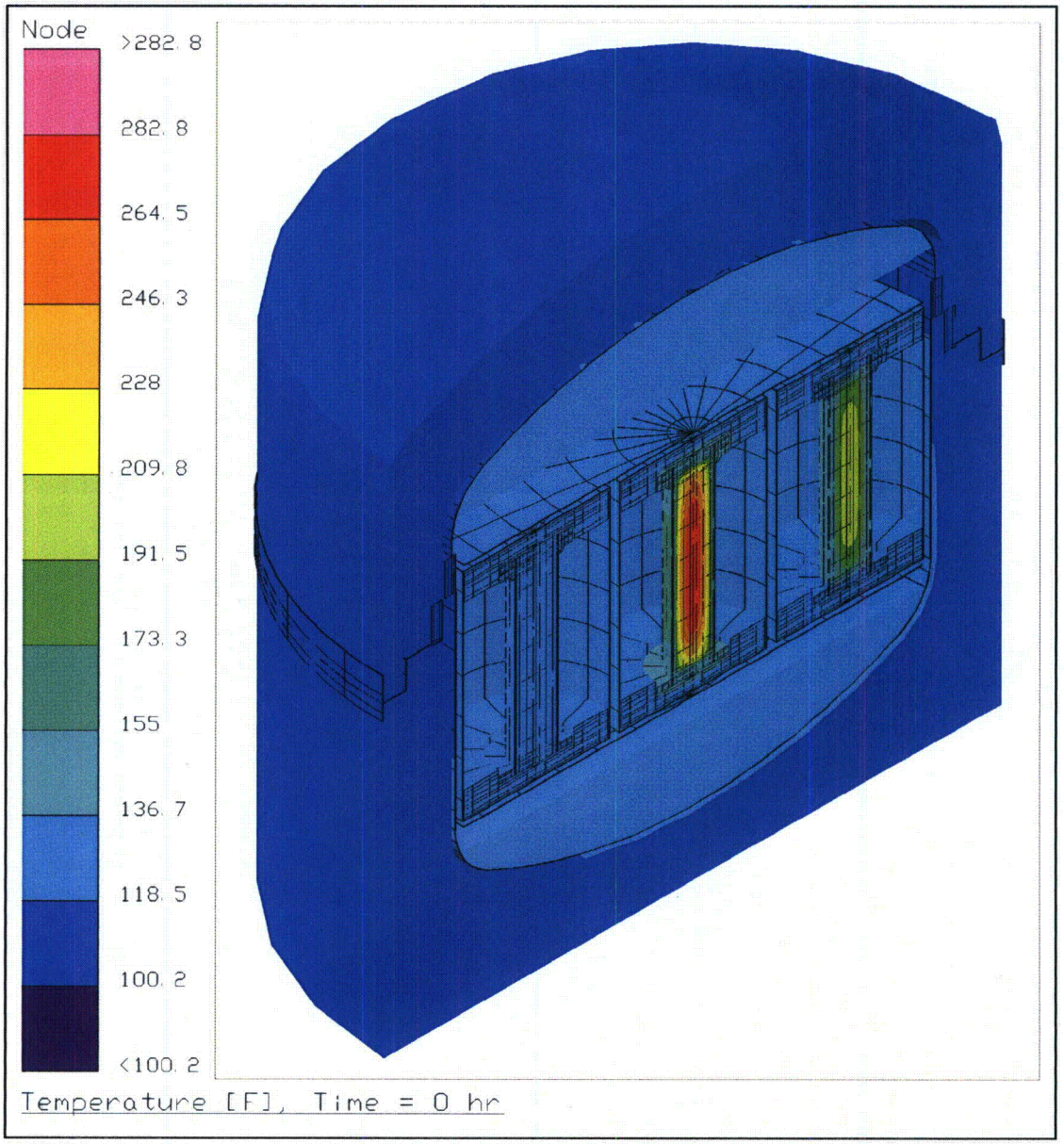

Figure 4-64 – HalfPACT Case 2 Package Temperatures without Insolation

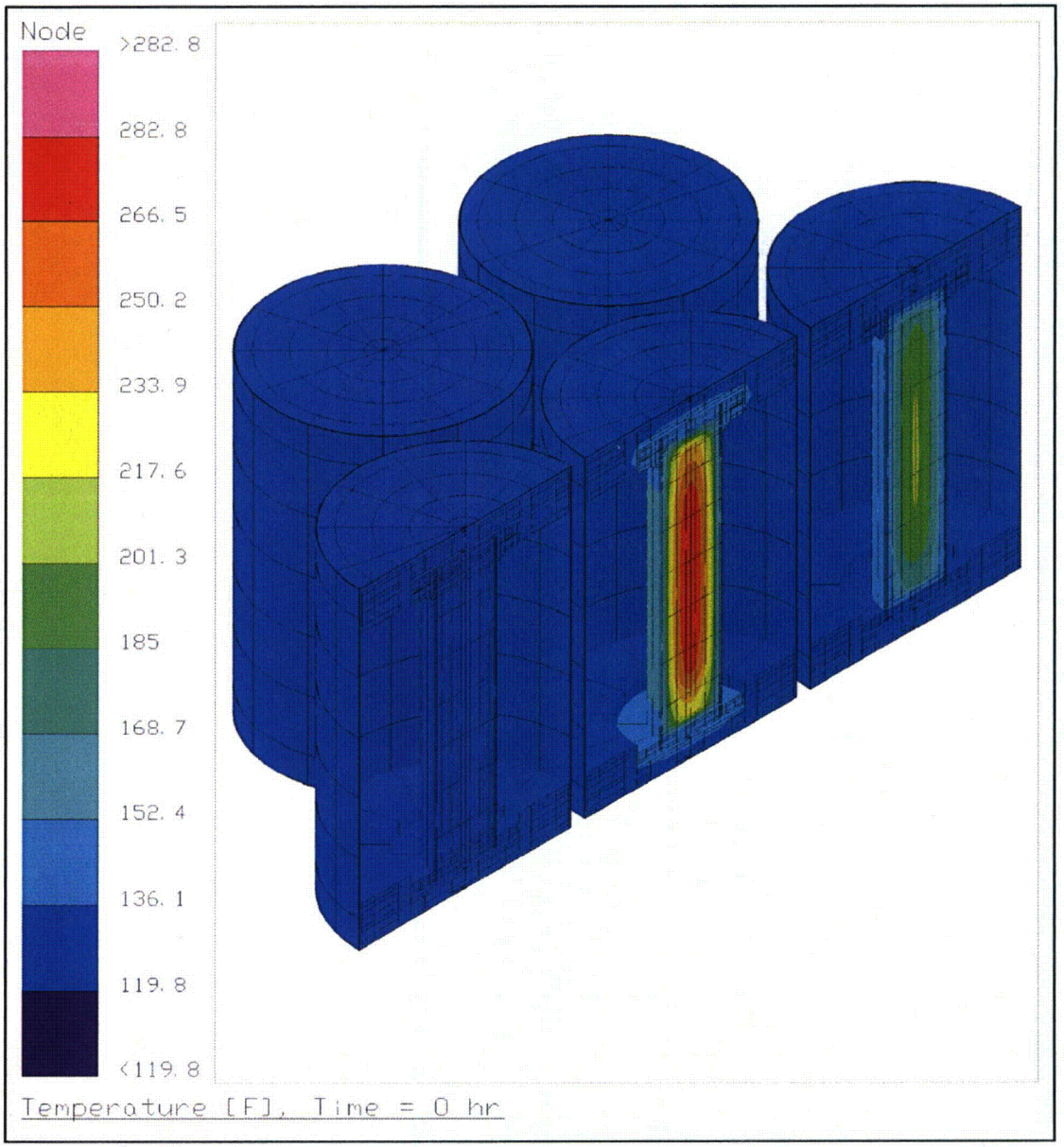

Figure 4-65 – HalfPACT Case 2 Payload Temperatures without Insolation

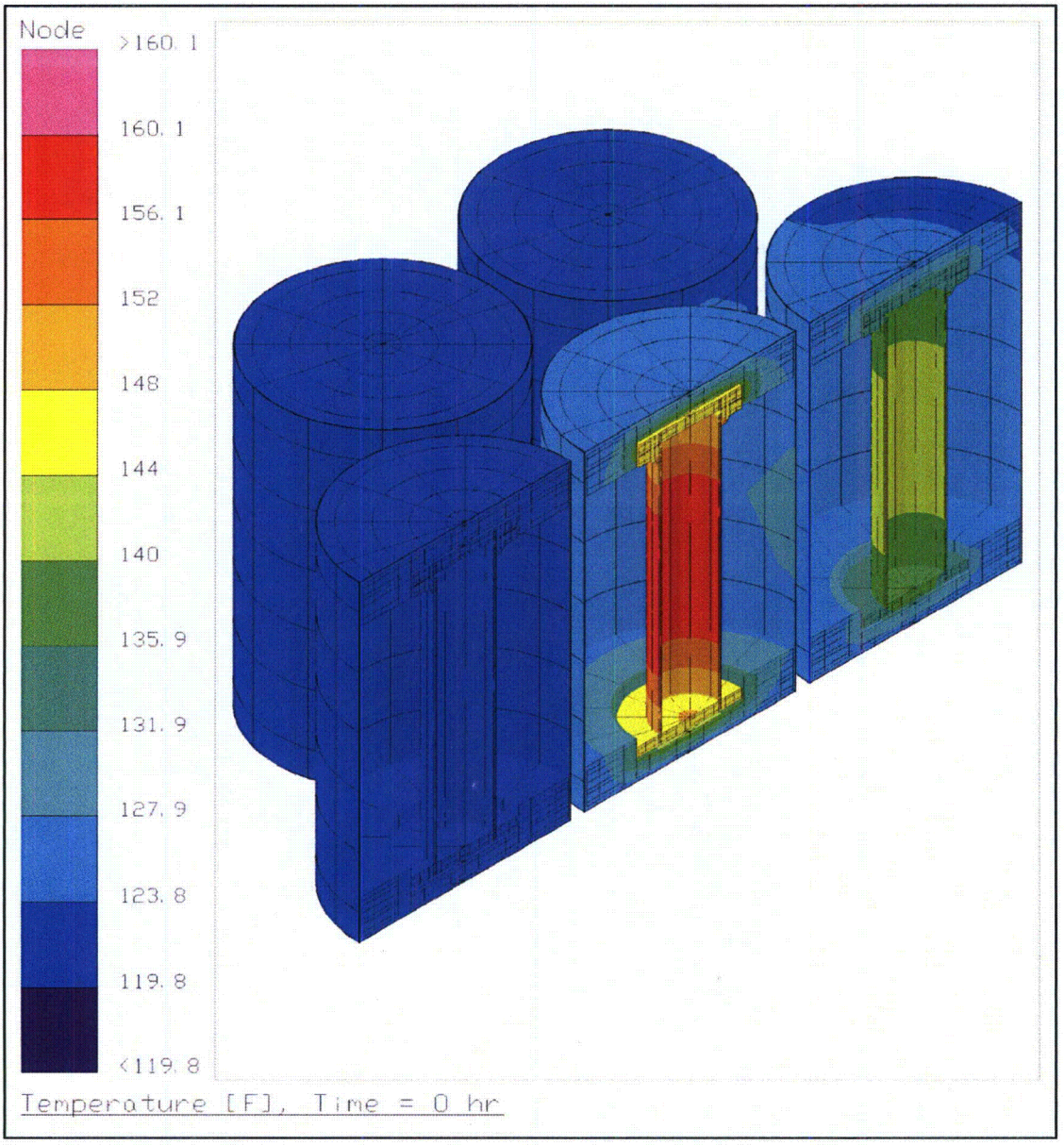

Figure 4-66 – HalfPACT Case 2 CCO Temperatures without Insolation

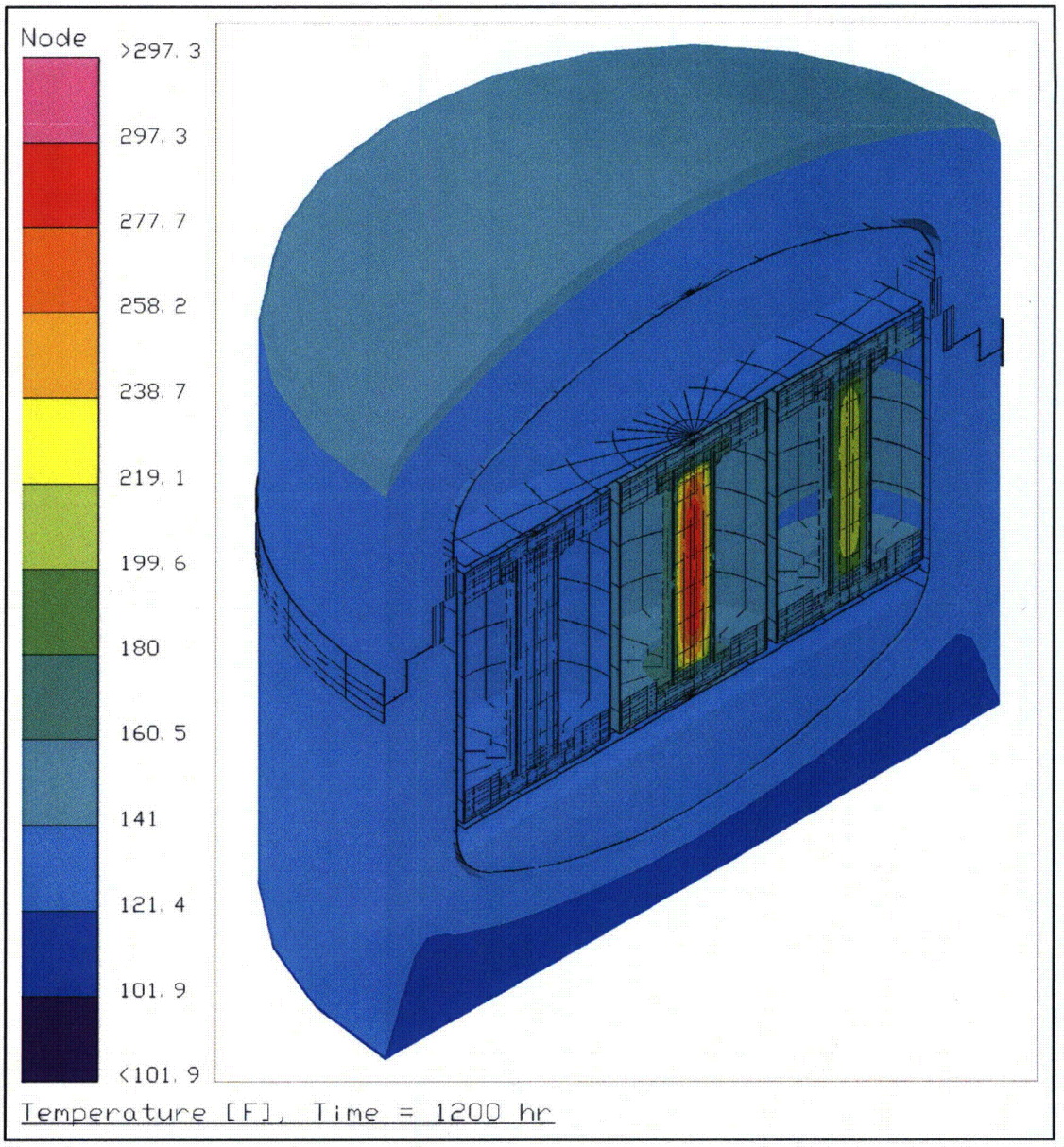

Figure 4-67 – HalfPACT Case 2 Package Temperatures with Insolation

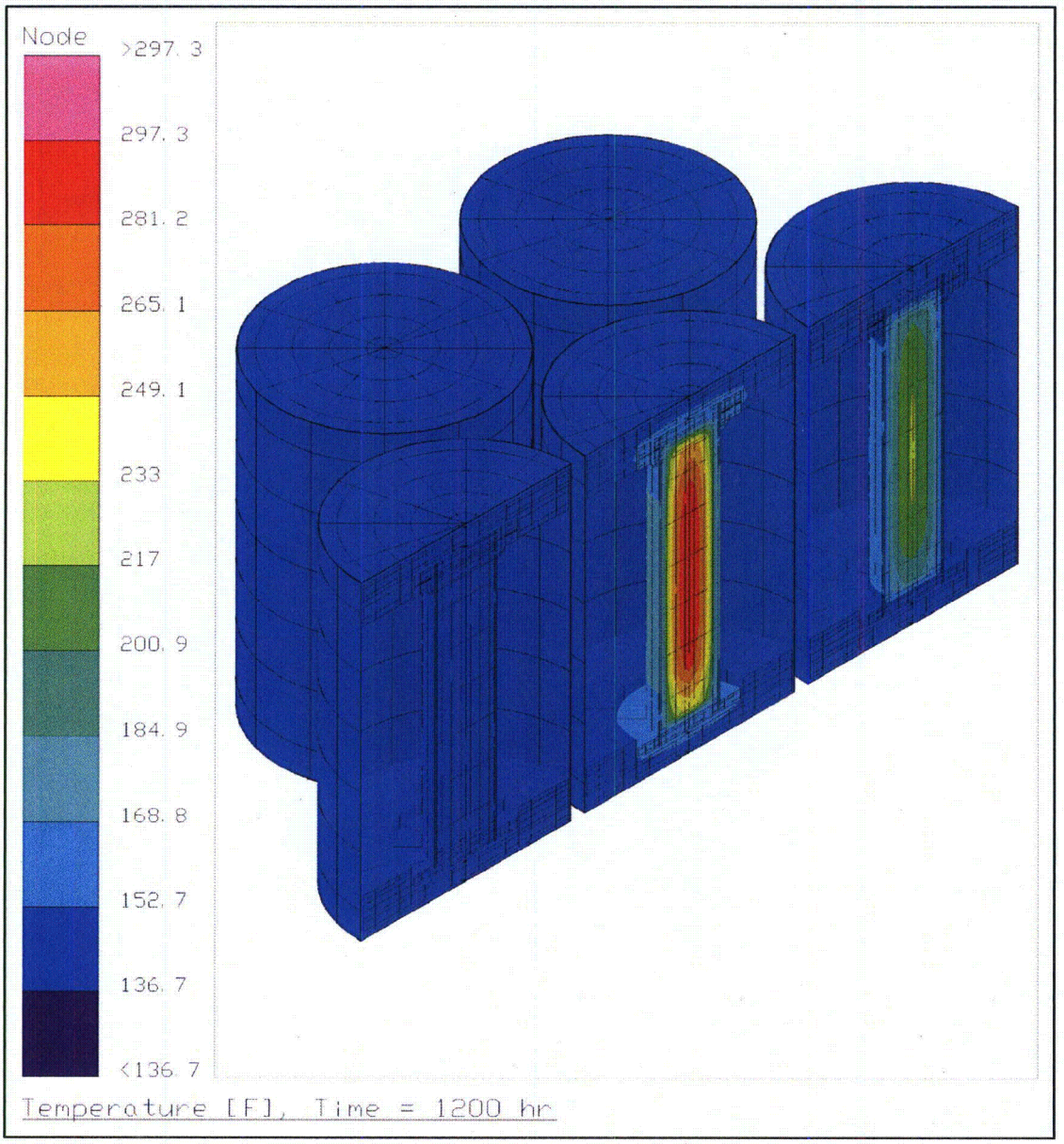

Figure 4-68 – HalfPACT Case 2 Payload Temperatures with Insolation

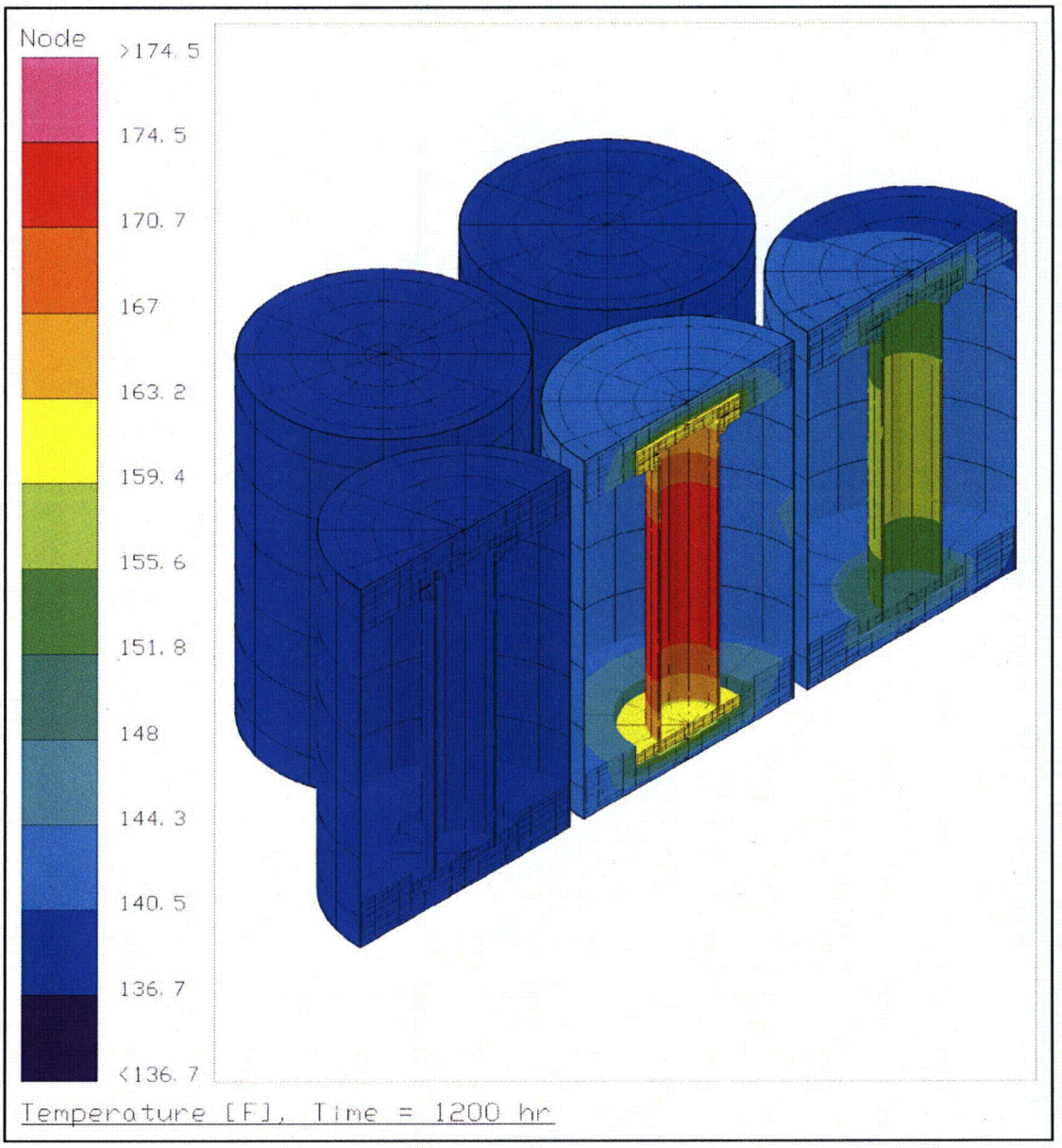

Figure 4-69 – HalfPACT Case 2 CCO Temperatures with Insolation

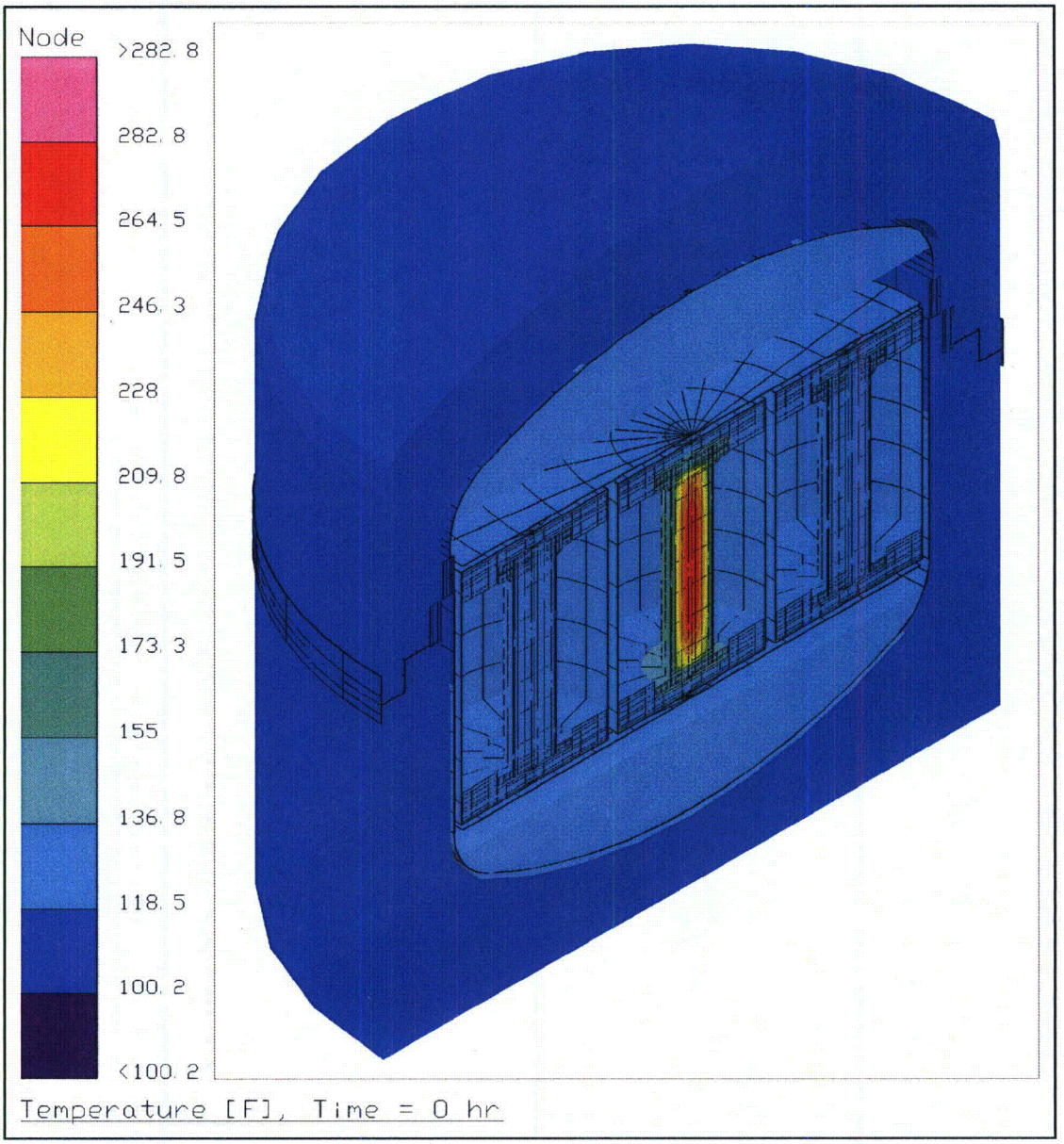

Figure 4-70 – HalfPACT Case 3 Package Temperatures without Insolation

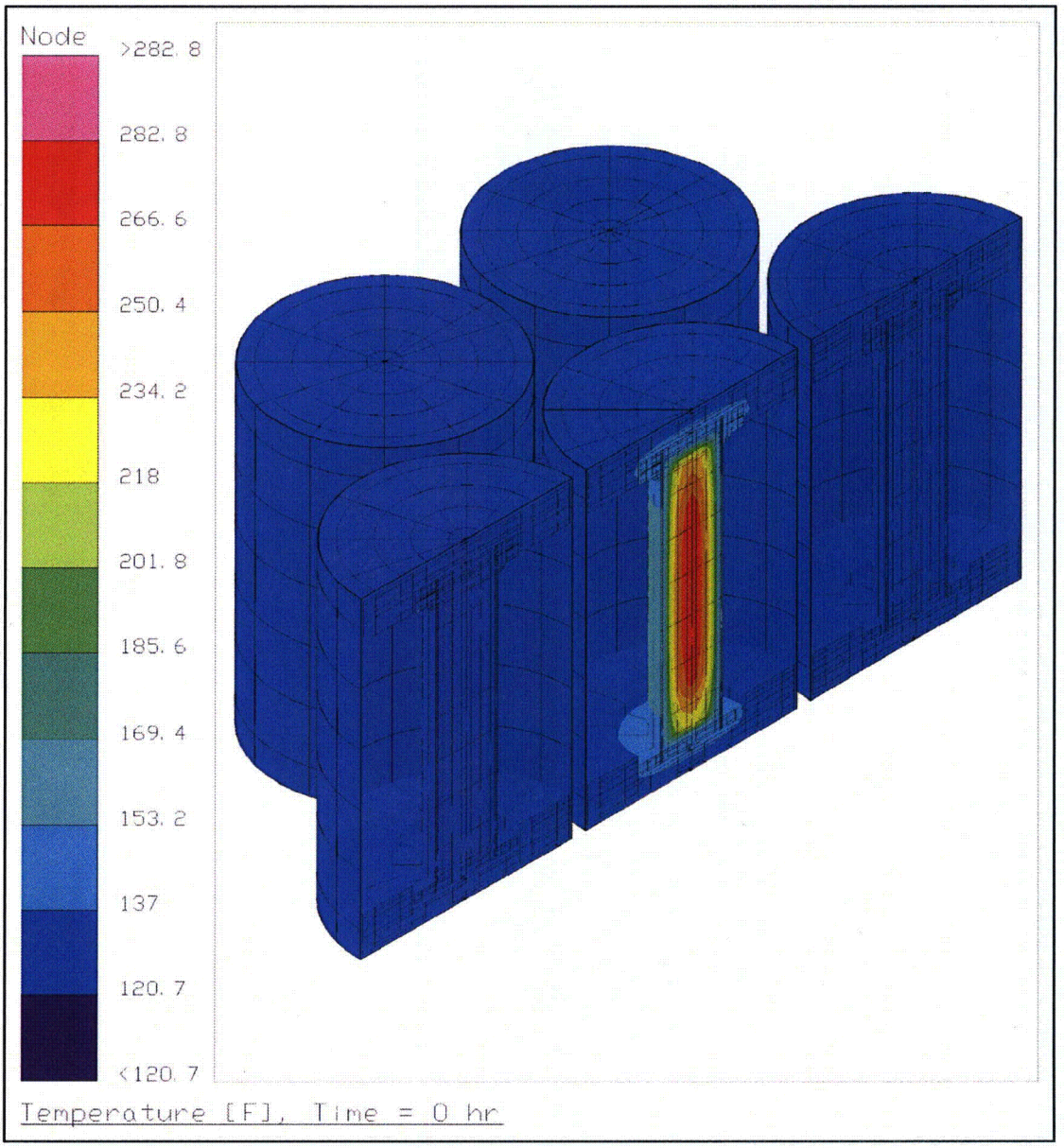

Figure 4-71 – HalfPACT Case 3 Payload Temperatures without Insolation

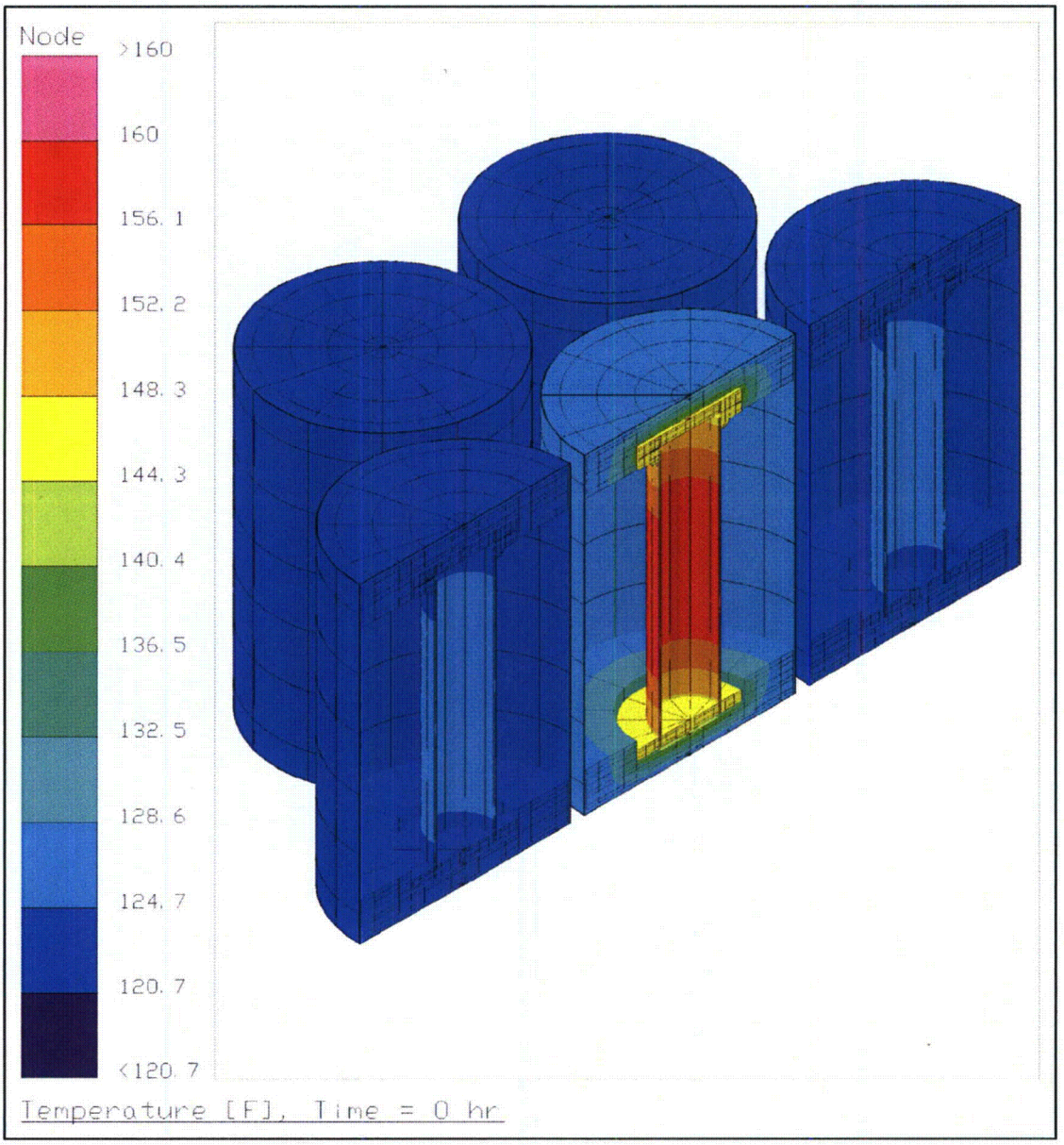

Figure 4-72 – HalfPACT Case 3 CCO Temperatures without Insolation

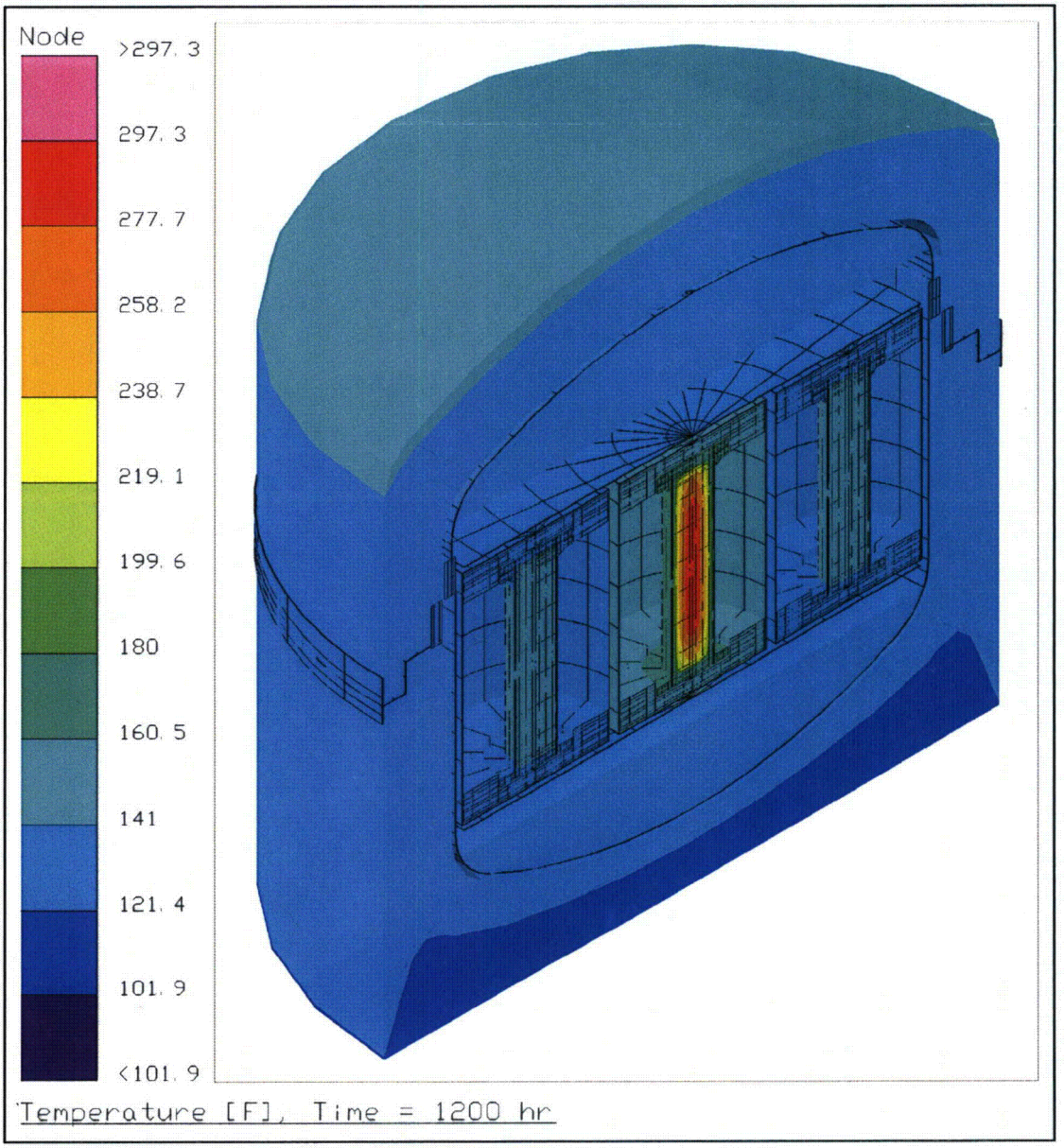

Figure 4-73 – HalfPACT Case 3 Package Temperatures with Insolation

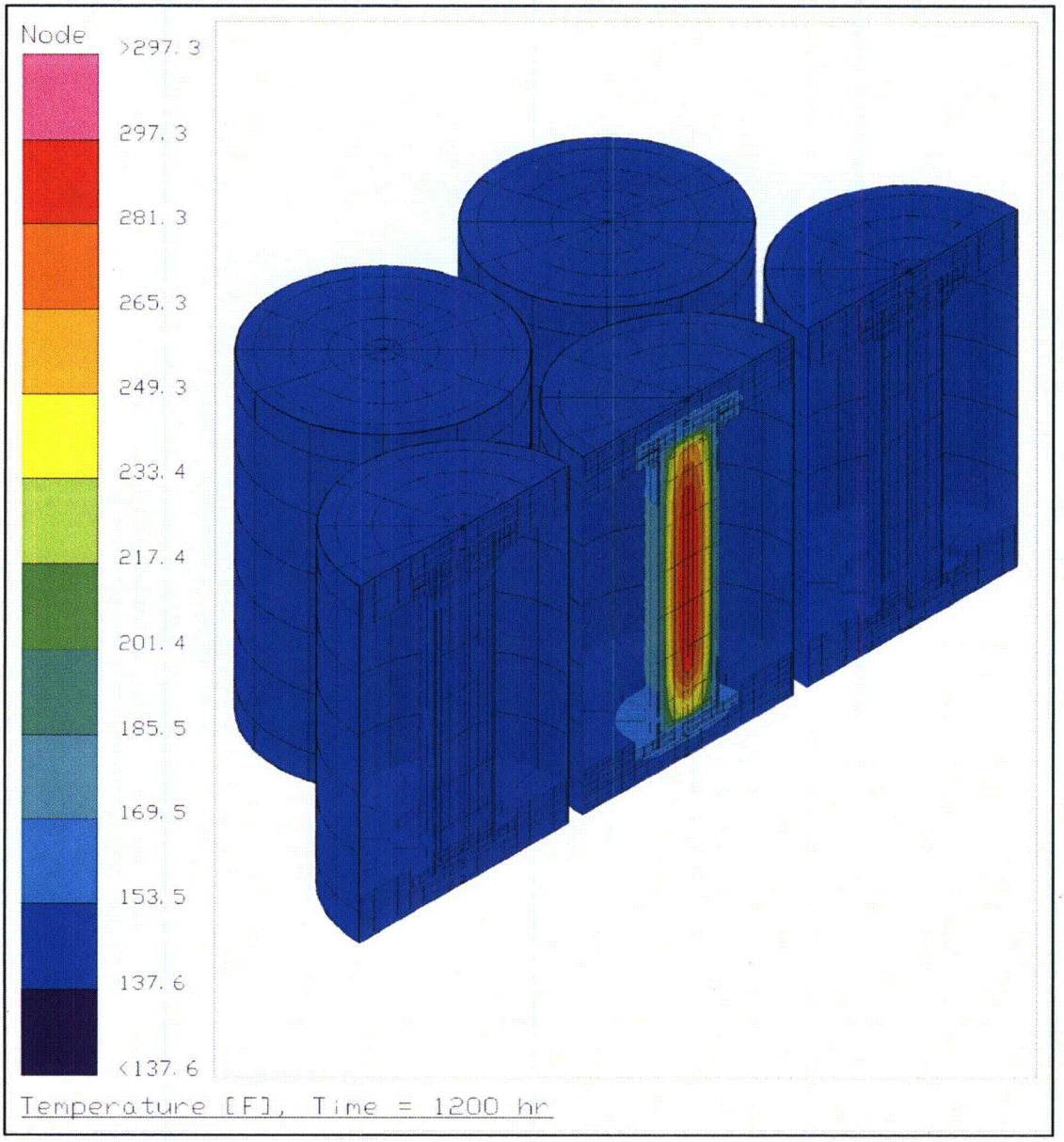

Figure 4-74 – HalfPACT Case 3 Payload Temperatures with Insolation

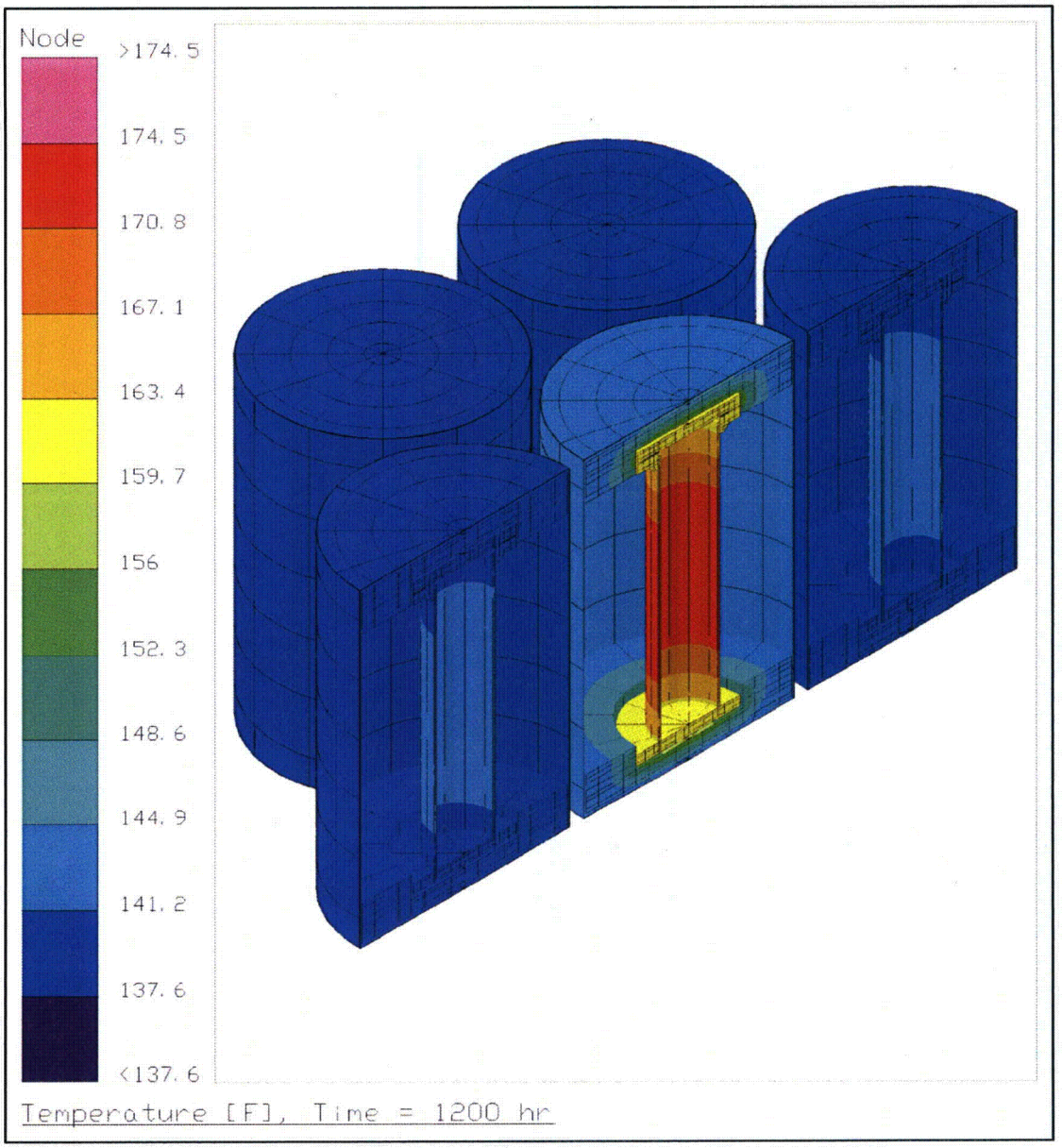

Figure 4-75 – HalfPACT Case 3 CCO Temperatures with Insolation

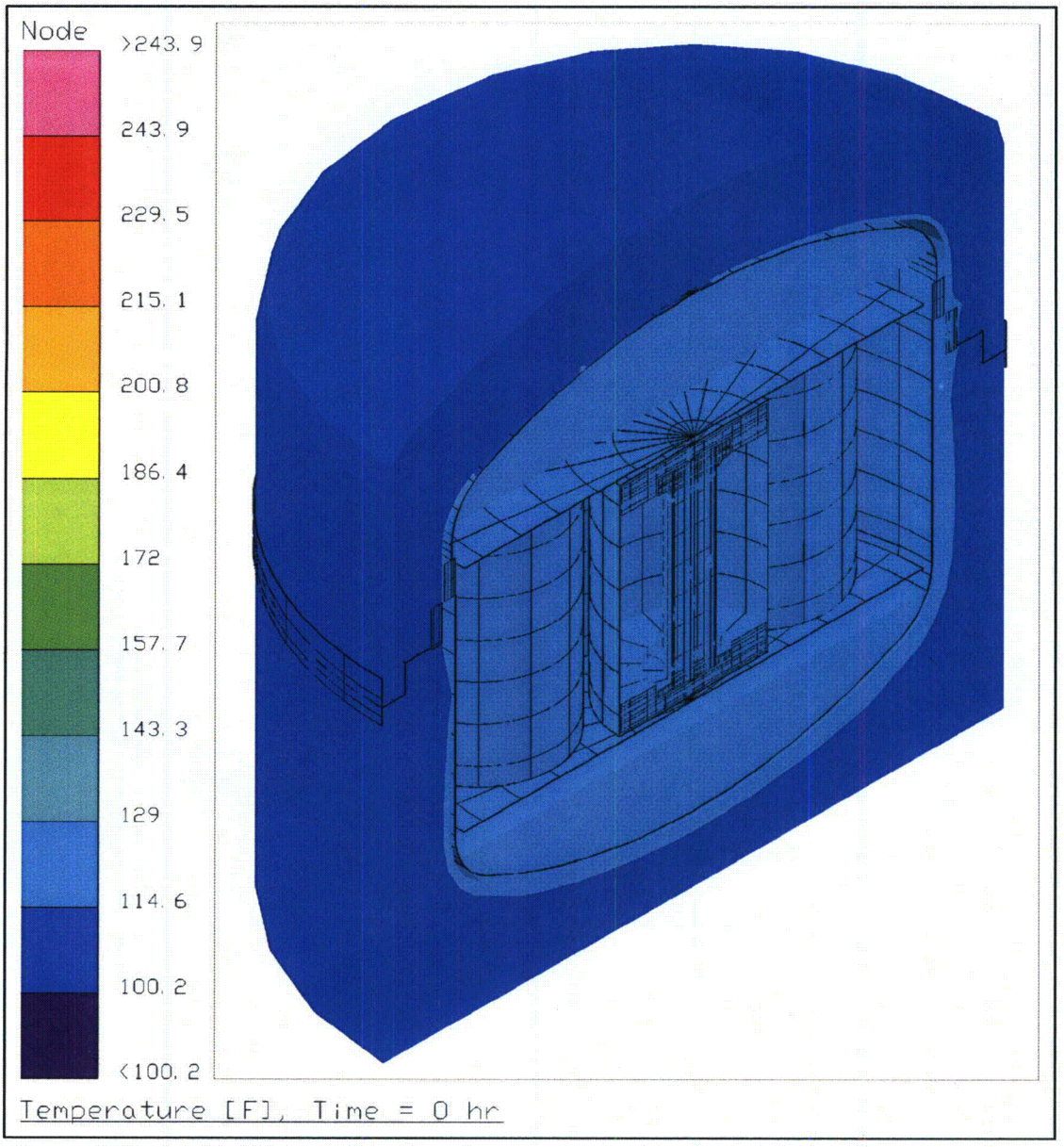

Figure 4-76 – HalfPACT Case 4 Package Temperatures without Insolation

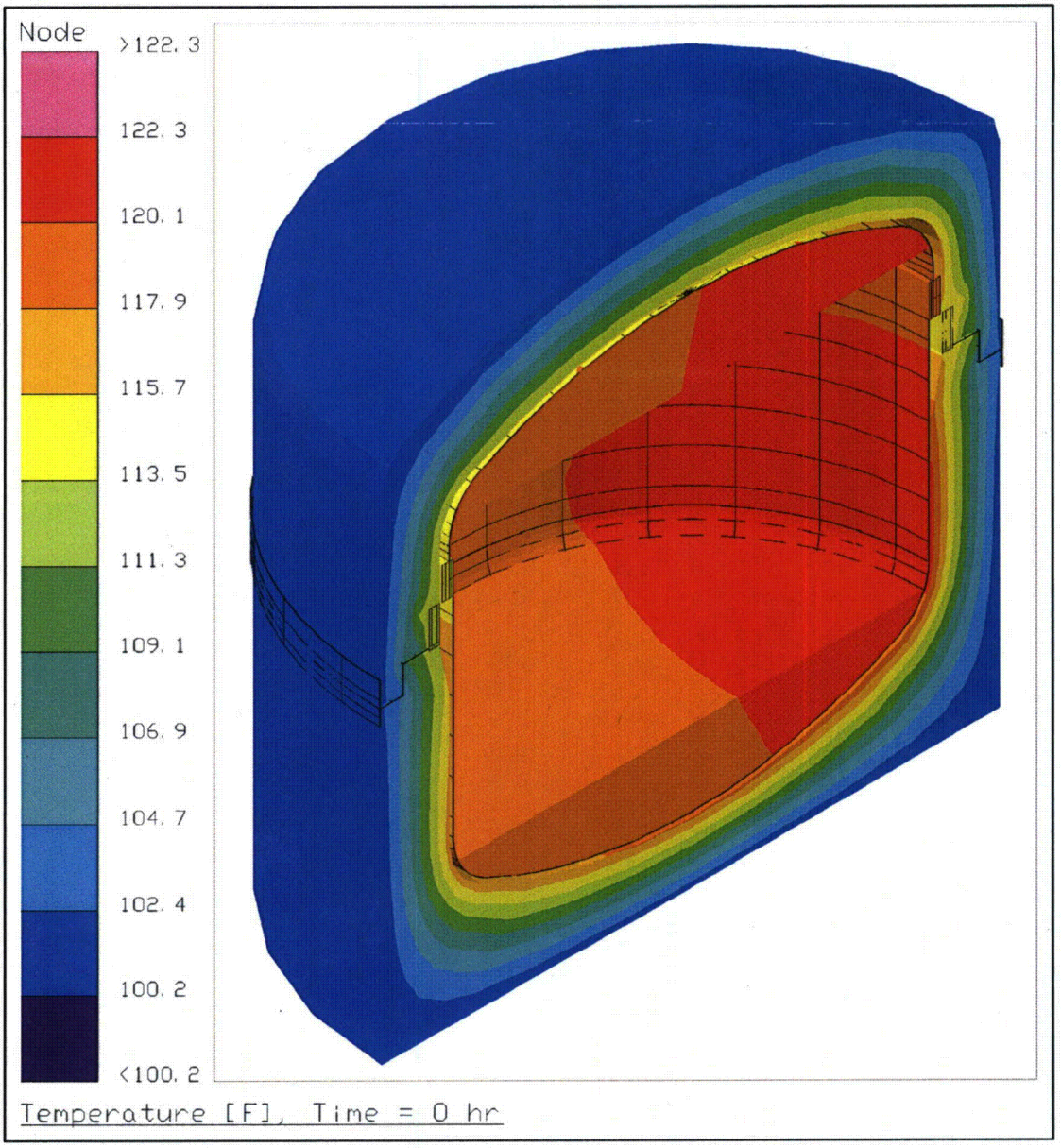

Figure 4-77 – HalfPACT Case 4 Packaging Temperatures without Insolation

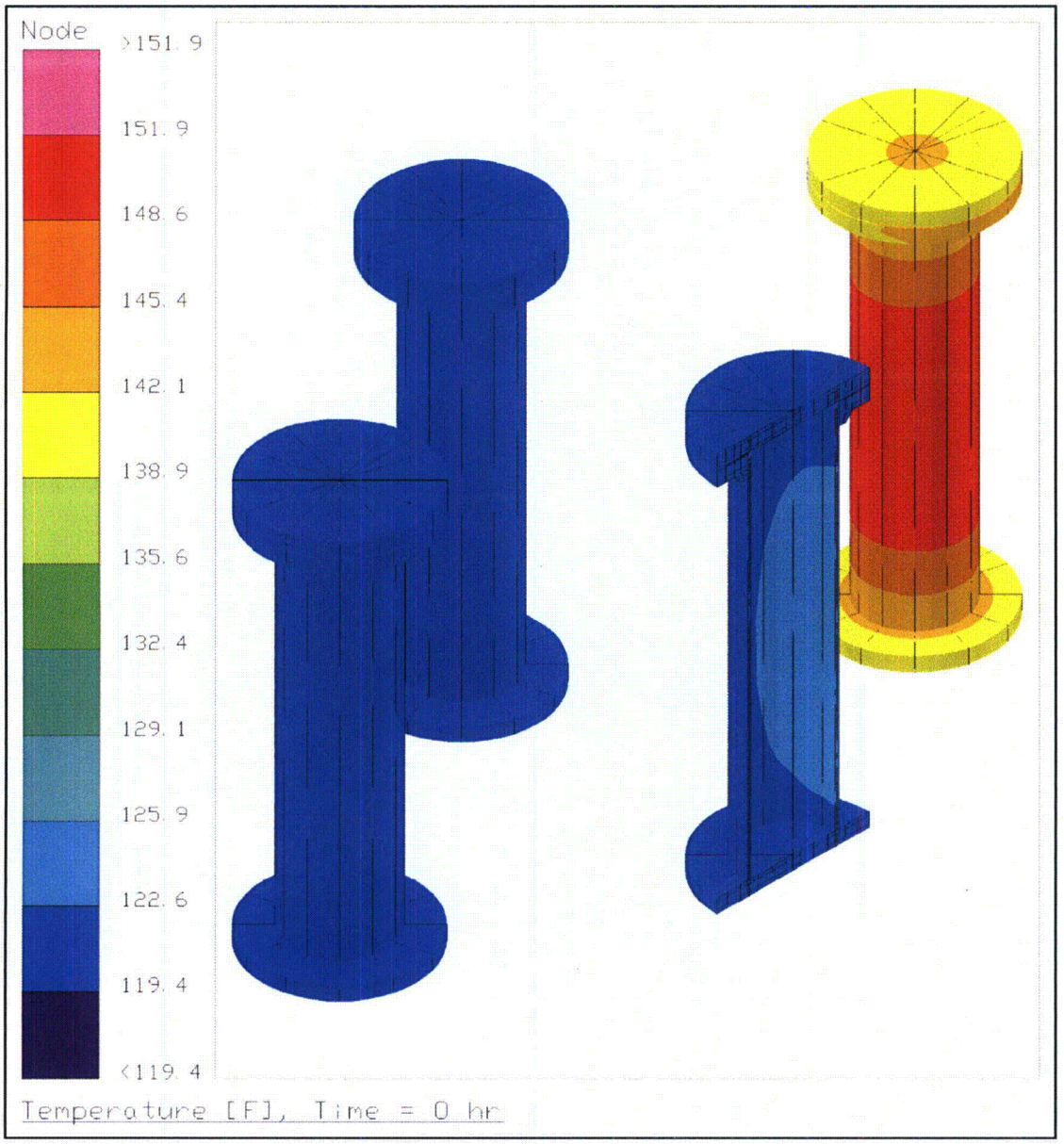

Figure 4-78 – HalfPACT Case 4 CCO Temperatures without Insolation

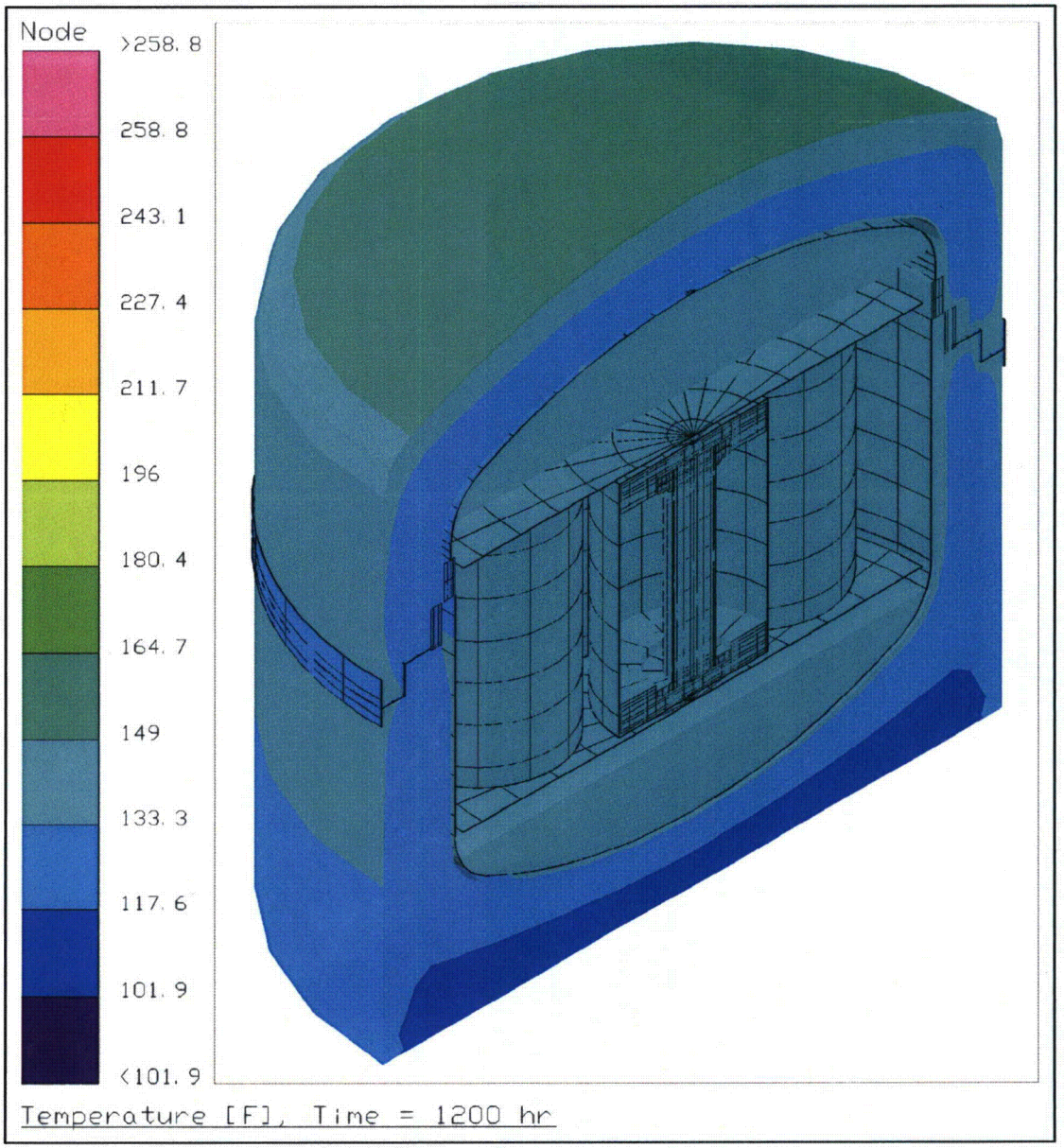

Figure 4-79 – HalfPACT Case 4 Package Temperatures with Insolation

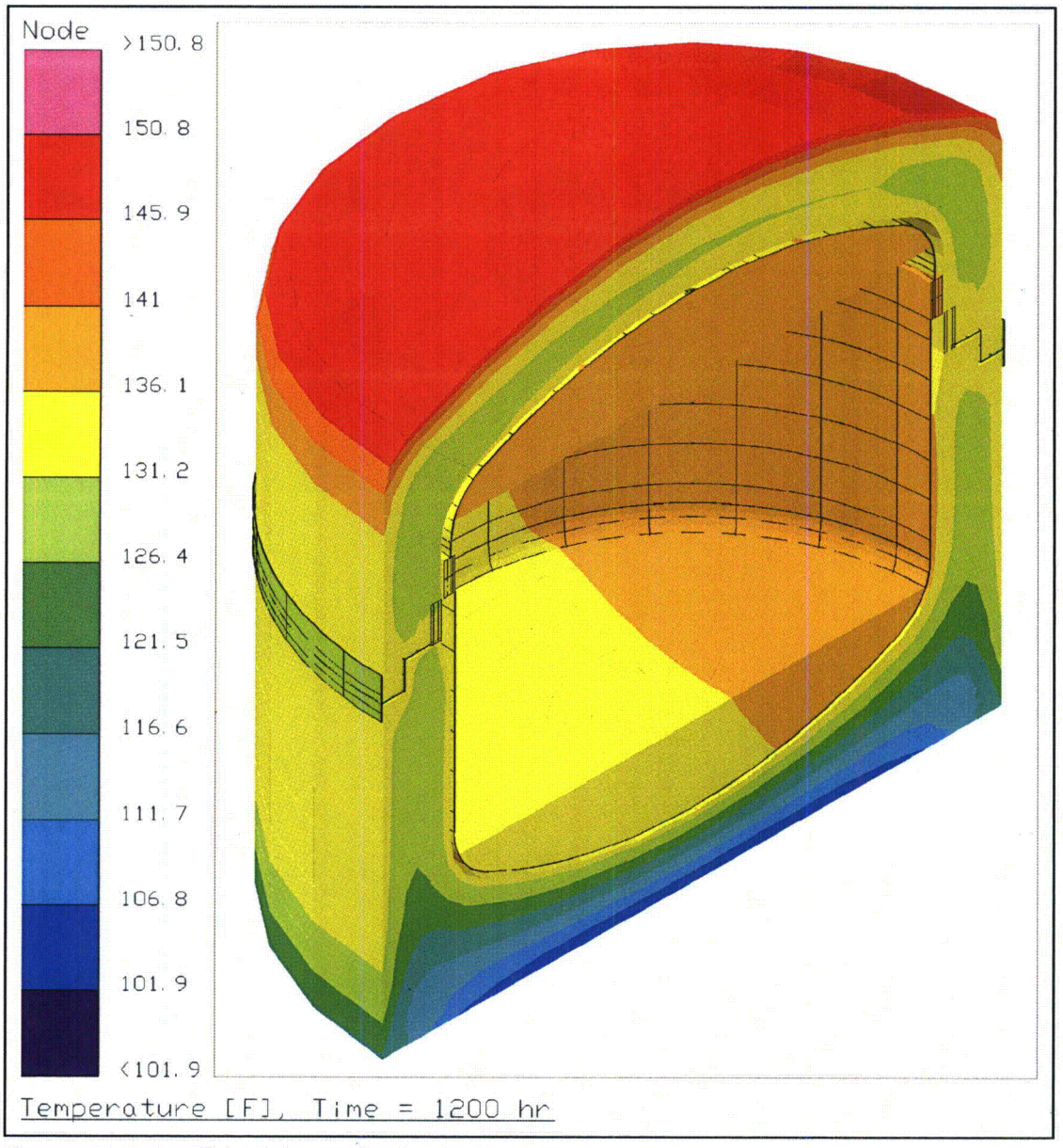

Figure 4-80 – HalfPACT Case 4 Packaging Temperatures with Insolation

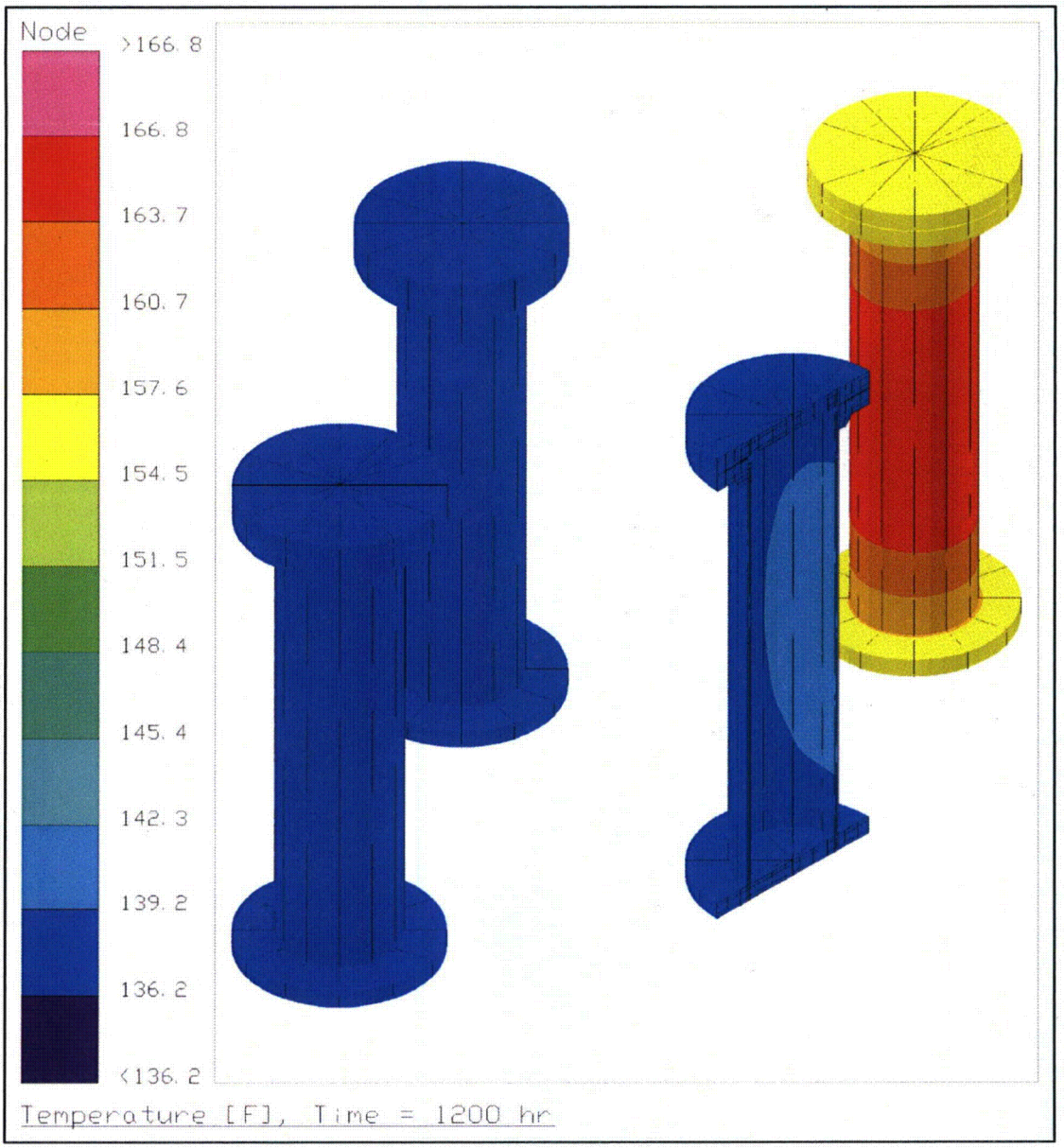

Figure 4-81 – HalfPACT Case 4 CCO Temperatures with Insolation

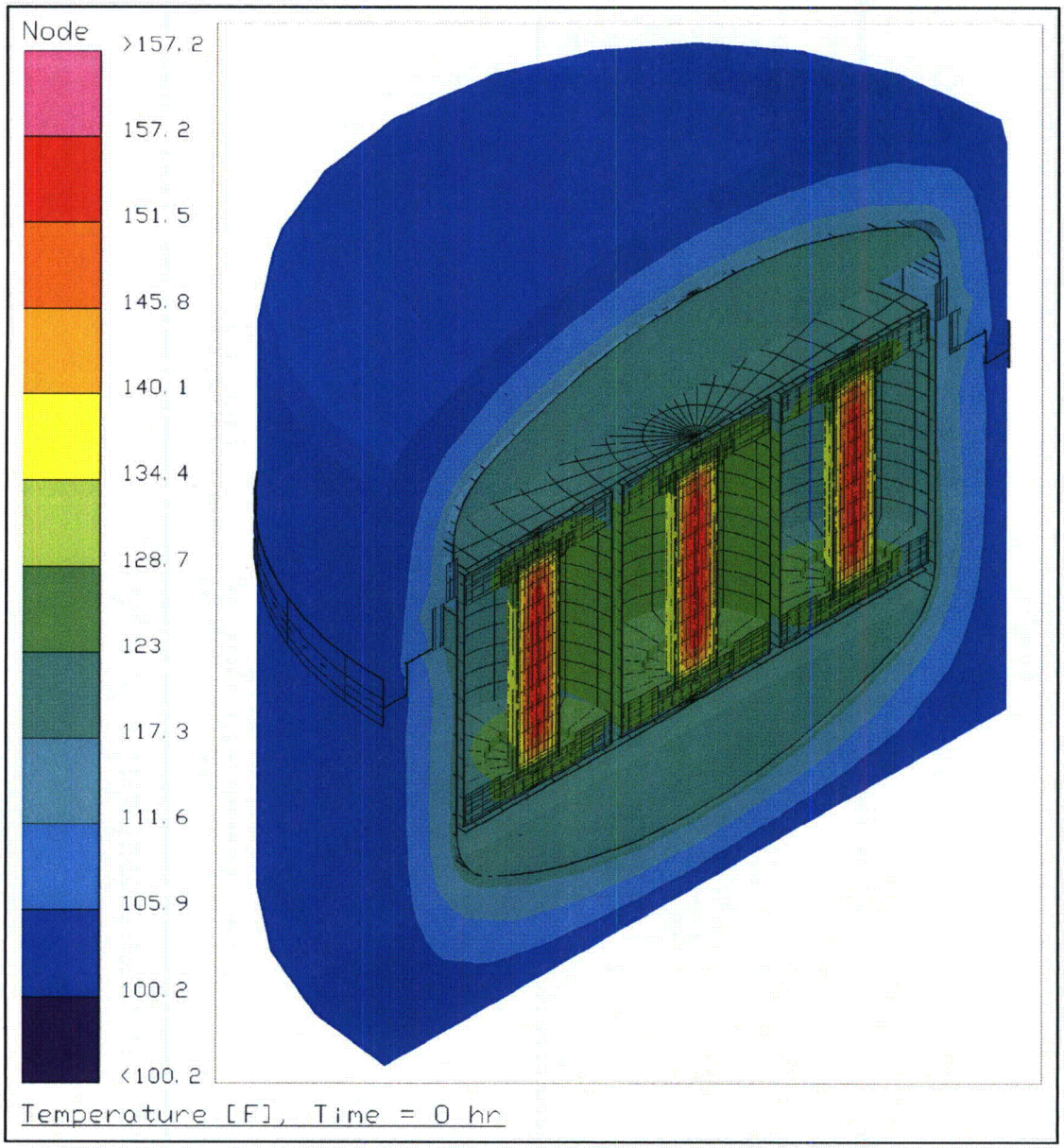

Figure 4-82 – HalfPACT Case 1H Package Temperatures without Insolation (Sensitivity Study)

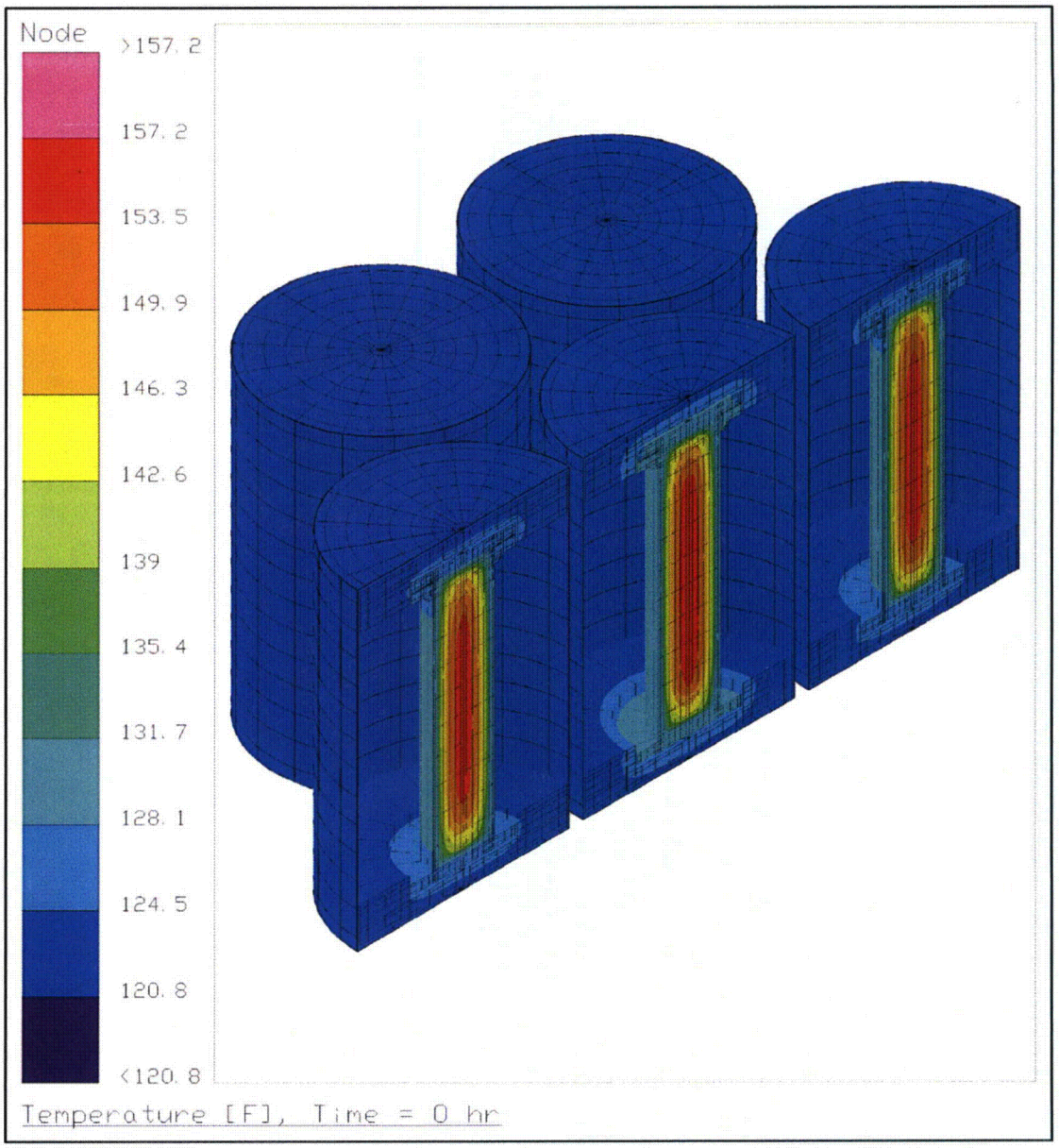

Figure 4-83 – HalfPACT Case 1H Payload Temperatures without Insolation (Sensitivity Study)

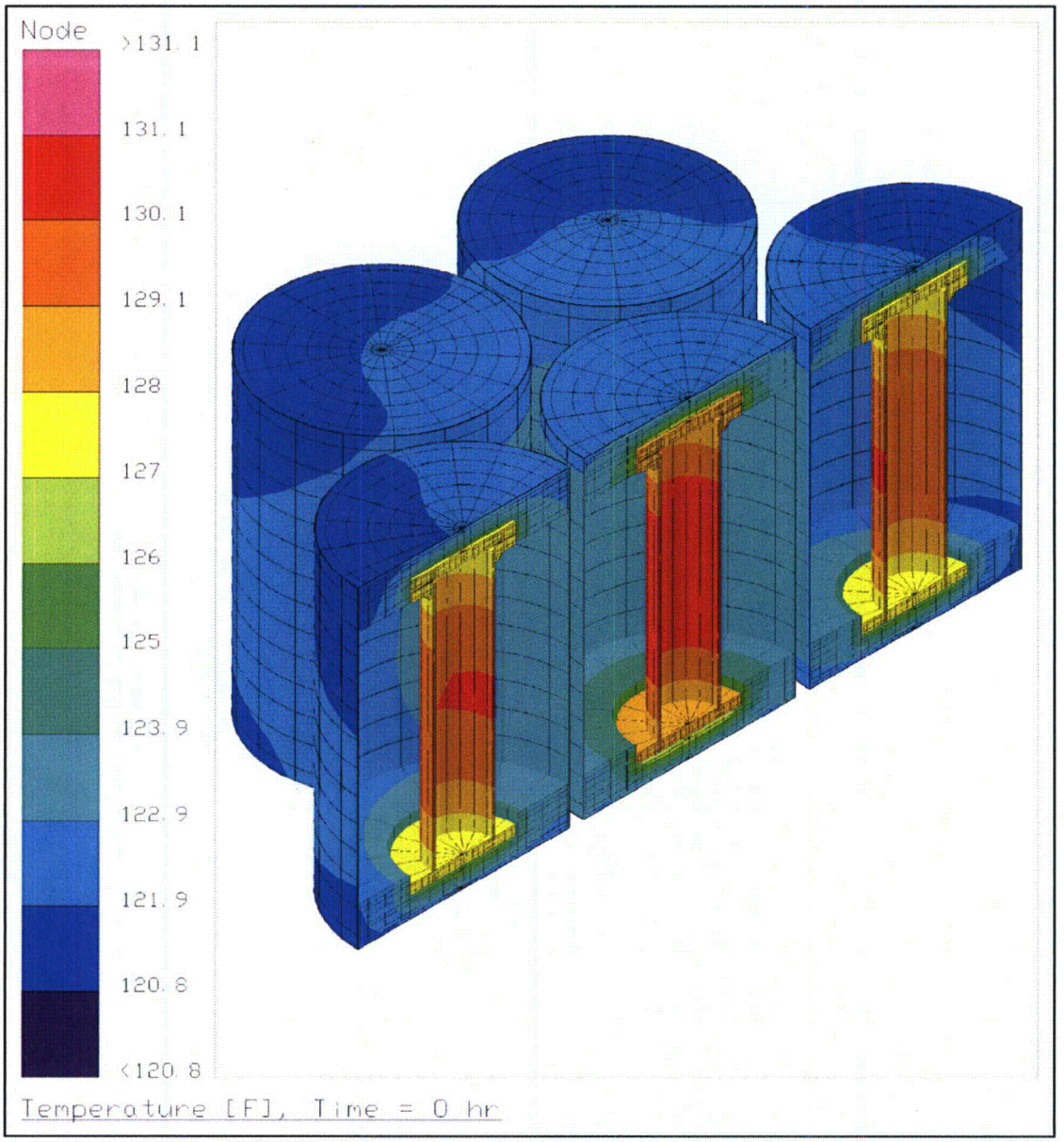

Figure 4-84 – HalfPACT Case 1H CCO Temperatures without Insolation (Sensitivity Study)

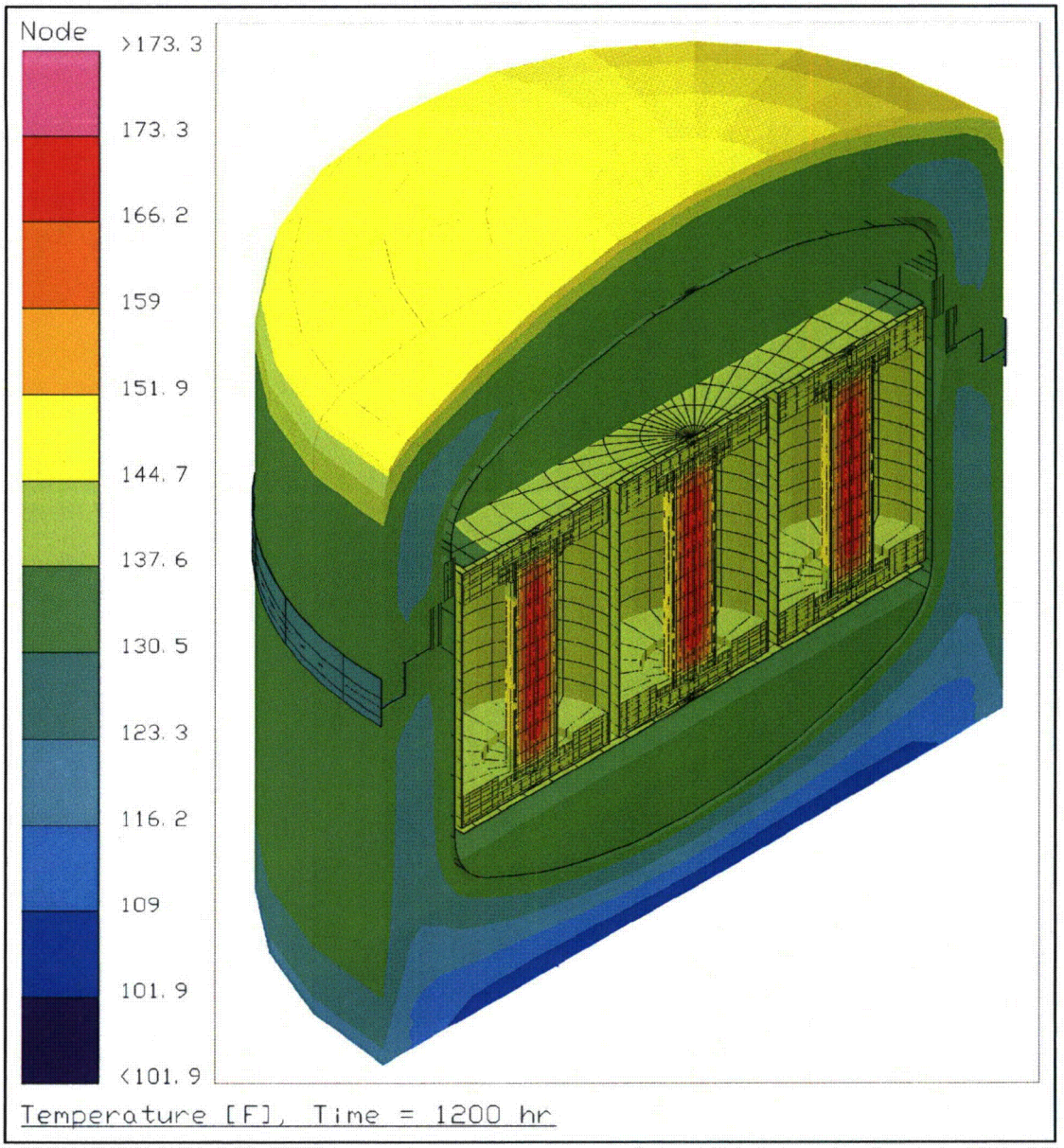

Figure 4-85 – HalfPACT Case 1H Package Temperatures with Insolation (Sensitivity Study)

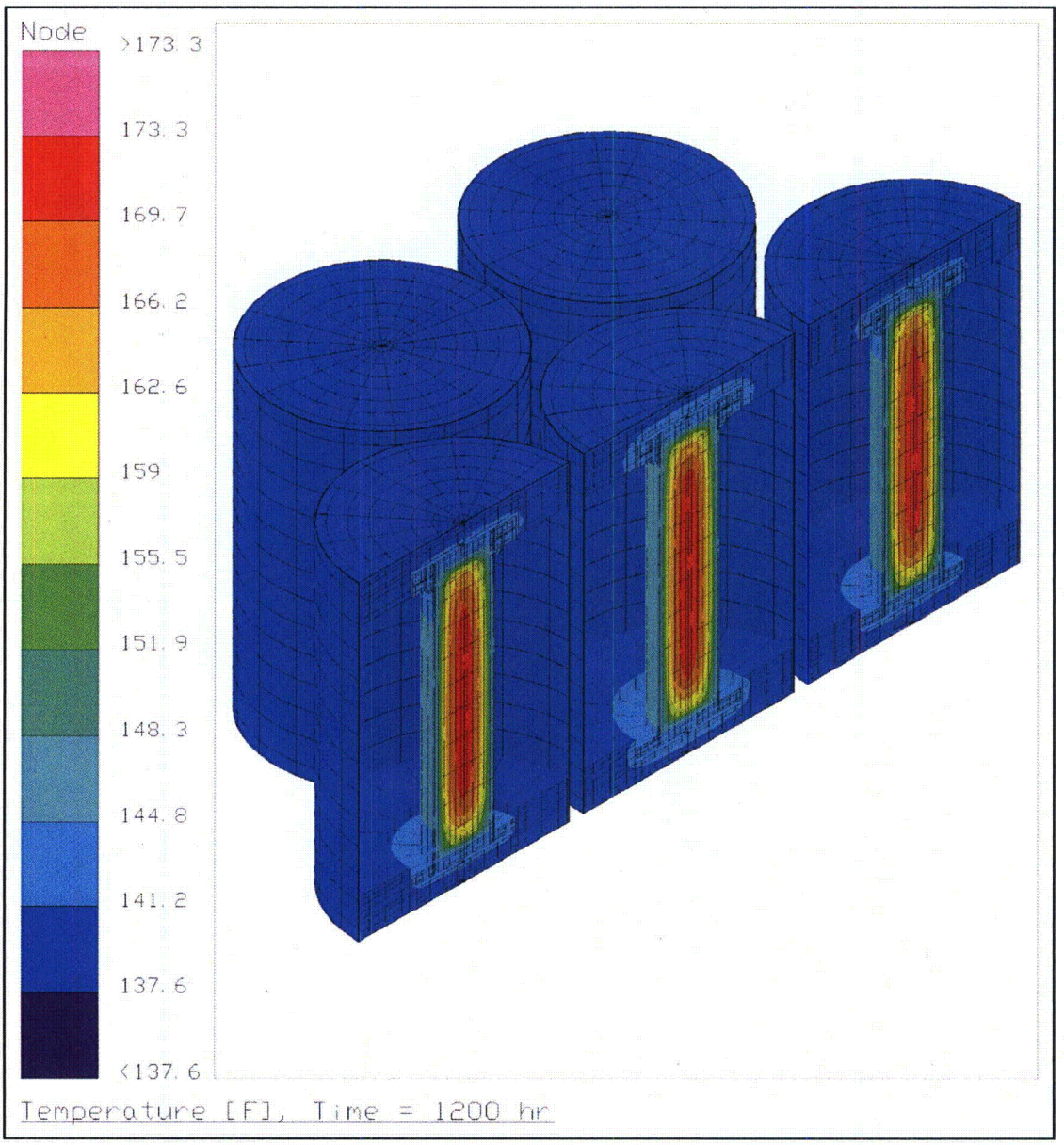

Figure 4-86 – HalfPACT Case 1H Payload Temperatures with Insolation (Sensitivity Study)

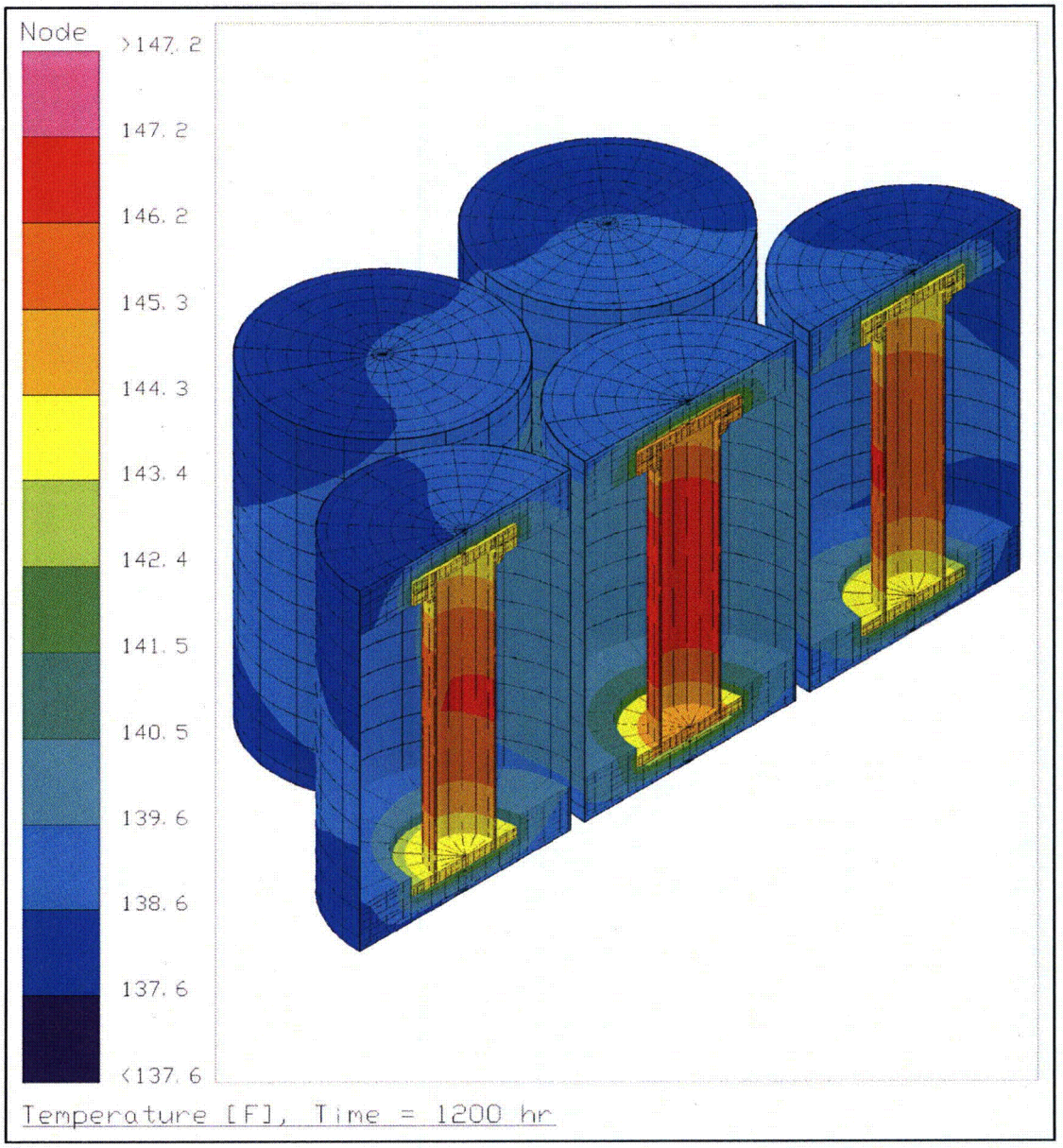

Figure 4-87 – HalfPACT Case 1H CCO Temperatures with Insolation (Sensitivity Study)

4.4 Minimum Temperatures

The minimum temperatures within the TRUPACT-II and HalfPACT packages are not evaluated for the analytically trivial NCT ambient condition of -40 °F, no insolation, and zero decay heat load for the evaluated payload configurations. Given sufficient time, the package temperatures will sink to the -40 °F ambient temperatures for these thermal load conditions.

The assumed conditions for minimum temperatures of -40 °F yield component temperature levels that are within the allowable temperature limits according to Section 3.0, *Technical Specifications of Components.*

4.5 Maximum Internal Pressure

The design maximum pressure in the ICV under normal conditions of transport is 50 psig. The major factors affecting the ICV internal pressure are radiolytic gas generation, thermal expansion of gases, and the vapor pressure of water within the ICV cavity. The determination of the maximum normal operating pressure (MNOP) is not within the scope of this calculation. However, decay heat/temperature equations are presented to support internal pressure calculations.

As shown in Table 3.4-1 through Table 3.4-5 in Section 3.4.4, *Maximum Internal Pressure*, of the TRUPACT-II Safety Analysis Report, and in Table 3.4-2 in Section 3.4.4, *Maximum Internal Pressure*, of the HalfPACT Safety Analysis Report, component temperatures are essentially linearly proportional to the decay heat load for the various analysis cases. With reference to Table 4-3 for the TRUPACT-II package and Table 4-5 for the HalfPACT package, Table 4-7 and Table 4-8 present the linear equation coefficients for the components used in the internal pressure calculations based on the equation:

$$T = a + bQ$$

where T is the temperature (degrees Fahrenheit) and Q is the decay heat load (watts). The bounding linear equation coefficients for each package, case, and condition are presented in Table 4-9.

4.6 Maximum Thermal Stresses

Determination of maximum thermal stresses in the TRUPACT-II and HalfPACT packagings is not within the scope of this calculation.

4.7 Evaluation of Package Performance for Normal Conditions of Transport

The combined thermal performance of the CCOs within the TRUPACT-II and HalfPACT packagings is evaluated for the applicable NCT conditions and for a variety of decay heat distributions within the packagings. The evaluations found that the resulting component temperatures remained within their specified allowable limits for all cases. Furthermore, the computed temperatures for the TRUPACT-II and HalfPACT packaging components are bounded by those currently predicted in the TRUPACT-II and HalfPACT SARs[1,2], respectively. Thus, the CCO payload will not impact the safety basis of either the TRUPACT-II or HalfPACT packages for NCT.

Table 4-7 – Linear Equation Coefficients for Temperatures (°F) Based on Decay Heat Load (W) for the TRUPACT-II Package

Case	Condition	Temperature		Coefficients	
		T_{0W}	T_{40W}	a	b
1	Contents Centerline Average – Maximum CCOs	117.7	161.2	117.7	1.0875
	Contents Bulk Average – Maximum CCOs	117.7	153.0	117.7	0.8825
	Contents Centerline Average – All CCOs	117.7	160.5	117.7	1.0700
	Contents Bulk Average – All CCOs	117.7	152.3	117.7	0.8650
	Air Bulk Average	117.7	139.7	117.7	0.5500
	ICV Wall Minimum	116.5	134.4	116.5	0.4475
2	Contents Centerline Average – Maximum CCOs	117.7	280.8	117.7	4.0775
	Contents Bulk Average – Maximum CCOs	117.7	223.6	117.7	2.6475
	Contents Centerline Average – All CCOs	117.7	161.0	117.7	1.0825
	Contents Bulk Average – All CCOs	117.7	152.8	117.7	0.8775
	Air Bulk Average	117.7	140.2	117.7	0.5625
	ICV Wall Minimum	116.5	134.5	116.5	0.4500
3	Contents Centerline Average – Maximum CCOs	117.7	281.7	117.7	4.1000
	Contents Bulk Average – Maximum CCOs	117.7	224.5	117.7	2.6700
	Contents Centerline Average – All CCOs	117.7	160.1	117.7	1.0600
	Contents Bulk Average – All CCOs	117.7	151.9	117.7	0.8550
	Air Bulk Average	117.7	139.6	117.7	0.5475
	ICV Wall Minimum	116.5	133.6	116.5	0.4275
4	Contents Centerline Average – Maximum CCOs	117.7	282.6	117.7	4.1225
	Contents Bulk Average – Maximum CCOs	117.7	225.4	117.7	2.6925
	Contents Centerline Average – All CCOs	117.7	159.4	117.7	1.0425
	Contents Bulk Average – All CCOs	117.7	151.3	117.7	0.8400
	Air Bulk Average	117.7	139.7	117.7	0.5500
	ICV Wall Minimum	116.5	134.2	116.5	0.4425

Table 4-8 – Linear Equation Coefficients for Temperatures (°F) Based on Decay Heat Load (W) for the HalfPACT Package

Case	Condition	Temperature		Coefficients	
		T_{0W}	T_{40W}	a	b
1	Contents Centerline Average – Maximum CCO	117.6	169.4	117.6	1.2950
	Contents Bulk Average – Maximum CCO	117.6	157.1	117.6	0.9875
	Contents Centerline Average – All CCOs	117.6	168.6	117.6	1.2750
	Contents Bulk Average – All CCOs	117.6	156.3	117.6	0.9675
	Air Bulk Average	117.5	137.8	117.5	0.5075
	ICV Wall Minimum	116.6	133.2	116.6	0.4150
2	Contents Centerline Average – Maximum CCO	117.6	278.7	117.6	4.0275
	Contents Bulk Average – Maximum CCO	117.6	221.5	117.6	2.5975
	Contents Centerline Average – All CCOs	117.6	168.8	117.6	1.2800
	Contents Bulk Average – All CCOs	117.6	156.6	117.6	0.9750
	Air Bulk Average	117.5	138.1	117.5	0.5150
	ICV Wall Minimum	116.6	133.0	116.6	0.4100
3	Contents Centerline Average – Maximum CCO	117.6	278.7	117.6	4.0275
	Contents Bulk Average – Maximum CCO	117.6	221.5	117.6	2.5975
	Contents Centerline Average – All CCOs	117.6	168.9	117.6	1.2825
	Contents Bulk Average – All CCOs	117.6	156.6	117.6	0.9750
	Air Bulk Average	117.5	138.1	117.5	0.5150
	ICV Wall Minimum	116.6	133.2	116.6	0.4150
4	Contents Centerline Average – Maximum CCO	117.6	244.9	117.6	3.1825
	Contents Bulk Average – Maximum CCO	117.6	201.9	117.6	2.1075
	Contents Centerline Average – All CCOs	117.6	168.2	117.6	1.2650
	Contents Bulk Average – All CCOs	117.6	155.9	117.6	0.9575
	Air Bulk Average	117.5	137.7	117.5	0.5050
	ICV Wall Minimum	116.6	132.4	116.6	0.3950

Table 4-9 – Bounding Linear Equation Coefficients for Temperatures (°F) Based on Decay Heat Load (W) for the TRUPACT-II and HalfPACT Packages

Package	Case	Condition	Coefficients	
			a	b
TRUPACT-II	4	Contents Centerline Average – Maximum CCOs	117.7	4.1225
	4	Contents Bulk Average – Maximum CCOs	117.7	2.6925
	2	Contents Centerline Average – All CCOs	117.7	1.0825
	2	Contents Bulk Average – All CCOs	117.7	0.8775
	2	Air Bulk Average	117.7	0.5625
	3	ICV Wall Minimum	116.5	0.4275
HalfPACT	2 & 3	Contents Centerline Average – Maximum CCO	117.6	4.0275
	2 & 3	Contents Bulk Average – Maximum CCO	117.6	2.5975
	3	Contents Centerline Average – All CCOs	117.6	1.2825
	2 & 3	Contents Bulk Average – All CCOs	117.6	0.9750
	2 & 3	Air Bulk Average	117.5	0.5150
	4	ICV Wall Minimum	116.6	0.3950

5.0 THERMAL EVALUATION FOR HYPOTHETICAL ACCIDENT CONDITIONS

The maximum temperatures for the CCO components within the TRUPACT-II and HalfPACT packagings from the HAC fire event may be determined by conservatively combining the experimentally derived differential temperatures measured from HAC fire testing of each package (given in Table 3.5-5 of the TRUPACT-II SAR and Table 3.5-2 of the HalfPACT SAR) with the worst-case initial pre-fire temperatures from Table 4-2 for the TRUPACT-II package and Table 4-4 for the HalfPACT package. The worst-case initial pre-fire temperatures are based on the maximum temperature for each component, regardless of the case number. Further conservatism is attained by upwardly adjusting maximum temperatures to account for the difference in the tested payload mass versus the CCO payload mass.

The bounding estimate for the increase in TRUPACT-II and HalfPACT packaging component temperatures due to the lighter CCO payload is determined by taking the heat absorbed by the test payload (i.e., concrete-filled 55-gallon drums) and proportionally redistributing all of that thermal energy to packaging components interior to the OCA outer shell (which is already at the maximum fire temperature of 1,475 °F and incapable of absorbing additional energy). The heat absorbed by the test payload is conservatively calculated by assuming a uniform temperature increase such that the payload bulk average temperature is assumed to be equal to the measured drum shell temperature. The adjusted absorbed heat values are subsequently used to calculate adjusted bulk average temperatures for the packaging components (i.e., OCA foam, OCV structure, ICV structure, honeycomb spacers, and payload pallet) by using their respective component masses and specific heats. The adjusted packaging component bulk average temperatures are then used to calculate a bounding temperature change (percentage increase) due to a fire event for the package with "no payload" mass.

The "no payload" temperature change percentages are conservatively applied to the packaging components and CCO payload by assuming that the CCO 55-gallon drum adjusted maximum temperature is equal to the adjusted ICV bulk average temperature, with all other packaging component adjusted maximum temperatures equal to the maximum measured fire temperatures increased by the bulk average temperature change percentage for each component. It is conservative to assume that the CCO 55-gallon drum shell is at the bulk average temperature of the ICV structure because, at the point of maximum temperature, heat flow is primarily inward such that the magnitude of temperature increase due to the fire event is progressively less for each component as the heat moves from the OCV to the ICV and into the payload. Additionally, previous fire tests have demonstrated that the maximum surface temperature of the payload container(s) is less than the bulk average temperature of the ICV structure. To account for the pre-fire temperature gradients within the CCO that are due to the insulating effects of the radial gap between the CCC structure and the 55-gallon drum, the maximum temperature differential for each CCO component is assumed to be a function of the maximum temperature differential for the 55-gallon drum and proportional to the pre-fire temperature gradients within the CCO.

5.1 Maximum HAC Fire Temperatures for TRUPACT-II with a CCO Payload

Table 5-1 summarizes the weights, dominant materials, specific heats, pre-fire temperatures, bulk average fire temperatures, differential temperatures, and the heat absorbed for each TRUPACT-II packaging and payload component. Table notes provide corresponding references to the data provided in the tables.

With reference to Table 5-1, the total absorbed heat in a TRUPACT-II package with 500-pound concrete-filled payload drums is calculated to be 1,478,677 Btu. As a check, the average "time-integrated" heat flux due to a 30-minute HAC fire event is 31.6 kW-hr/m^2 (≈10,000 Btu/ft^2) based on a thermal experiment performed by Sandia.[18] The time-integrated absorbed heat for the TRUPACT-II package with a 320 ft^2 external surface area is 10,000 × 320 = 3,200,000 Btu. Therefore, the corresponding ratio of calculated

[18] J. J. Gregory, N. R. Keltner, R. Mata, Jr., *Thermal Measurements in Large Pool Fires*, SAND87-0094C, Thermal Test and Analysis Division, Sandia National Laboratories, Albuquerque, NM, 1987.

absorbed heat versus the Sandia-derived maximum absorbed heat is 1,478,677/3,200,000 = 0.46. Considering that austenitic stainless steel exhibits an emissivity of approximately 0.45 at 1,475 °F,[19] the calculated absorbed heat is reasonable.

Table 5-2 presents the adjusted heat absorbed by each packaging component when 33,815 Btu of tested payload heat from Table 5-1 is proportionally redistributed to the packaging components. For example, the adjusted heat absorbed by the ICV structure is:

$$17{,}540 \times \frac{524{,}092 + 29{,}884 + 17{,}540 + 2{,}810 + 1{,}950 + 33{,}815}{524{,}092 + 29{,}884 + 17{,}540 + 2{,}810 + 1{,}950} = 18{,}569\,\text{Btu}$$

The corresponding adjusted bulk average fire temperature, given an ICV weight of 2,420 pounds, a specific heat of 0.121 Btu/lb-°F, and a pre-fire temperature of 127.0 °F (all from Table 5-1), is:

$$127.0 + \frac{18{,}569}{(2{,}420 \times 0.121)} = 190.4\,°\text{F}$$

The corresponding temperature change for the ICV structure, given a bulk average fire temperature for the ICV structure of 186.9 °F from Table 5-1 and an adjusted bulk average fire temperature for the ICV structure of 190.4 °F from Table 5-2, is:

$$\frac{190.4 - 186.9}{186.9} \times 100 = 1.9\%$$

Table 5-3 presents the bulk average ICV cavity air temperature and maximum fire temperatures for the CCO components, ICV structure and O-ring seal region, and OCV structure and O-ring seal region based on data from Table 5-1, Table 5-2, and Table 5-3.

Again, using the ICV structure as the example, the adjusted maximum fire temperature, given an adjusted bulk average fire temperature of 190.4 °F and temperature change of 1.9% from Table 5-2, and a measured maximum fire temperature of 220.0 °F from Table 5-3, is:

$$220.0 \times (1 + 0.019) = 224.2\,°\text{F}$$

The corresponding maximum differential temperature for the ICV structure, given an adjusted maximum fire temperature of 224.2 °F and a CTU-2 pre-fire temperature of 127.0 °F, is:

$$224.2 - 127.0 = 97.2\,°\text{F}$$

The resulting maximum CCO fire temperature for the ICV structure, given a maximum CCO pre-fire temperature of 126.9 °F and a maximum differential temperature of 97.2 °F, is:

$$126.9 + 97.2 = 224.1\,°\text{F}$$

The adjusted bulk average fire temperature of 190.4 °F for the ICV structure from Table 5-2 is conservatively applied to the CCO 55-gallon drums. The corresponding maximum temperature differential for the CCO 55-gallon drums, given an adjusted bulk average fire temperature of 190.4 °F and a CTU-2 pre-fire temperature of 127 °F, is:

$$190.4 - 127.0 = 63.4\,°\text{F}$$

The 63.4 °F maximum temperature differential for the CCO 55-gallon drums is proportionally reduced for CCO components within the drums based on the ratio of the maximum CCO pre-fire temperature for the CCO 55-gallon drum of 133.1 °F and the maximum CCO pre-fire temperature for the CCO component.

---

[19] Infrared emissivity is taken from W. D. Wood, H. W. Deem, and C. F. Lucks, *Thermal Radiation Properties of Selected Materials*, Volume I, DMIC Report 177, November 1962; normal total emittance for clean-and-smooth, Type 301 stainless steel, p56.

For example, the maximum differential temperature for the CCC structure, given a maximum differential temperature of 63.4 °F for the CCO 55-gallon drum, a maximum CCO pre-fire temperature of 133.1 °F for the CCO 55-gallon drum, and a maximum CCO pre-fire CCC structure temperature of 163.8 °F, is:

$$63.4 \times \frac{133.1}{163.8} = 51.5\,°F$$

The resulting maximum CCC structure temperature, given a maximum CCO pre-fire temperature of 163.8 °F and a maximum differential temperature of 51.5 °F, is:

$$163.8 + 51.5 = 215.3\,°F$$

As stated earlier, the maximum pre-fire CCO temperatures from Table 4-2 are based on the maximum temperature for each component, regardless of the case number, resulting in the bounding maximum fire CCO temperatures reported in Table 5-3.

The adjusted maximum fire temperatures for the remaining packaging components (i.e., the bulk average ICV cavity air, the maximum ICV structure and O-ring seal, and maximum OCV structure and O-ring seal) are equal to the CTU-2 measured fire temperatures increased by the temperature change percentage from Table 5-2 for each packaging component for the "no payload" condition.

For example, the adjusted maximum fire temperature for the OCV structure, given a CTU-2 measured fire temperature of 439.0 °F, and a temperature change of 2.6% from Table 5-2, is:

$$439.0 \times (1 + 0.026) = 450.4\,°F$$

The corresponding maximum temperature differential for the OCV structure, given an adjusted maximum fire temperature of 450.4 °F and a CTU-2 pre-fire temperature of 127.0 °F, is:

$$450.4 - 127.0 = 323.4\,°F$$

The resulting maximum CCO fire temperature for the OCV structure, given a maximum CCO pre-fire temperature of 125.1 °F and a maximum temperature differential of 323.4 °F, is:

$$125.1 + 323.4 = 448.5\,°F$$

5.2 Maximum HAC Fire Temperatures for HalfPACT with a CCO Payload

Table 5-4 summarizes the weights, dominant materials, specific heats, pre-fire temperatures, bulk average fire temperatures, differential temperatures, and the heat absorbed for each HalfPACT packaging and payload component. Table notes provide corresponding references to the data provided in the tables.

With reference to Table 5-4, the total absorbed heat in a HalfPACT package with 1,000-pound concrete-filled payload drums is calculated to be 1,368,362 Btu. As a check, the average "time-integrated" heat flux due to a 30-minute HAC fire event is 31.6 kW-hr/m^2 (≈10,000 Btu/ft^2) based on a thermal experiment performed by Sandia.[18] The time-integrated absorbed heat for the HalfPACT package with a 260 ft^2 external surface area is 10,000 × 260 = 2,600,000 Btu. Therefore, the corresponding ratio of calculated absorbed heat versus the Sandia-derived maximum absorbed heat is 1,368,362/2,600,000 = 0.53. Considering that austenitic stainless steel exhibits an emissivity of approximately 0.45 at 1,475 °F,[19] the calculated absorbed heat is reasonable.

Table 5-5 presents the adjusted heat absorbed by each packaging component when 87,234 Btu of tested payload heat from Table 5-4 is proportionally redistributed to the packaging components. For example, the adjusted heat absorbed by the ICV structure is:

$$15{,}875 \times \frac{437{,}977 + 34{,}576 + 15{,}875 + 2{,}854 + 4{,}995 + 3{,}568 + 87{,}234}{437{,}977 + 34{,}576 + 15{,}875 + 2{,}854 + 4{,}995 + 3{,}568} = 18{,}646\,\text{Btu}$$

The corresponding adjusted bulk average fire temperature, given an ICV weight of 2,050 pounds, a specific heat of 0.121 Btu/lb-°F, and a pre-fire temperature of 43.0 °F (all from Table 5-4), is:

$$43.0 + \frac{18{,}646}{(2{,}050 \times 0.121)} = 118.2\,°F$$

The corresponding temperature change for the ICV structure, given a bulk average fire temperature for the ICV structure of 107.0 °F from Table 5-4 and an adjusted bulk average fire temperature for the ICV structure of 118.2 °F from Table 5-5, is:

$$\frac{118.2 - 107.0}{107.0} \times 100 = 10.5\%$$

Table 5-6 presents the bulk average ICV cavity air temperature and maximum fire temperatures for the CCO components, ICV structure and O-ring seal region, and OCV structure and O-ring seal region based on data from Table 5-4, Table 5-5, and Table 5-6.

Again, using the ICV structure as the example, the adjusted maximum fire temperature, given an adjusted bulk average fire temperature of 118.2 °F and temperature change of 10.5% from Table 5-5, and a measured maximum fire temperature of 110.0 °F from Table 5-6, is:

$$110.0 \times (1 + 0.105) = 121.6\,°F$$

The corresponding maximum differential temperature for the ICV structure, given an adjusted maximum fire temperature of 121.6 °F and a CTU pre-fire temperature of 43.0 °F, is:

$$121.6 - 43.0 = 78.6\,°F$$

The resulting maximum CCO fire temperature for the ICV structure, given a maximum CCO pre-fire temperature of 122.3 °F and a maximum differential temperature of 78.6 °F, is:

$$122.3 + 78.6 = 200.9\,°F$$

The adjusted bulk average fire temperature of 118.2 °F for the ICV structure from Table 5-5 is conservatively applied to the CCO 55-gallon drums. The corresponding maximum temperature differential for the CCO 55-gallon drums, given an adjusted bulk average fire temperature of 118.2 °F and a CTU pre-fire temperature of 43 °F, is:

$$118.2 - 43.0 = 75.2\,°F$$

The 75.2 °F maximum temperature differential for the CCO 55-gallon drums is proportionally reduced for CCO components within the drums based on the ratio of the maximum CCO pre-fire temperature for the CCO 55-gallon drum of 128.1 °F and the maximum CCO pre-fire temperature for the CCO component.

For example, the maximum differential temperature for the CCC structure, given a maximum differential temperature of 75.2 °F for the CCO 55-gallon drum, a maximum CCO pre-fire temperature of 128.1 °F for the CCO 55-gallon drum, and a maximum CCO pre-fire CCC structure temperature of 160.1 °F, is:

$$75.2 \times \frac{128.1}{160.1} = 60.2\,°F$$

The resulting maximum CCC structure temperature, given a maximum CCO pre-fire temperature of 160.1 °F and a maximum differential temperature of 60.2 °F, is:

$$160.1 + 60.2 = 220.3\,°F$$

As stated earlier, the maximum pre-fire CCO temperatures from Table 4-4 are based on the maximum temperature for each component, regardless of the case number, resulting in bounding maximum fire CCO temperatures in Table 5-6.

The adjusted maximum fire temperatures for the remaining packaging components (i.e., the bulk average ICV cavity air, the maximum ICV structure and O-ring seal, and maximum OCV structure and O-ring seal) are equal to the CTU measured fire temperatures increased by the temperature change percentage from Table 5-5 for each packaging component for the "no payload" condition.

For example, the adjusted maximum fire temperature for the OCV structure, given a CTU measured fire temperature of 200.0 °F, and a temperature change of 13.2% from Table 5-5, is:

$$200.0 \times (1 + 0.132) = 226.4\ ^\circ F$$

The corresponding maximum temperature differential for the OCV structure, given an adjusted maximum fire temperature of 226.4 °F and a CTU pre-fire temperature of 43.0 °F, is:

$$226.4 - 43.0 = 183.4\ ^\circ F$$

The resulting maximum CCO fire temperature for the OCV structure, given a maximum CCO pre-fire temperature of 120.7 °F and a maximum temperature differential of 183.4 °F, is:

$$120.7 + 183.4 = 304.1^\circ F$$

5.3 Summary of Maximum HAC Fire Temperatures for TRUPACT-II and HalfPACT with a CCO Payload

Summarized in Table 5-3 and Table 5-6 for the TRUPACT-II and HalfPACT packages, respectively, are the predicted HAC fire temperatures with a CCO payload for the major components in each package, none of which exceed defined temperature limits for the materials of construction. The redistribution of the payload's thermal energy based on a "no payload" configuration results in modest increases in component temperatures compared to TRUPACT-II and HalfPACT package fire test results. Thus, the CCO payload will not impact the safety basis of either the TRUPACT-II or HalfPACT packages for the HAC fire event.

Table 5-1 – Heat Absorbed for the HAC Fire Event for TRUPACT-II CTU-2 with 500-lb Concrete-Filled Payload Drums

TRUPACT-II Component	Material	Component Weight① (lb)	Specific Heat② (Btu/lb-°F)	Pre-Fire Temperature③ (°F)	Bulk Avg Fire Temperature④ (°F)	Differential Temperature (°F)	Heat Absorbed⑤ (Btu)	Fraction of Total Heat Absorbed
Packaging:								
• OCA Structure	Stainless Steel	4,937	0.121	21.0	1,475.0	1,454.0	868,586	58.7%
• OCA Foam⑥	Polyurethane	1,913	0.353	74.0	850.1	776.1	524,092	35.4%
• OCV Structure	Stainless Steel	2,515	0.121	127.0	225.2	98.2	29,884	2.0%
• ICV Structure	Stainless Steel	2,420	0.121	127.0	186.9	59.9	17,540	1.2%
• Honeycomb Spacers	Aluminum	200	0.223	127.0	190.0	63.0	2,810	0.2%
• Payload Pallet	Aluminum	265	0.223	127.0	160.0	33.0	1,950	0.1%
Packaging Totals		*12,250*					*1,444,862*	*97.7%*
Tested Payload:								
• 55-Gallon Drums⑦	Carbon Steel	840	0.112	127.0	152.5	25.5	2,399	0.2%
• Concrete Payload⑧	Concrete	6,160	0.200	127.0	152.5	25.5	31,416	2.1%
Payload Totals		*7,000*					*33,815*	*2.3%*
Totals		*19,250*					*1,478,677*	*100.0%*

Notes for Table 5-1 and Table 5-3:

① Component weights are estimated based on AutoCAD and Mathcad models that are normalized to the weight values presented in Table 2.2-1 of the TRUPACT-II SAR.[1]

② With the exception of concrete and polyurethane foam which are constants independent of temperature, Specific Heat is based on a temperature of 200 °F.

③ With the exception of the OCA Foam temperature, the Pre-Fire Temperatures are taken from Section 3.5.2.2, *CTU-2 Package Conditions and Environment*, of the TRUPACT-II SAR.

④ With the exception of the OCA Structure and OCA Foam temperatures, the Bulk Average Fire Temperatures are simple averages of passive temperature indicating strip data for each component from Table 3.5-4 of the TRUPACT-II SAR; the OCA Structure temperature is taken from Section 3.5.3, *Package Temperatures*, of the TRUPACT-II SAR.

⑤ The Heat Absorbed, $Q_a = mc_p\Delta T$, where m is the mass (i.e., Weight), c_p is the Specific Heat, and ΔT is the change in temperature (i.e., Differential Temperature).

⑥ Both the Pre-Fire Temperature and Bulk Average Fire Temperature for the polyurethane foam are taken as the average of the temperatures for the OCA Shells and OCV Shells.

⑦ The nominal weight of the 55-Gallon Drums is assumed to be 60 pounds each.

⑧ The specific heat of concrete is taken from M. K. Kassir, K. K. Bandyopadhyay and M. Reich, *Thermal Degradation of Concrete in the Temperature Range from Ambient to 315 °C (600 °F)*, BNL 52384, October 1996.

❶ The CTU-2 Measured Fire Temperatures are taken from Table 3.5-5 of the TRUPACT-II SAR.

❷ The Adjusted Maximum Fire Temperature for the 55-Gallon Drums is assumed to be equal to the Adjusted Bulk Average Fire Temperature for the ICV Structure; all other Adjusted Maximum Fire Temperatures are equal to the CTU-2 Measured Fire Temperatures increased by the Temperature Change percentage in Table 5-2 for each packaging component.

❸ The Maximum Pre-Fire CCO Temperatures are taken from Table 4-2 referencing the maximum temperature for each component regardless of the case number.

❹ The minimum ignition temperature of wood is taken as 250 °C (482 °F) from Table 5 of Vytenis Babrauskas, *Ignition of Wood: A Review of the State of the Art*, pp71-88 in Interflam 2001, Interscience Communications Ltd., London (2001).

Table 5-2 – Adjusted Heat Absorbed During the HAC Fire Event for TRUPACT-II CTU-2 with No Payload

TRUPACT-II Component	Adjusted Heat Absorbed (Btu)	Adjusted Bulk Average Fire Temperature (°F)	Temperature Change
Packaging:			
• OCA Structure	868,586	1,475.0	0.0%
• OCA Foam	554,845	895.6	5.4%
• OCV Structure	31,638	231.0	2.6%
• ICV Structure	18,569	190.4	1.9%
• Honeycomb Spacers	2,975	193.7	1.9%
• Payload Pallet	2,064	161.9	1.2%
Packaging Totals	*1,478,677*		

Table 5-3 – Adjusted Maximum HAC Fire Temperatures for TRUPACT-II with a CCO Payload

Component/Location	TRUPACT-II – Adjusted for No Payload				CCO Analysis		Temperature Limit (°F)
	CTU-2 Pre-Fire Temperature (°F)	CTU-2 Measured Fire Temperature° (°F)	Adjusted Maximum Fire Temperature° (°F)	Maximum Differential Temperature (°F)	Maximum CCO Pre-Fire Temperature° (°F)	Maximum CCO Fire Temperature (°F)	
Maximum CCC Structure	—	—	—	51.5	163.8	215.3	2,600
Maximum CCC Gasket	—	—	—	55.6	151.8	207.4	548
Maximum CCO Plywood Dunnage°	—	—	—	57.9	145.7	203.6	482
Maximum CCO 55-Gallon Drum	127.0	—	190.4	63.4	133.1	196.5	2,750
Bulk Average ICV Cavity Air	127.0	179.0	182.4	55.4	123.4	178.8	N/A
Maximum ICV Structure	127.0	220.0	224.2	97.2	126.9	224.1	2,600
Maximum ICV O-ring Seal	127.0	200.0	203.8	76.8	123.2	200.0	360
Maximum OCV Structure	127.0	439.0	450.4	323.4	125.1	448.5	2,600
Maximum OCV O-ring Seal	127.0	253.0	259.6	132.6	118.4	251.0	360

Table 5-4 – Heat Absorbed for the HAC Fire Event for HalfPACT CTU with 1,000-lb Concrete-Filled Payload Drums

HalfPACT Component	Material	Component Weight① (lb)	Specific Heat② (Btu/lb-°F)	Pre-Fire Temperature③ (°F)	Bulk Avg Fire Temperature④ (°F)	Differential Temperature (°F)	Heat Absorbed⑤ (Btu)	Fraction of Total Heat Absorbed
Packaging:								
• OCA Structure	Stainless Steel	4,509	0.121	43.0	1,475.0	1,432.0	781,283	57.1%
• OCA Foam⑥	Polyurethane	1,586	0.353	43.0	825.3	782.3	437,977	32.0%
• OCV Structure	Stainless Steel	2,155	0.121	43.0	175.6	132.6	34,576	2.5%
• ICV Structure	Stainless Steel	2,050	0.121	43.0	107.0	64.0	15,875	1.2%
• Honeycomb Spacers	Aluminum	200	0.223	43.0	107.0	64.0	2,854	0.2%
• Payload Pallet	Aluminum	350	0.223	43.0	107.0	64.0	4,995	0.4%
• Payload Spacer	Aluminum	250	0.223	43.0	107.0	64.0	3,568	0.3%
Packaging Totals		*11,100*					*1,281,128*	*93.6%*
Tested Payload:								
• 55-Gallon Drums⑦	Carbon Steel	420	0.112	43.0	107.0	64.0	3,010	0.2%
• Concrete Payload⑧	Concrete	6,580	0.200	43.0	107.0	64.0	84,224	6.2%
Payload Totals		*7,000*					*87,234*	*6.4%*
Totals		*18,100*					*1,368,362*	*100.0%*

Notes for Table 5-4 and Table 5-6:

① Component weights are estimated based on AutoCAD and Mathcad models that are normalized to the weight values presented in Table 2.2-1 of the HalfPACT SAR.[2]

② With the exception of concrete and polyurethane foam which are constants independent of temperature, Specific Heat is based on a temperature of 200 °F.

③ With the exception of the OCA Foam temperature, the Pre-Fire Temperatures are taken from Section 3.5.2, *Package Conditions and Environment*, of the HalfPACT SAR.

④ With the exception of the OCA Structure and OCA Foam temperatures, the Bulk Average Fire Temperatures are simple averages of passive temperature indicating strip data for each component from Table 3.5-2 of the HalfPACT SAR; the OCA Structure temperature is assumed to be 1,475 °F based on TRUPACT-II OCA Structure temperature results.

⑤ The Heat Absorbed, $Q_a = mc_p\Delta T$, where m is the mass (i.e., Weight), c_p is the Specific Heat, and ΔT is the change in temperature (i.e., Differential Temperature).

⑥ Both the Pre-Fire Temperature and Bulk Average Fire Temperature for the polyurethane foam are taken as the average of the temperatures for the OCA Shells and OCV Shells.

⑦ The nominal weight of the 55-Gallon Drums is assumed to be 60 pounds each.

⑧ The specific heat of concrete is taken from M. K. Kassir, K. K. Bandyopadhyay and M. Reich, *Thermal Degradation of Concrete in the Temperature Range from Ambient to 315 °C (600 °F)*, BNL 52384, October 1996.

❶ The CTU Measured Fire Temperatures are taken from Table 3.5-2 of the HalfPACT SAR.

❷ The Adjusted Maximum Fire Temperature for the 55-Gallon Drums is assumed to be equal to the Adjusted Bulk Average Fire Temperature for the ICV Structure; all other Adjusted Maximum Fire Temperatures are equal to the CTU-2 Measured Fire Temperatures increased by the Temperature Change percentage in Table 5-5 for each packaging component.

❸ The Maximum Pre-Fire CCO Temperatures are taken from Table 4-4 referencing the maximum temperature for each component regardless of the case number.

❹ The minimum ignition temperature of wood is taken as 250 °C (482 °F) from Table 5 of Vytenis Babrauskas, *Ignition of Wood: A Review of the State of the Art*, pp71-88 in Interflam 2001, Interscience Communications Ltd., London (2001).

Table 5-5 – Adjusted Heat Absorbed for the HAC Fire Event for HalfPACT CTU with No Payload

HalfPACT Component	Adjusted Heat Absorbed (Btu)	Adjusted Bulk Average Fire Temperature (°F)	Temperature Change
Packaging:			
• OCA Structure	781,283	1,475.0	0.0%
• OCA Foam	514,414	961.8	16.5%
• OCV Structure	40,610	198.7	13.2%
• ICV Structure	18,646	118.2	10.5%
• Honeycomb Spacers	3,352	118.2	10.5%
• Payload Pallet	5,867	118.2	10.5%
• Payload Spacer	4,191	118.2	10.5%
Packaging Totals	*1,368,363*		

Table 5-6 – Adjusted Maximum HAC Fire Temperatures for HalfPACT with a CCO Payload

Component/Location	HalfPACT – Adjusted for No Payload				CCO Analysis		Temperature Limit (°F)
	CTU Pre-Fire Temperature (°F)	CTU Measured Fire Temperature° (°F)	Adjusted Maximum Fire Temperature° (°F)	Maximum Differential Temperature (°F)	Maximum CCO Pre-Fire Temperature° (°F)	Maximum CCO Fire Temperature (°F)	
Maximum CCC Structure	—	—	—	60.2	160.1	220.3	2,600
Maximum CCC Gasket	—	—	—	65.1	147.9	213.0	548
Maximum CCO Plywood Dunnage°	—	—	—	68.2	141.2	209.4	482
Maximum CCO 55-Gallon Drum	43.0	—	118.2	75.2	128.1	203.3	2,750
Bulk Average ICV Cavity Air	43.0	110.0	121.6	78.6	121.5	200.1	N/A
Maximum ICV Structure	43.0	110.0	121.6	78.6	122.3	200.9	2,600
Maximum ICV O-ring Seal	43.0	110.0	121.6	78.6	119.1	197.7	360
Maximum OCV Structure	43.0	200.0	226.4	183.4	120.7	304.1	2,600
Maximum OCV O-ring Seal	43.0	200.0	226.4	183.4	115.6	299.0	360

6.0 APPENDIX

6.1 Aluminum Honeycomb End Spacer Conductivity Calculation

The thermal conductivity of aluminum honeycomb reported by Hexcel in TSB-120[20] provides little or no supporting information for how those values were obtained, or for what honeycomb orientation they are valid. The *Spacecraft Thermal Control Handbook*[21] provides a computationally derived method for determining the effective thermal conductivity of honeycomb structures based on cell size, material thickness, and orientation. Thermal conductivity calculated by this method is lower than the value reported by Hexcel, and is therefore conservatively used in the thermal model. The following figure, derived from the *Spacecraft Thermal Control Handbook*, serves to illustrate the dimensional parameters considered.

The effective conductivity for the x, y and z directions (W, L and T directions, respectively, on the above drawing) are calculated as follows:

$$k_x = \frac{3}{2}\left(\frac{k_{Al}\delta}{S}\right), \quad k_y = \frac{k_{Al}\delta}{S}, \quad k_z = \left(\frac{8}{3}\right)\frac{k_{Al}\delta}{S}$$

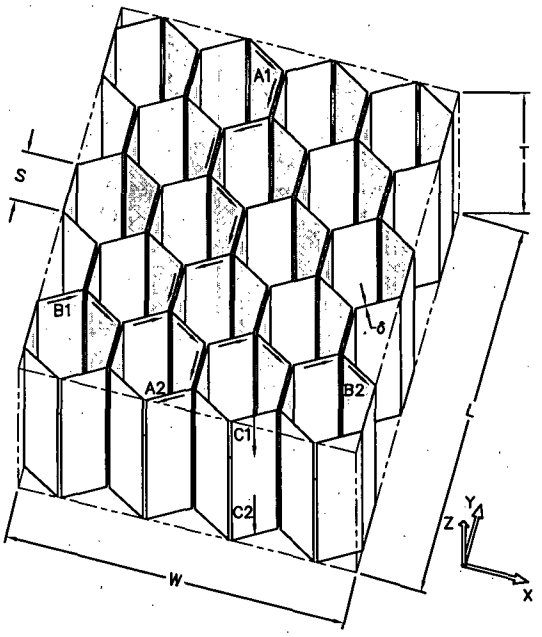

Note that for the thermal calculations k_y and k_z represent radial and axial conductivity, respectively. The end spacers used in the ICV torispherical heads have a foil thickness, δ = 0.003 inches, and a nominal cell dimension, S = 0.375 inches. Therefore:

$$k_x = (0.0120)k_{Al}$$

$$k_y = (0.0080)k_{Al}$$

$$k_z = (0.0213)k_{Al}$$

Thus, the effective thermal conductivity is 0.80% of the thermal conductivity of Alloy 5052 aluminum in the radial direction (k_x is ignored since it results in a higher value), and 2.13% of the thermal conductivity of Alloy 5052 aluminum in the axial direction.

6.2 Polyethylene Plastic Wrap Transmittance Calculation

As many as 18 layers of optional, 0.002-inch thick, polyethylene plastic stretch wrap may be used to restrain the payload drums during transport. Data on the transmittance of polyethylene is available from Figure 659 of *Thermophysical Properties of Matter*[22]. Assuming a plastic wrap stretch temperature of 200 °F to 250 °F, Curves 1 through 4 from Figure 659 are applicable. Wien's displacement law states:

$$\lambda_{max} T = 5215.6\ \mu m - {}^{\circ}R$$

---

[20] HexWeb Honeycomb Attributes and Properties, TSB 120, Hexcel Corporation.

[21] David G. Gilmore, Editor, Spacecraft Thermal Control Handbook – Volume I: Fundamental Technologies, 2nd Edition, American Institute of Aeronautics and Astronautics, Inc.; Appendix B: Material Thermal Properties – Honeycomb Panel Thermal Properties.

[22] Y. S. Touloukian and C. Y. Ho, Editors, *Thermophysical Properties of Matter*, Thermophysical Properties Research Center (TPRC) Data Series, Purdue University, 1970, IFI/Plenum, New York.

Thus, at 250 °F the wavelength of maximum intensity is:

$$\lambda_{max} = \frac{5215.6}{(250 + 460)} = 7.436 \ \mu m$$

The number of wraps is of secondary importance to the overall transmittance since the first few layers perform essentially all of the filtering. The maximum monochromatic radiation is near 10 μm, and since the low end of the transmittance curves is near $\tau = 0.75$, an overall transmittance of 0.75 is applicable.

CHAPTER 7

Thermal Decomposition of Polymers

Craig L. Beyler and Marcelo M. Hirschler

Introduction

Solid polymeric materials undergo both physical and chemical changes when heat is applied; this will usually result in undesirable changes to the properties of the material. A clear distinction needs to be made between thermal decomposition and thermal degradation. The American Society for Testing and Materials' (ASTM) definitions should provide helpful guidelines. Thermal decomposition is "a process of extensive chemical species change caused by heat."[1] Thermal degradation is "a process whereby the action of heat or elevated temperature on a material, product, or assembly causes a loss of physical, mechanical, or electrical properties."[1] In terms of fire, the important change is thermal decomposition, whereby the chemical decomposition of a solid material generates gaseous fuel vapors, which can burn above the solid material. In order for the process to be self-sustaining, it is necessary for the burning gases to feed back sufficient heat to the material to continue the production of gaseous fuel vapors or volatiles. As such, the process can be a continuous feedback loop if the material continues burning. In that case, heat transferred to the polymer causes the generation of flammable volatiles; these volatiles react with the oxygen in the air above the polymer to generate heat, and a part of this heat is transferred back to the polymer to continue the process. (See Figure 1-7.1.) This chapter is concerned with chemical and physical aspects of thermal decomposition of polymers. The chemical processes are responsible for the generation of flammable volatiles while physical changes, such as melting and charring, can markedly alter the decomposition and burning characteristics of a material.

The gasification of polymers is generally much more complicated than that of flammable liquids. For most flammable liquids, the gasification process is simply evaporation. The liquid evaporates at a rate required to maintain the equilibrium vapor pressure above the liquid. In the case of polymeric materials, the original material itself is essentially involatile, and the quite large molecules must be broken down into smaller molecules that can vaporize. In most cases, a solid polymer breaks down into a variety of smaller molecular fragments made up of a number of different chemical species. Hence, each of the fragments has a different equilibrium vapor pressure. The lighter of the molecular fragments will vaporize immediately upon their creation while other heavier molecules will remain in the condensed phase (solid or liquid) for some time. While remaining in the condensed phase, these heavier molecules may undergo further decomposition to lighter fragments which are more easily vaporized. Some polymers break down completely so that virtually no solid residue remains. More often, however, not all the original fuel becomes fuel vapors since solid residues are left behind. These residues can be carbonaceous (char), inorganic (originating from heteroatoms contained in the original polymer, either within the structure or as a result of additive incorporations), or a combination of both. Charring materials, such as wood, leave large fractions of the original carbon content as carbonaceous residue, often as a porous char. When thermal decomposition of deeper layers of such a material continues, the volatiles produced must pass through the char above them to reach the surface. During this travel, the hot char may cause secondary reactions to occur in the volatiles. Carbonaceous chars can be intumescent layers, when appropriately formed, which slow down further thermal decomposition considerably. Inorganic residues, on the other hand, can form glassy lay-

Dr. Craig L. Beyler is the technical director of Hughes Associates, Fire Science and Engineering. He was the founding editor of the *Journal of Fire Protection Engineering* and serves on a wide range of committees in the fire research community.

Dr. Marcelo M. Hirschler is an independent consultant on fire safety with GBH International. He has over two decades of experience researching fire and polymers and has managed a plastics industry fire testing and research laboratory for seven years. He now serves on a variety of committees addressing the development of fire standards and codes, has published extensively, and is an associate editor of the journal *Fire and Materials*.

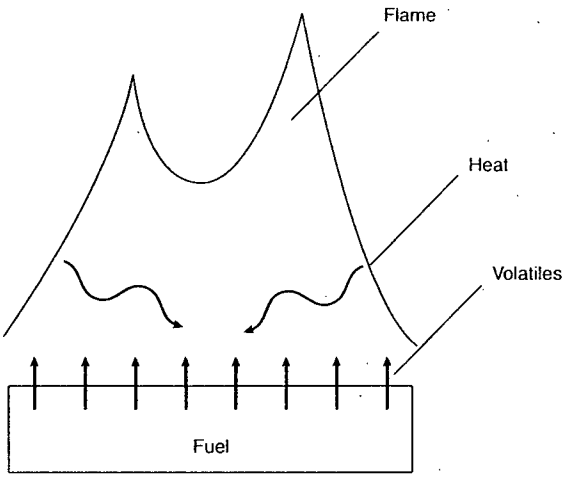

Figure 1-7.1. ***Energy feedback loop required for sustained burning.***

ers that may then become impenetrable to volatiles and protect the underlying layers from any further thermal breakdown. Unless such inorganic barriers form, purely carbonaceous chars can always be burned by surface oxidation at higher temperatures.

As this brief description of the thermal decomposition process indicates, the chemical processes are varied and complex. The rate, mechanism, and product composition of these thermal decomposition processes depend both on the physical properties of the original material and on its chemical composition.

Polymeric Materials

Polymeric materials can be classified in a variety of ways.[2] First, polymers are often classified, based on their origin, into natural and synthetic (and sometimes including a third category of seminatural or synthetic modifications of natural polymers). However, more useful is a classification based on physical properties, in particular the elastic modulus and the degree of elongation. Following this criterion, polymers can be classified into elastomers, plastics, and fibers. Elastomers (or rubbers) are characterized by a long-range extensibility that is almost completely reversible at room temperature. Plastics have only partially reversible deformability, while fibers have very high tensile strength but low extensibility. Plastics can be further subdivided into thermoplastics (whose deformation at elevated temperatures is reversible) and thermosets (which undergo irreversible changes when heated). Elastomers have elastic moduli between 10^5 and 10^6 N/m^2, while plastics have moduli between 10^7 and 10^8 N/m^2, and fibers have moduli between 10^9 and 10^{10} N/m^2. In terms of the elongation, elastomers can be stretched roughly up to 500 to 1000 percent, plastics between 100 to 200 percent, and fibers only 10 to 30 percent before fracture of the material is complete.

Polymers can also be classified in terms of their chemical composition; this gives a very important indication as to their reactivity, including their mechanism of thermal decomposition and their fire performance.

The main carbonaceous polymers with no heteroatoms are polyolefins, polydienes, and aromatic hydrocarbon polymers (typically styrenics). The main polyolefins are thermoplastics: polyethylene [repeating unit: $-(CH_2-CH_2)-$] and polypropylene [repeating unit: $-[CH(CH_3)-CH_2]-$], which are two of the three most widely used synthetic polymers. Polydienes are generally elastomeric and contain one double bond per repeating unit. Other than polyisoprene (which can be synthetic or natural, e.g., natural rubber) and polybutadiene (used mostly as substitutes for rubber), most other polydienes are used as copolymers or blends with other materials [e.g., in ABS (acrylonitrile butadiene styrene terpolymers), SBR (styrene butadiene rubbers), MBS (methyl methacrylate butadiene styrene terpolymers), and EPDM (ethylene propylene diene rubbers)]. They are primarily used for their high abrasion resistance and high impact strength. The most important aromatic hydrocarbon polymers are based on polystyrene [repeating unit: $-[CH(phenyl)-CH_2]-$]. It is extensively used as a foam and as a plastic for injection-molded articles. A number of styrenic copolymers also have tremendous usage, e.g., principally, ABS, styrene acrylonitrile polymers (SAN), and MBS.

The most important oxygen-containing polymers are cellulosics, polyacrylics, and polyesters. Polyacrylics are the only major oxygen-containing polymers with carbon–carbon chains. The most important oxygen-containing natural materials are cellulosics, mostly wood and paper products. Different grades of wood contain 20 to 50 percent cellulose. The most widely used polyacrylic is poly(methyl methacrylate) (PMMA) [repeating unit: $-[CH_2-C(CH_3)-CO-OCH_3]-$]. PMMA is valued for its high light transmittance, dyeability, and transparency. The most important polyesters are manufactured from glycols, for example, polyethylene terephthalate (PET) or polybutylene terephthalate (PBT), or from biphenol A (polycarbonate). They are used as engineering thermoplastics, as fibers, for injection-molded articles, and unbreakable replacements for glass. Other oxygenated polymers include phenolic resins (produced by the condensation of phenols and aldehydes, which are often used as polymeric additives), polyethers [such as polyphenylene oxide (PPO), a very thermally stable engineering polymer], and polyacetals (such as polyformaldehyde, used for its intense hardness and resistance to solvents).

Nitrogen-containing materials include nylons, polyurethanes, polyamides, and polyacrylonitrile. Nylons, having repeating units containing the characteristic group $-CO-NH-$, are made into fibers and also into a number of injection-molded articles. Nylons are synthetic aliphatic polyamides. There are also natural polyamides (e.g., wool, silk, and leather) and synthetic aromatic polyamides (of exceptionally high thermal stability and used for protective clothing). Polyurethanes (PU), with repeating units containing the characteristic group $-NH-COO-$, are normally manufactured from the condensation of polyisocyanates and polyols. Their principal area of application is as foams (flexible and rigid), or as thermal insulation.

Other polyurethanes are made into thermoplastic elastomers, which are chemically very inert. Both these types of polymers have carbon–nitrogen chains, but nitrogen can also be contained in materials with carbon–carbon chains, the main example being polyacrylonitrile [repeating unit: $-(CH_2-CH-CN-)$]. It is used mostly to make into fibers and as a constituent of engineering copolymers (e.g., SAN, ABS).

Chlorine-containing polymers are exemplified by poly(vinyl chloride) [PVC, repeating unit: $-(CH_2-CHCl)-$]. It is the most widely used synthetic polymer, together with polyethylene and polypropylene. It is unique in that it is used both as a rigid material (unplasticized) and as a flexible material (plasticized). Flexibility is achieved by adding plasticizers or flexibilizers. Through the additional chlorination of PVC, another member of the family of vinyl materials is made: chlorinated poly(vinyl chloride) (CPVC) with very different physical and fire properties from PVC. Two other chlorinated materials are of commercial interest: (1) polychloroprene (a polydiene, used for oil-resistant wire and cable materials and resilient foams) and (2) poly(vinylidene chloride) [PVDC, with a repeating unit: $-(CH_2-CCl_2)-$ used for making films and fibers]. All these polymers have carbon–carbon chains.

Fluorine-containing polymers are characterized by high thermal and chemical inertness and low coefficient of friction. The most important material in the family is polytetrafluoroethylene (PTFE); others are poly(vinylidene fluoride) (PVDF), poly(vinyl fluoride) (PVF), and fluorinated ethylene polymers (FEP).

Physical Processes

The various physical processes that occur during thermal decomposition can depend on the nature of the material. For example, as thermosetting polymeric materials are infusible and insoluble once they have been formed, simple phase changes upon heating are not possible. Thermoplastics, on the other hand, can be softened by heating without irreversible changes to the material, provided heating does not exceed the minimum thermal decomposition temperature. This provides a major advantage for thermoplastic materials in the ease of molding or thermo forming of products.

The physical behavior of thermoplastics in heating is dependent on the degree of order in molecular packing, i.e., the degree of crystallinity. For crystalline materials, there exists a well-defined melting temperature. Materials that do not possess this ordered internal packing are amorphous. An example of an amorphous material is window glass. While it appears to be a solid, it is in fact a fluid that over long periods of time (centuries) will flow noticeably. Despite this, at low temperatures amorphous materials do have structural properties of normal solids. At a temperature known as the glass transition temperature in polymers, the material starts a transition toward a soft and rubbery state. For example, when using a rubber band, one would hope to use the material above its glass transition temperature. However, for materials requiring

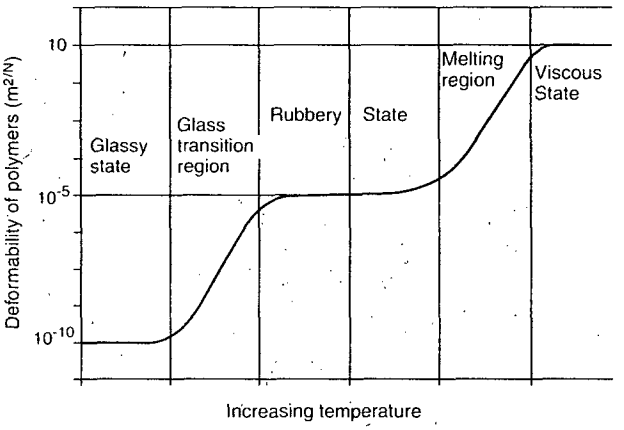

Figure 1-7.2. ***Idealized view of effect on deformability of thermoplastics with increasing temperature.***

rigidity and compressive strength, the glass transition temperature is an upper limit for practical use. In theoretical terms, this "deformability" of a polymer can be expressed as the ratio of the deformation (strain) resulting from a constant stress applied. Figure 1-7.2 shows an idealized view of the effect on the deformability of thermoplastics of increasing the temperature: a two-step increase. In practice, it can be stated that the glass transition temperature is the upper limit for use of a plastic material (as defined above, based on its elastic modulus and elongation) and the lower limit for use of an elastomeric material. Furthermore, many materials may not achieve a viscous state since they begin undergoing thermal decomposition before the polymer melts. Some typical glass transition temperatures are given in Table 1-7.1. As this type of physical transformation is less well defined than a phase transformation, it is known as a second order transition. Typically, materials are only partially crystalline, and, hence, the melting temperature is less well defined, usually extending over a range of 10°C or more.

Neither thermosetting nor cellulosic materials have a fluid state. Due to their structure, it is not possible for the original material to change state at temperatures below that at which thermal decomposition occurs. Hence, there are no notable physical transformations in the material before decomposition. In cellulosic materials, there is an important semi-physical change that always occurs on heating: desorption of the adsorbed water. As the water is both physically and chemically adsorbed, the temperature and rate of desorption will vary with the material. The activation energy for physical desorption of water is 30 to 40 kJ/mol, and it starts occurring at temperatures somewhat lower than the boiling point of water (100°C).

Many materials (whether cellulosic, thermosetting, or thermoplastic) produce carbonaceous chars on thermal decomposition. The physical structure of these chars will strongly affect the continued thermal decomposition

Table 1-7.1 ***Glass Transition and Crystalline Melting Temperatures***

Polymer	% Crystalline	Glass Transition Temperature (°C)	Crystalline Melting Temperature (°C)
Acetal	high	91–110	175–181
Acrylonitrile-butadiene-styrene	low		110–125
Cellulose	high		decomposes
Ethylene-vinyl acetate	high		65–110
Fluorinated ethylene propylene	high		275
High-density polyethylene	95	–125	130–135
Low-density polyethylene	60	–25	109–125
Natural rubber	low		30
Nylon 11	high		185–195
Nylon 6		75	215–220
Nylon 6-10		50	215
Nylon 6-6		57	250–260
Polyacrylonitrile	low	140	317
Poly(butene 1)		124–142	124–142
Polybutylene		126	126
Poly(butylene terephthalate)	high	40	232–267
Polycarbonate	low	145–150	215–230
Polychlorotrifluoroethylene	high	45	220
Poly(ether ether ketone)	high	143	334
Poly(ether imide)		217	
Poly(ethylene terephthalate)	high	70	265
Poly(hexene 1)			55
Poly(methylbutene 1)			300
Polymethylene	100		136
Poly(methyl methacrylate)	low	50	90–105
Polyoxymethylene	75–80	–85	175–180
Poly(pentene 1)			130
Poly(3-phenylbutene 1)			360
Poly(phenylene oxide)/polystyrene	low	100–135	110–135
Poly(phenylene sulphide)	high	88–93	277–282
Polypropylene	65	–20	170
Polystyrene	low	>80	230
Polysulphone	low	190	190
Polytetrafluoroethylene	100	125	327
Poly(vinyl chloride)	5–15	80–85	75–105 (212)
Poly(vinylidene chloride)	high	–18	210
Poly(vinylidene fluoride)	high	–30– –20	160–170
Poly(p-xylene)			>400
Styrene-acrylonitrile	low	100–120	120

process. Very often the physical characteristics of the char will dictate the rate of thermal decomposition of the remainder of the polymer. Among the most important characteristics of char are density, continuity, coherence, adherence, oxidation-resistance, thermal insulation properties, and permeability.[3] Low-density–high-porosity chars tend to be good thermal insulators; they can significantly inhibit the flow of heat from the gaseous combustion zone back to the condensed phase behind it, and thus slow down the thermal decomposition process. This is one of the better means of decreasing the flammability of a polymer (through additive or reactive flame retardants).[1,3,4] As the char layer thickens, the heat flux to the virgin material decreases, and the decomposition rate is reduced. The char itself can undergo glowing combustion when it is exposed to air. However, it is unlikely that both glowing combustion of the char and significant gas-phase combustion can occur simultaneously in the same zone above the surface, since the flow of volatiles through the char will tend to exclude air from direct contact with the char. Therefore, in general, solid-phase char combustion tends to occur after volatilization has largely ended.

Chemical Processes

The thermal decomposition of polymers may proceed by oxidative processes or simply by the action of heat. In many polymers, the thermal decomposition processes are accelerated by oxidants (such as air or oxygen). In that case, the minimum decomposition temperatures are lower in the presence of an oxidant. This significantly complicates the problem of predicting thermal decomposition rates, as the prediction of the concentration of oxygen at the polymer surface during thermal decomposition or combustion is quite difficult. Despite its importance to fire, there have been many fewer studies of thermal decomposition processes in oxygen or air than in inert atmospheres.

It is worthwhile highlighting, however, that some very detailed measurements of oxygen concentrations and of the effects of oxidants have been made by Stuetz et al. in the 1970s[5] and more recently by Kashiwagi et al.,[6–10] Brauman,[11] and Gijsman et al.[12] Stuetz found that oxygen can penetrate down to at least 10 mm below the surface of polypropylene. Moreover, for both polyethylene and polypropylene, this access to oxygen is very important in determining thermal decomposition rates and mechanisms. Another study of oxygen concentration inside polymers during thermal decomposition, by Brauman,[11] suggests that the thermal decomposition of polypropylene is affected by the presence of oxygen (a fact confirmed more recently by Gijsman et al.[12]) while poly(methyl methacrylate) thermal decomposition is not. Kashiwagi found that a number of properties affect the thermal and oxidative decomposition of thermoplastics, particularly molecular weight, prior thermal damage, weak linkages, and primary radicals. Of particular interest is the fact that the effect of oxygen (or air) on thermal decomposition depends on the mechanism of polymerization: free-radical polymerization leads to a neutralization of the effect of oxygen. A study on poly(vinylidene fluoride) indicated that the effect of oxygen can lead to changes in both reaction rate and kinetic order of reaction.[13]

Kashiwagi's work in particular has resulted in the development of models for the kinetics of general random-chain scission thermal decomposition,[14] as well as for the thermal decomposition of cellulosics[15] and thermoplastics.[16]

There are a number of general classes of chemical mechanisms important in the thermal decomposition of polymers: (1) random-chain scission, in which chain scissions occur at apparently random locations in the polymer chain; (2) end-chain scission, in which individual monomer units are successively removed at the chain end; (3) chain-stripping, in which atoms or groups not part of the polymer chain (or backbone) are cleaved; and (4) cross-linking, in which bonds are created between polymer chains. These are discussed in some detail under General Chemical Mechanisms, later in this chapter. It is sufficient here to note that thermal decomposition of a polymer generally involves more than one of these classes of reactions. Nonetheless, these general classes provide a conceptual framework useful for understanding and classifying polymer decomposition behavior.

Interaction of Chemical and Physical Processes

The nature of the volatile products of thermal decomposition is dictated by the chemical and physical properties of both the polymer and the products of decomposition. The size of the molecular fragments must be small enough to be volatile at the decomposition temperature. This effectively sets an upper limit on the molecular weight of the volatiles. If larger chain fragments are created, they will remain in the condensed phase and will be further decomposed to smaller fragments, which can vaporize.

Figure 1-7.3 shows examples of the range of chemical or physical changes that can occur when a solid polymer

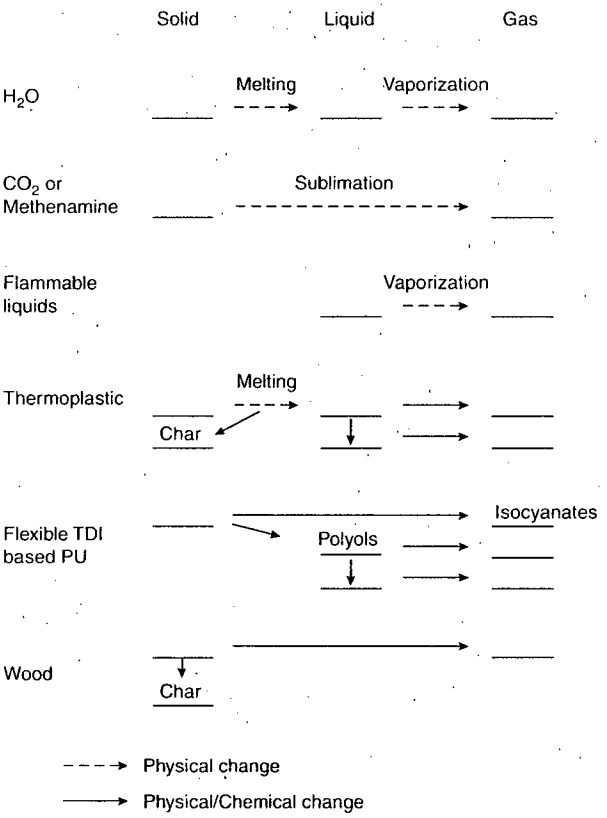

Figure 1-7.3. ***Physical and chemical changes during thermal decomposition.***

is volatilized. The changes range from simple phase transformations (solid going to liquid and then to gas, at the top of the figure), to complex combinations of chemical and physical changes (in the lower part of the figure). Water and many other liquids forming crystalline solids on freezing (e.g., most flammable liquids) undergo straightforward physical phase changes. Sublimation, i.e., the direct phase change from a solid to a gas, without going through the liquid phase, will happen with materials such as carbon dioxide (e.g., CO_2, dry gas) or methenamine at normal temperatures and pressures. Methenamine is of interest in fires because methenamine pills are the ignition source in a standard test for carpets, ASTM D2859,[17] used in mandatory national regulations.[18,19] Thermoplastics can melt without chemical reaction to form a viscous state (polymer melt), but they often decompose thermally before melting. This polymer melt can then decompose into smaller liquid or gaseous fragments. The liquid fragments will then decompose further until they, too, are sufficiently volatile to vaporize. Some polymers, especially thermosets or cellulosics, have even more complex decomposition mechanisms. Polyurethanes (particularly flexible foams) can decompose by three different mechanisms. One of them involves the formation of gaseous isocyanates, which can then repolymerize in the gas phase and condense as a "yellow smoke." These iso-

cyanates are usually accompanied by liquid polyols, which can then continue to decompose. Cellulosics, such as wood, decompose into three types of products: (1) laevoglucosan, which quickly breaks down to yield small volatile compounds; (2) a new solid, char; and (3) a series of high molecular weight semi-liquid materials generally known as tars. Figure 1-7.3 illustrates the complex and varied physicochemical decomposition pathways available, depending on the properties of the material in question. These varied thermal degradation/decomposition mechanisms have clear effects on fire behavior.

Experimental Methods

By far, the most commonly used thermal decomposition test is thermogravimetric analysis (TGA). In TGA experiments, the sample (mg size) is brought quickly up to the desired temperature (isothermal procedure) and the weight of the sample is monitored during the course of thermal decomposition. Because it is impossible in practice to bring the sample up to the desired temperature before significant thermal decomposition occurs, it is common to subject the sample to a linearly increasing temperature at a predetermined rate of temperature rise. One might hope to obtain the same results from one nonisothermal test that were possible only in a series of isothermal tests. In practice, this is not possible since the thermogram (plot of weight vs. temperature) obtained in a nonisothermal test is dependent on the heating rate chosen. Traditional equipment rarely exceed heating rates of 0.5 K/s, but modifications can be made to obtain rates of up to 10 K/s.[20,21] This dependence of thermal decomposition on heating rate is due to the fact that the rate of thermal decomposition is not only a function of the temperature, but also of the amount and nature of the decomposition process that has preceded it.

There are several reasons why the relevance of thermogravimetric studies to fire performance can be questioned: heating rate, amount of material, and lack of heat feedback are the major ones. For example, it is well known that heating rates of 10 to 100 K/s are common under fire conditions but are rare in thermal analysis. However, low heating rates *can* occur in real fires. More seriously, thermogravimetric studies are incapable of simulating the thermal effects due to large amounts of material burning and resupplying energy to the decomposing materials at different rates. However, analytical thermogravimetric studies do give important information about the decomposition process even though extreme caution must be exercised in their direct application to fire behavior.

Differential thermogravimetry (DTG) is exactly the same as TGA, except the mass loss versus time output is differentiated automatically to give the mass loss rate versus time. Often, both the mass loss and the mass loss rate versus time are produced automatically. This is, of course, quite convenient as the rate of thermal decomposition is proportional to the volatilization or mass loss rate. One of the main roles where DTG is useful is in mechanistic studies. For example, it is the best indicator of the temperatures at which the various stages of thermal decomposition take

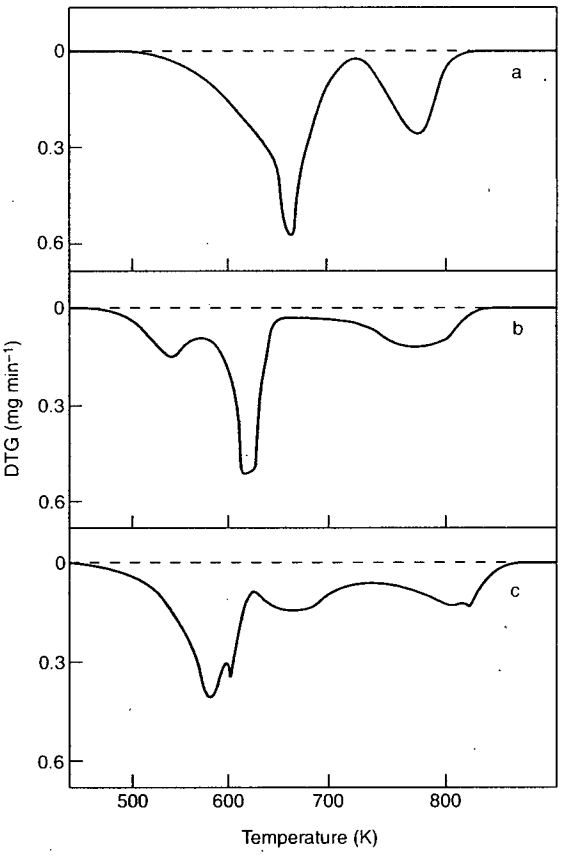

Figure 1-7.4. ***Effect of hydrated alumina and of antimony oxide-decabromobiphenyl (DBB) on DTG of ABS copolymer: (a) ABS; (b) ABS (60%) $A\ell_2O_3$, 3 H_2O (40%); (c) ABS (70%) + DBB (22.5%) + Sb_2O_3 (7.5%).***

place and the order in which they occur as illustrated in Figure 1-7.4. Part (a) of this figure shows the DTG of a thermoplastic polymer, acrylonitrile-butadiene-styrene (ABS), and part (b) shows the same polymer containing 40 percent alumina trihydrate.[22] The polymer decomposes in two main stages. The addition of alumina trihydrate has a dual effect: (1) it makes the material less thermally stable, and (2) it introduces a third thermal decomposition stage. Moreover, the first stage is now the elimination of alumina trihydrate. A more complex example is shown in Figure 1-7.5, where the effects of a variety of additives are shown;[23] some of these additives are effective flame retardants and others are not: the amount of overlap between the thermal decomposition stages of polymer and additives is an indication of the effectiveness of the additive.

Another method for determining the rate of mass loss is thermal volatilization analysis (TVA).[24] In this method, a sample is heated in a vacuum system (0.001 Pa) equipped with a liquid nitrogen trap (77 K) between the sample and the vacuum pump. Any volatiles produced will increase the pressure in the system until they reach the liquid nitrogen and condense out. The pressure is proportional to the mass volatilization rate, and a pressure transducer, rather

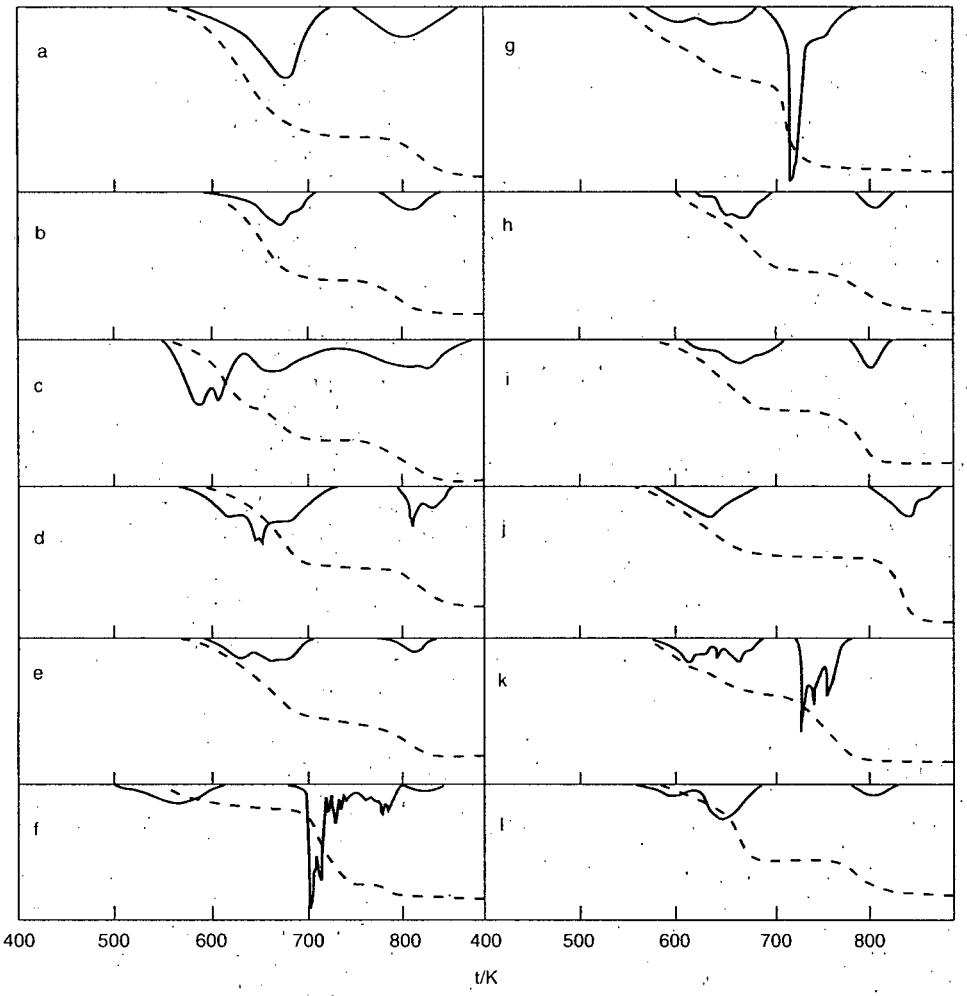

Figure 1-7.5. ***Thermal analyses of systems containing ABS, decabromobiphenyl (DBB), and one metal oxide, where DTG curves are indicated by a continuous line and TGA curves by a dashed line: (a) ABS; (b) ABS + DBB; (c) ABS + DBB + Sb_2O_3; (d) ABS + DBB + SnO; (e) ABS + DBB + $Sno_2 \cdot H_2O$; (f) ABS + DBB + ZnO; (g) ABS + DBB + Fe_2O_3; (h) ABS + DBB + AlOOH; (i) ABS + DBB + Al_2O_3; (j) ABS + DBB + $Al_2O_3 \cdot 3H_2O$; (k) ABS + DBB + ammonium molybdate; (l) ABS + DBB + talc. DTG (—); TGA (----).***

than a sample microbalance, is used to measure the decomposition rate.

In addition to the rate of decomposition, it is also of interest to determine the heat of reaction of the decomposition process. In almost all cases, heat must be supplied to the sample to get it to a temperature where significant thermal decomposition will occur. However, once at such a temperature, the thermal decomposition process may either generate or utilize additional heat. The magnitude of this energy generation (exothermicity) or energy requirement (endothermicity) can be determined in the following ways.

In differential thermal analysis (DTA), a sample and a reference inert material with approximately the same heat capacity are both subjected to the same linear temperature program. The sample and reference material temperatures are measured and compared. If the thermal decomposition of the sample is endothermic, the temperature of the sample will lag behind the reference material; if the decomposition is exothermic, the temperature of the sample will exceed the reference material temperature. Very often, the sample is held in a crucible, and an empty crucible is used as a reference. Such a test can be quite difficult to calibrate to get quantitative heats of reaction.

In view of the considerable importance of the exact process of thermal decomposition, it is advantageous to carry out simultaneously the measurements of TGA, DTG, and DTA. This can be achieved by using a simultaneous thermal analyzer (STA), which uses a dual sample/reference material system. In the majority of cases, polymeric materials are best represented by a reference material which is simply air, i.e., an empty crucible. STA instru-

ments can then determine, at the same time, the amounts of polymer decomposed, the rates at which these stages/processes occur, and the amount of heat evolved or absorbed in each stage. Examples of the application of this technique are contained in References 20 and 21. Recently, STA equipment is often being connected to Fourier transform infrared spectrometers (FTIR) for a complete chemical identification and analysis of the gases evolved at each stage, making the technique even more powerful.

Another method, which yields quantitative results more easily than DTA, is differential scanning calorimetry (DSC). In this test procedure, both the sample and a reference material are kept at the same temperature during the linear temperature program, and the heat of reaction is measured as the difference in heat input required by the sample and the reference material. The system is calibrated using standard materials, such as melting salts, with well-defined melting temperatures and heats of fusion. In view of the fact that DSC experiments are normally carried out by placing the sample inside sealed sample holders, this technique is seldom suitable for thermal decomposition processes. Thus, it is ideally suited for physical changes, but not for chemical processes. Interestingly, some of the commercial STA apparatuses are, in fact, based on DSC rather than DTA techniques for obtaining the heat input.

So far the experimental methods discussed have been concerned with the kinetics and thermodynamics of the thermal decomposition process. There is also concern with the nature of the decomposition process from the viewpoints of combustibility and toxicity. Chemical analysis of the volatiles exiting from any of the above instruments is possible. However, it is often convenient to design a special decomposition apparatus to attach directly to an existing analytical instrument. This is particularly important when the heating rate to be studied is much higher than that which traditional instruments can achieve. Thermal breakdown of cellulosic materials, for example, has been investigated at heating rates as high as 10 K/s[25,26] or even up to over 1000 K/s[27–29] in specialized equipment. The major reason this was done was in order to simulate the processes involved in "smoking," but the results are readily applicable to fire safety.

Given the vast numbers of different products that can result from the decomposition in a single experiment, separation of the products is often required. Hence, the pyrolysis is often carried out in the injector of a gas chromatograph (PGC). In its simplest but rarely used form, a gas chromatograph consists of a long tube with a well-controlled flow of a carrier gas through it. The tube or column is packed with a solid/liquid that will absorb and desorb constituents in the sample. A small sample of the decomposition products is injected into the carrier gas flow. If a particular decomposition product spends a lot of time adsorbed on the column packing, it will take a long time for it to reach the end of the column. Products with different adsorption properties relative to the column packing will reach the end of the column at different times. A detector placed at the exit of the gas chromatograph will respond to the flow rate of gases other than the carrier gas, and if separation is successful, the detector output will be a series of peaks. For a single peak, the time from injection is characteristic of the chemical species, and the area under the peak is proportional to the amount of the chemical species. Column packing, column temperature programming, carrier gas flow rate, sample size, and detector type must all be chosen and adjusted to achieve optimal discrimination of the decomposition products.

Once the gases have been separated, any number of analytical techniques can be used for identification. Perhaps the most powerful has been mass spectrometry (MS). Again speaking in very simple terms, in MS the chemical species is ionized, and the atomic mass of the ion can be determined by the deflection of the ion in a magnetic field. Generally, the ionization process will also result in the fragmentation of the molecule, so the "fingerprint" of the range of fragments and their masses must be interpreted to determine the identity of the original molecule. Gas chromatography and mass spectrometry are the subject of a vast literature, and many textbooks and specialized journals exist.

Useful physical data can be obtained by thermomechanical analysis (TMA). This is really a general name for the determination of a physical/mechanical property of a material subjected to high temperatures. Compressive and tensile strength, softening, shrinking, thermal expansion, glass transition, and melting can be studied by using TMA.

As displayed in Table 1-7.2, many of these tests can be performed *in vacuo*, in inert atmospheres, and in oxidizing atmospheres. Each has its place in the determination of the decomposition mechanism. Experiments performed *in vacuo* are of little practical value, but under vacuum the products of decomposition are efficiently carried away from the sample and its hot environment. Thus, secondary reactions are minimized so that the original decomposition product may reach a trap or analytical instrument intact. The practical significance of studies of thermal decomposition carried out in inert atmospheres may be

Table 1-7.2 ***Analytical Methods***

Method	Isothermal	Nonisothermal	In Vacuo	Inert	Air
Thermogravimetric analysis (TGA)	X	X	X	X	X
Differential thermogravimetry (DTG)	X	X	X	X	X
Thermal volatilization analysis (TVA)	X	X	X		
Differential thermal analysis (DTA)		X		X	X
Differential scanning calorimetry (DSC)		X		X	X
Pyrolysis gas chromatography (PGC)	X			X	
Thermomechanical aAnalysis (TMA)	X	X		X	X

argued. However, when a material burns, the flow of combustible volatiles from the surface and the flame above the surface effectively exclude oxygen at the material's surface. Under these conditions, oxidative processes may be unimportant. In other situations, such as ignition where no flame yet exists, oxidative processes may be critical. Whether or not oxygen plays a role in decomposition can be determined by the effect of using air rather than nitrogen in thermal decomposition experiments.

The decomposition reactions in the tests of Table 1-7.2 are generally monitored by the mass loss of the sample. With the exception of charring materials (e.g., wood or thermosets), analysis of the partially decomposed solid sample is rarely carried out. When it is done, it usually involves the search for heteroatom components due to additives. Analysis of the composition of the volatiles can be carried out by a wide range of analytical procedures. Perhaps the simplest characterization of the products is the determination of the fraction of the volatiles that will condense at various trap temperatures. Typically, convenient temperatures are room temperature (298 K), dry-ice temperature (193 K), and liquid nitrogen temperature (77 K). The products are classified as to the fraction of the sample remaining as residue; the fraction volatile at the pyrolysis temperature, but not at room temperature, V_{pyr}; the fraction volatile at room temperature, but not at dry-ice temperature, V_{298}; the fraction volatile at dry-ice temperature, but not at liquid nitrogen temperature, V_{-193}; and the fraction volatile at liquid nitrogen temperature, V_{-77}. This characterization gives a general picture of the range of molecular weights of the decomposition products. The contents of each trap can also be analyzed further, perhaps by mass spectroscopy.

The residual polymer can be analyzed to determine the distribution of molecular weights of the remaining polymer chains. This information can be of great value in determining the mechanism of decomposition. The presence of free radicals in the residual polymer can be determined by electron spin resonance spectroscopy (ESR, EPR), which simplistically can be considered the determination of the concentration of unpaired electrons in the sample. Other techniques, like infrared spectroscopy (IR), can be usefully employed to detect the formation of bonds not present in the original polymer. Such changes in bonding may be due to double-bond formation due to chain-stripping or the incorporation of oxygen into the polymer, for example.

General Chemical Mechanisms

Four general mechanisms common in polymer decomposition are illustrated in Figure 1-7.6. These reactions can be divided into those involving atoms in the main polymer chain and those involving principally side chains or groups. While the decomposition of some polymers can be explained by one of these general mechanisms, others involve combinations of these four general mechanisms. Nonetheless, these categorizations are useful in the identification and understanding of particular decomposition mechanisms.

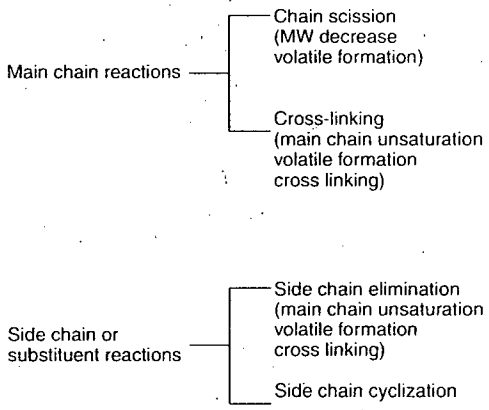

Figure 1-7.6. ***General decomposition mechanisms.***

Among simple thermoplastics, the most common reaction mechanism involves the breaking of bonds in the main polymer chain. These chain scissions may occur at the chain end or at random locations in the chain. End-chain scissions result in the production of monomer, and the process is often known as *unzipping*. Random-chain scissions generally result in the generation of both monomers and oligomers (polymer units with 10 or fewer monomer units) as well as a variety of other chemical species. The type and distribution of volatile products depend on the relative volatility of the resulting molecules.

Cross-linking is another reaction involving the main chain. It generally occurs after some stripping of substituents and involves the creation of bonds between two adjacent polymer chains. This process is very important in the formation of chars, since it generates a structure with a higher molecular weight that is less easily volatilized.

The main reaction types involving side chains or groups are elimination reactions and cyclization reactions. In elimination reactions, the bonds connecting side groups of the polymer chain to the chain itself are broken, with the side groups often reacting with other eliminated side groups. The products of these reactions are generally small enough to be volatile. In cyclization reactions, two adjacent side groups react to form a bond between them, resulting in the production of a cyclic structure. This process is also important in char formation because, as the reaction scheme shows, the residue is much richer in carbon than the original polymer as seen, for example, for poly(vinyl chloride):

$$-CH_2-CHCl- \Rightarrow -CH=CH- + HCl$$

which leads to a hydrogenated char or for poly(vinylidene chloride):

$$-CH_2-CCl_2- \Rightarrow -C\equiv C- + 2HCl$$

which yields a purely carbonaceous char with an almost graphitic structure. These chars will tend to continue

breaking down by chain scission, but only at very high temperatures.

Chain-Scission Mechanisms

Decomposition by chain scission is a very typical mechanism for polymer decomposition. The process is a multistep radical chain reaction with all the general features of such reaction mechanisms: initiation, propagation, branching, and termination steps.

Initiation reactions are of two basic types: (1) random-chain scission and (2) end-chain scission. Both, of course, result in the production of free radicals. The random scission, as the name suggests, involves the breaking of a main chain bond at a seemingly random location, all such main chain bonds being equal in strength. End-chain initiation involves the breaking off of a small unit or group at the end of the chain. This may be a monomer unit or some smaller substituent. These two types of initiation reactions may be represented by the following generalized reactions:

$$P_n \Rightarrow R_r + R_{n-r} \qquad \text{(random-chain scission)}$$

$$P_n \Rightarrow R_n + R_E \qquad \text{(end-chain initiation)}$$

where P_n is a polymer containing n monomer units, and R_r is a radical containing r monomer units. R_E refers to an end group radical.

Propagation reactions in polymer decomposition are often called *depropagation reactions*, no doubt due to the polymer chemist's normal orientation toward polymer formation (polymerization) rather than decomposition. Regardless, there are several types of reactions in this class [see Figure 1-7.7, parts (a), (b), and (c)]:

$$R_n \Rightarrow R_{n-m} + P_m \qquad \text{(intramolecular H transfer, random-chain scission)}$$

$$P_m + R_n \Rightarrow P_{m-j} + P_n + R_j \qquad \text{(intermolecular H transfer)}$$

$$R_n \Rightarrow R_{n-1} + P_1 \qquad \text{(unzipping, depropagation, depolymerization)}$$

The first of these reactions involves the transfer of a hydrogen atom within a single polymer chain, i.e., intramolecular hydrogen atom transfer. The value of m is usually between one and four as polymer molecules are often oriented such that the location of the nearest available H within the chain is one to four monomer units away from the radical site. The value of m need not be a constant for a specific polymer as the closest available hydrogen atom in the chain may vary due to conformational variations. Decomposition mechanisms based on this reaction are sometimes known as random-chain scission mechanisms. The second reaction involves the transfer of a hydrogen atom between polymer chains, i.e., intermolecular hydrogen atom transfer. The original radical, R_n, abstracts a hydrogen atom from the polymer, P_m. As this makes P_m radical with the radical site more often than not within the chain itself (i.e., not a terminal radical site), the newly formed radical breaks up into an unsaturated polymer, P_{m-j}, and a radical, R_j. In the final reaction, no hydrogen transfer occurs. It is essentially the reverse of the polymerization step and, hence, is called *unzipping, depropagation,* or *depolymerization*. Whether the decomposition involves principally hydrogen transfer reactions or unzipping can be determined by examining the structure of the polymer, at least for polymers with only carbon in the main chain. If hydrogen transfer is impeded, then it is likely that the unzipping reaction will occur.

Vinyl polymers, strictly speaking, are those derived from a vinyl repeating unit, namely

$$-[CH_2-CH_2]_n-$$

where n is the number of repeating monomers. Here, the hydrogen atoms can be substituted, leading to a repeating unit of the following form:

$$-[\underset{X}{\overset{W}{C}}-\underset{Z}{\overset{Y}{C}}]_n-$$

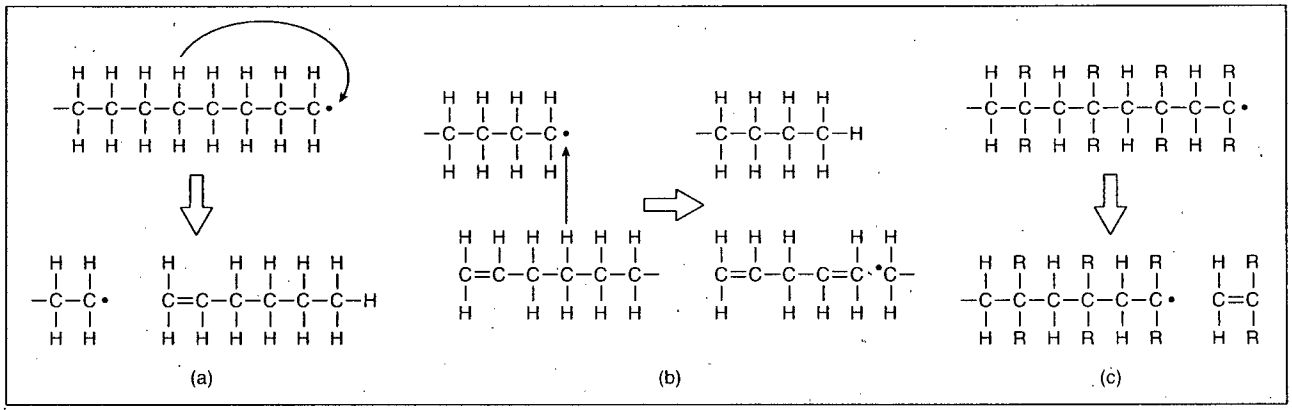

Figure 1-7.7. ***(a) Intramolecular H transfer, (b) intermolecular H transfer, (c) unzipping.***

where W, X, Y, and Z are substituent groups, perhaps hydrogen, methyl groups, or larger groups. Consider that the C–C bond connecting monomer units is broken and that a radical site results from the scission shown as

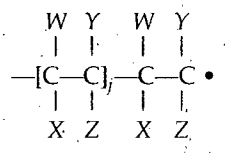

where the symbol • indicates an unpaired electron and, hence, a radical site. In order for a hydrogen atom to be transferred from the chain to the radical site, it must pass around either Y or Z. If Y and Z are hydrogens, this is not at all difficult due to their small size. However, if the alpha carbon has larger substituents bound to it (i.e., Y and Z are larger groups), the transfer of hydrogen to the radical site is more difficult. This type of interference with hydrogen transfer is known as *steric hindrance*. Table 1-7.3 shows this effect.[2] Polymers near the top of Table 1-7.3 have Y and Z substituents that are generally large, with a resulting high monomer yield, characteristic of unzipping reactions. Near the bottom of Table 1-7.3, where Y and Z are small, the polymers form negligible amounts of monomer as other mechanisms dominate.

While chain-branching reactions seem to be of little importance in polymer decomposition, termination reactions are required in all chain mechanisms. Several types of termination reactions are common.

$$R_m \Rightarrow P_m \qquad \text{(unimolecular termination)}$$

$$R_m + R_n \Rightarrow P_{m+n} \qquad \text{(recombination)}$$

$$R_n + R_m \Rightarrow P_m + P_n \qquad \text{(disproportionation)}$$

Table 1-7.3 ***Monomer Yield from Thermal Decomposition of Polymers of the General Form*** **[CWX – CYZ]$_n$**[2]

Polymer	W	X	Y	Z	Monomer Yield (wt. %)	Decomposition Mechanism[a]
PMMA	H	H	CH_3	CO_2CH_3	91–98	E
Polymethacrylonitrile	H	H	CH_3	CN	90	E
E Poly (a-methylstyrene)	H	H	CH_3	C_6H_5	95	E
Polyoxymethylene[b]	—	—	—	—	100	E
Polytetrafluoroethylene	F	F	F	F	95	E
Poly (methyl atropate)	H	H	C_6H_5	CO_2CH_3	>99	E
Poly (*p*-bromostyrene[c]	H	H	H	C_6H_4Br	91–93	E
Poly (*p*-chlorostyrene[c]	H	H	H	C_6H_4Cl	82–94	E
Poly (*p*-methyoxystyrene[c]	H	H	H	C_7H_7O	84–97	E
Poly (*p*-methylstyrene)	H	H	H	C_7H_7	82–94	E
Poly (a-deuterostyrene)	H	H	D	C_6H_5	70	E
Poly (a,β,β-trifluorostyrene)	F	F	F	C_6H_5	44	E/R
Polystyrene	H	H	H	C_6H_5	42–45	E/R
Poly (*m*-methylstyrene	H	H	H	C_7H_8	44	E/R
Poly (β-deuerostyrene)	H	D	H	C_6H_5	42	E/R
Poly (β-methylstyrene)	H	CH_3	H	C_6H_5		E/R
Poly (*p*-methoxystvrene[d]	H	H	H	C_7H_7O	36–40	E/R
Polyisobutene	H	H	CH_3	CH_3	18–25	E/R
Polychlorotrifluoroethylene	F	F	Cl	F	28	E/S
Poly (ethylene oxide)[b]	—	—	—	—	4	R/E
Poly (propylene oxide)[b]	—	—	—	—	4	R/E
Poly (4-methyl pent-1-ene)	H	H	H	C_4H_9	2	R/E
Polyethylene	H	H	H	H	0.03	R
Polypropylene	H	H	H	CH_3	0.17	R
Poly (methyl acrylate)	H	H	H	CO_2CH_3	0.7	R
Polytrifluoroethylene	F	F	H	F	—	R
Polybutadiene[b]	—	—	—	—	1	R
Polyisoprene[b]	—	—	—	—	5	R
Poly (vinyl chloride)	H	H	H	Cl	0–0.07	S
Poly (vinylidene fluoride)	H	H	F	F	—	S
Poly (vinyl fluoride)	H	H	H	F	—	S
Poly (vinyl alcohol)	H	H	H	OH	—	S
Polyacrylonitrile	H	H	H	CN	5	C

[a]R, random-chain scission; E, end-chain scission (unzipping); S, chain-stripping; C, cross-linking.

[b]Not of general form [CWX – CYZ]$_n$

[c]Cationic polymerization

[d]Free-radical polymerization

The first of these reactions is, strictly speaking, not generally possible. Nonetheless, there are instances where the observed termination reaction appears to be first order (at least empirically). It is impossible to remove the radical site from a polymer radical without adding or subtracting at least one hydrogen atom while still satisfying the valence requirements of the atoms. What probably occurs is that the termination reaction is, in fact, second order, but the other species involved is so little depleted by the termination reaction that the termination reaction appears not to be affected by the concentration of that species. This is known as a pseudo first-order reaction. The recombination reaction is a classical termination step that is actually just the reverse of the random-chain scission initiation reaction. Finally, the disproportionation reaction involves the transfer of a hydrogen atom from one radical to the other. The hydrogen donor forms a double bond as a result of the hydrogen loss, and the acceptor is fully saturated. If this sort of reaction occurs immediately after an initiation reaction, no unzipping or other propagation reaction occurs, and the polymer decomposition is fully characterized by a random process of bond scissions.

There is a natural tendency to regard all materials with the same generic name, such as poly(methyl methacrylate), as being the same material with the same properties. As these are commercial products, the preparation methods (including the polymerization process) are dictated by the required physical and chemical properties of the material for normal use. Additives, both intentional and inadvertent, may be present, and the method of polymerization and the molecular weight of the polymer chains may vary. This is particularly important in the case of polymeric "compounds" (the actual polymeric material that is used commercially to fabricate a product of any kind) that contain a large fraction of additives. In some polyolefins, the fraction of polymer (known as *resin*) may be much less than half of the total mass of the compound, because of the presence of large amounts of fillers. In some compounds derived from poly(vinyl chloride), flexibility is introduced by means of *plasticizers*.

In this regard, it is interesting and important to note that polymers tend to be less stable than their oligomer counterparts. This results from several effects involved in the production and aging of polymers as well as simply the chain length itself. Initiation reactions in a polymer can lead to far more monomer units being involved in decomposition reactions, relative to the polymer's short-chain oligomeric analog. In the production and aging of polymers, there are opportunities for the production of abnormalities in the polymer chains due to the mode of synthesis and thermal, mechanical, and radiation effects during aging.

In the synthesis of the polymer, abnormalities may result from several sources. Unsaturated bonds result from chain termination by free-radical termination reactions. End-chain unsaturation results from second-order disproportionation reactions, and midchain unsaturation often occurs due to chain-transfer reactions with subsequent intramolecular hydrogen transfer. Chain branching may result from the formation of midchain radicals. During synthesis, chain transfer reactions may cause midchain radicals that then go on to react with monomers or polymers to create a branched polymer structure. Termination of the polymerization reaction may also result in *head-to-head linkages*; i.e., monomer units are attached such that some of the monomers are oriented opposite to the remainder of the chain. Lastly, foreign atoms or groups may be incorporated into the polymer chain. This may occur due to impurities, polymerization initiators, or catalysts. Oxygen is often a problem in this regard.

The purity and the molecular weight of the polymer can markedly affect not only the decomposition rates, but also the mechanism of decomposition. An example of such a change might involve chain initiations occurring at the location of impurities in the chain of a polymer which, if pure, would principally be subject to end-chain initiation. Both the mechanism and the decomposition rate would be affected. Not all polymer "defects" degrade polymer thermal performance. In a polymer that decomposes by unzipping, a head-to-head linkage can stop the unzipping process. Thus, for an initiation that would have led to the full polymer being decomposed, only the part between the initiation site and the head-to-head link is affected. At least one additional initiation step is required to fully decompose the chain. This has been studied in detail by Kashiwagi et al.[6–10]

Kinetics

Eight generic types of reaction involved in simple decomposition processes have been addressed in the previous sections. Even if only a subset of these reaction types are required and the reaction rates are not a strong function of the size of the polymer chains and radicals, the kinetics describing the process can be quite complex. In engineering applications, such complex reaction mechanisms are not used. Rather, simple overall kinetic expressions are generally utilized if, in fact, decomposition kinetics are considered at all. The most common assumption is that the reactions can be described by an Arrhenius expression of first order in the remaining polymer mass. Often one goes even further and ignores any dependence of the reaction rate on the remaining polymer or the thickness of the decomposition zone and simply expresses the volatilization rate per unit surface area as a zero-order Arrhenius expression. This effectively assumes that the decomposition zone is of constant thickness and fresh polymer replaces the decomposed polymer by surface regression. Such an approach would clearly not be satisfactory for charring materials where decomposition is clearly not a surface phenomenon. As some of the work quoted earlier has indicated (e.g., Reference 13), it is also not suitable for many thermoplastic polymers.

Despite the fact that detailed kinetic models are not used in engineering calculations, it is instructive to consider some very simple cases, by the use of overall kinetic expressions, to indicate what is being lost. The effect of the initiation mechanism on decomposition kinetics can be easily demonstrated by considering either random- or end-chain initiation with propagation by unzipping and no termination reactions other than exhaustion of the

polymer chain by unzipping. The rate of weight loss for random-chain initiation can be expressed as

$$\frac{dW}{dt} = D_p \cdot k_{ir} \cdot W$$

where D_p, the degree of polymerization, is the number of monomer units per polymer chain; and k_{ir} is the rate constant for the random-chain initiation reaction. Notice that the rate constant of the propagation reaction is not included in the expression. A further assumption that the propagation rate is much faster than the initiation rate has also been made. The initiation reaction is said to be the *rate-limiting step*. The degree of polymerization arises in the equation since, for each initiation, D_p monomer units will be released; and the remaining weight, W, arises because the number of bonds available for scission is proportional to W. Since the polymer unzips completely, the molecular weight of all remaining polymer chains is the same as the initial molecular weight.

Considering end-chain initiation, the rate of mass loss is given by

$$\frac{dW}{dt} = D_p \cdot (2n) \cdot k_{ie}$$

where n is the number of polymer chains, and, hence, $2n$ is the number of chain ends, and k_{ie} is the rate constant for end-chain initiation. The number of polymer chains is simply the mass of the sample divided by the molecular weight of each chain, or

$$n = \frac{W}{D_p \cdot MW_m}$$

where MW_m is the molecular weight of the monomer. Using this expression yields

$$\frac{dW}{dt} = \frac{2 \cdot k_{ie} \cdot W}{MW_m}$$

Comparing this with the random initiation expression, one can see that, for random initiation, the rate is dependent on the original degree of polymerization; whereas for end-chain initiation the rate is independent of the degree of polymerization or, equivalently, the original molecular weight of the polymer. In both cases, however, the rate is first order in the mass of the sample. This derivation has been for a monodisperse polymer; i.e., all chains have been considered to be the same length initially.

Returning to the random-chain initiation expression, it is clear that longer chains are decomposed preferentially. If the initial sample had a range of molecular weights, the longer chains would disappear more quickly than shorter chains, and the molecular weight distribution would change with time, unlike in the monodisperse case. It can be shown that in this case the reaction order is no longer unity, but is between one and two, depending on the breadth of the distribution.[30] Thus,

$$\frac{dW}{dt} \sim W^n$$

with

$$1 < n < 2$$

for random-chain initiation and complete unzipping of a polydisperse system.

This simple comparison illustrates some of the ways in which the details of the polymerization process, which control variables like the molecular weight distribution, can alter the decomposition process. For a particular polymer sample, no single initiation reaction need be dominant, in general. The activation energies for the different initiation steps may be quite different, leading to large variations in the relative rates with temperature. For instance, in PMMA, the dominant initiation step at low temperatures (around 570 K) is end-chain initiation. At higher temperatures (around 770 K), the random-chain initiation step dominates. In a single nonisothermal TGA experiment, this temperature range can easily be traversed, and overall interpretation of the results in terms of a single mechanism would be unsatisfactory and misleading.

Nonetheless, simple overall kinetic expressions are likely to be dominant in engineering for some time. The pitfalls with this approach simply serve to reinforce the need to determine the kinetic parameters in an experiment that is as similar to the end use as is practical. This is one of the major reasons why the use of TGA results has been brought into question. As stated before, the heating rates often are far less than those generally found in fire situations. The low heating rates in TGA experiments tend to emphasize lower-temperature kinetics, which may be much less important at the heating rates characteristic of most fire situations.

One interesting study worth presenting here is a theoretical analysis of thermal decomposition that presents a technique for calculating the temperature at the beginning and end of thermal decomposition, based on structural data from the polymer and on scission at the weakest bond, with considerable degree of success, particularly for successive members of a polymeric family.[31] A subsequent analysis has also been published that is much simpler, but it has not been validated against experimental data.[32]

General Physical Changes During Decomposition

The physical changes that occur on heating a material are both important in their own right and also impact the course of chemical decomposition significantly. The nature of the physical changes and their impact on decomposition vary widely with material type. This section addresses the general physical changes that occur for thermoplastic (glass transition, melting) and thermosetting (charring, water desorption) materials.

Melting and Glass Transition

On heating a thermoplastic material, the principal physical change is the transformation from a glass or solid to the fluid state. (See Figure 1-7.2.) If this transformation

occurs at temperatures well below the decomposition temperature, it becomes more likely that the material will drip and/or flow. While such behavior is a complication, in terms of fire safety it can either improve or degrade the performance of the material. In some configurations, flowing of the material can remove it from the source of heat and thus avoid ignition or further fire growth. In other situations, the flow of material may be toward the heat source, leading to a worsened fire situation. Many standard fire tests that allow materials to flow away from the heat source have been shown to be unsuitable for assessing the hazards of flowing or dripping materials. Care must be taken in the evaluation of standard test results in this regard. However, many thermoplastics do not show marked tendencies to flow during heating and combustion. Whereas polyethylene melts and flows readily, high-quality cast poly(methyl methacrylate) shows only slight tendencies to flow under fire conditions.

When designing a material, there are several techniques that can be utilized to increase the temperature at which physical transformations occur. These strategies are generally aimed at increasing the stiffness of the polymer or increasing the interactions between polymer chains. It is clear that increasing the crystallinity of the polymer increases the interaction between polymer chains. In the highly ordered state associated with crystalline materials, it is less possible for polymer chains to move relative to one another, as additional forces must be overcome in the transformation to the unordered fluid state. Crystallinity is enhanced by symmetric regular polymer structure and highly polar side groups. Regular structure allows adjacent polymer chains to pack in a regular and tight fashion. As such, isotactic polymers are more likely to crystallize than atactic polymers, and random copolymers do not tend to crystallize. Polar side groups enhance the intermolecular forces. Regular polar polymers, such as polyesters and polyamides, crystallize readily. Even atactic polymers with OH and CN side groups will crystallize due to polarity. The melting temperature of a polymer is also increased with increasing molecular weight up to a molecular weight of about 10,000 to 20,000 g/mol.

Melting temperatures can also be increased by increasing the stiffness of the polymer chain. Aromatic polyamides melt at much higher temperatures than their aliphatic analogs due to stiffness effects. Aromatics are particularly useful for chain stiffening, as they provide stiffness without bulk which would hinder crystallinity. At the opposite extreme, the increased flexibility of the oxygen atom links in polyethers is responsible for a lowering of the melting temperature of polyethers relative to polymethylene. Chain stiffening must be accompanied by suitable thermal stability and oxidation resistance in order to achieve increased service temperatures. Many aromatic polymers have melting temperatures in excess of their decomposition temperatures, making these materials thermosetting.

Cross-linking also increases the melting temperature and, like chain stiffening, can render a material infusible. Cross-links created in fabrication or during heating are also important in thermoplastics. The glass transition temperature can be increased in amorphous polymers by the inclusion of cross-links during fabrication. Random-chain scissions can quickly render a material unusable by affecting its physical properties unless cross-linking occurs. Such cross-linking in thermoplastics on heating may be regarded as a form of repolymerization. The temperature above which depolymerization reactions are faster than polymerization reactions is known as *ceiling temperature*. Clearly, above this temperature catastrophic decomposition will occur.

Charring

While char formation is a chemical process, the significance of char formation is largely due to its physical properties. Clearly, if material is left in the solid phase as char, less flammable gas is given off during decomposition. More importantly, the remaining char can be a low-density material and is a barrier between the source of heat and the virgin polymer material. As such, the flow of heat to the virgin material is reduced as the char layer thickens, and the rate of decomposition is reduced, depending on the properties of the char.[3] If the heat source is the combustion energy of the burning volatiles, not only will the fraction of the incident heat flux flowing into the material be reduced, but the incident heat flux as a whole will be reduced as well. Unfortunately, char formation is not always an advantageous process. The solid-phase combustion of char can cause sustained smoldering combustion. Thus, by enhancing the charring tendency of a material, flaming combustion rates may be reduced, but perhaps at the expense of creating a source of smoldering combustion that would not otherwise have existed.

Charring is enhanced by many of the same methods used to increase the melting temperature. Thermosetting materials are typically highly cross-linked and/or chain-stiffened. However, charring is not restricted to thermosetting materials. Cross- linking may occur as a part of the decomposition process, as is the case in poly(vinyl chloride) and polyacrylonitrile.

Implications for Fire Performance

As explained earlier, one of the major reasons why thermal decomposition of polymers is studied is because of its importance in terms of fire performance. This issue has been studied extensively.

Early on, Van Krevelen[33,34] showed that, for many polymers, the limiting oxygen index (LOI, an early measure of flammability)[35] could be linearly related to char yield as measured by TGA under specified conditions. Then, since Van Krevelen showed how to compute char yield to a good approximation from structural parameters, LOI should be computable; and for pure polymers having substantial char yields, it is fairly computable. Somewhat later, comparisons were made between the minimum decomposition temperature (or, even better, the temperature for 1 percent thermal decomposition) and the LOI.[2,22] The conclusion was that, although in general low flammability resulted from high minimum thermal decomposition

temperatures, no easy comparison could be found between the two. There were some notable cases of polymers with both low thermal stability and low flammability. This type of approach has since fallen into disrepute, particularly in view of the lack of confidence remaining today in the LOI technique.[36] Table 1-7.4 shows some thermal decomposition temperatures and limiting oxygen indices[22] as well as heat release rate values, the latter as measured in the cone calorimeter.[37,38] It is clear from the data in Table 1-7.4 that thermal decomposition is *not* a stand-alone means of predicting fire performance. Promising work in this regard is being made by Lyon,[39] who appears to be able to preliminarily predict some heat release information from thermoanalytical data.

However, mechanisms of action of fire retardants and potential effectiveness of fire retardants can be well predicted from thermal decomposition activity (for example, see Figures 1-7.4 and 1-7.5).[22,23] It is often necessary to have some additional understanding of the chemical reactions involved. In Figure 1-7.5, for example, the systems containing ABS, decabromobiphenyl, and either antimony oxide (c) or ferric oxide (g) have very similar TGA/DTG curves, with continuous weight loss. This indicates that the Sb system is effective but the iron one is not, because antimony bromide can volatilize while iron bromide does not. On the other hand, the system containing zinc oxide (f) is inefficient because the zinc bromide volatilizes too early, i.e., before the polymer starts breaking down. Some authors have used thermal decomposition techniques via the study of the resulting products to understand the mechanism of fire retardance (e.g., Grassie[40]), or together with a variety of other techniques (e.g., Camino et al.[41,42]).

Whatever the detailed degree of predictability of fire performance data from thermal decomposition data, its importance should not be underestimated: *polymers cannot burn if they do not break down.*

Table 1-7.4 ***Thermal Stability and Flammability of Polymers***

Polymer	T_d[a] (K)	T_1%[b] (K)	LOI[c] (-)	Pk RHR[d] (kW/m²)
Polyacetal	503	548	15.7	360
Poly(methyl methacrylate)	528	555	17.3	670
Polypropylene	531	588	17.4	1500
Polyethylene (LDPE)	490	591	17.4	800[e]
Polyethylene (HDPE)	506	548	17.4	1400
Polystyrene	436	603	17.8	1100
ABS copolymer	440	557	18.0	950[e]
Polybutadiene	482	507	18.3	
Polyisoprene	460	513	18.5	
Cotton	379	488	19.9	450[e]
Poly(vinyl acohol)	337	379	22.5	
Wool	413	463	25.2	310[e]
Nylon-6	583		25.6	1300
Silicone oil	418	450	32	140[e]
Poly(vinylidene fluoride)	628	683	43.7	30[e]
Poly(vinyl chloride)	356	457	47	180
Polytetrafluoroethylene	746	775	95	13

[a] T_d: Minimum thermal decomposition temperature from TGA (10-mg sample, 10-K/min heating rate, nitrogen atmosphere)[22]

[b] $T_{1\%}$: Temperature for 1% thermal decomposition, conditions as above[22]

[c] LOI: Limiting oxygen index[22]

[d] Pk RHR: Peak rate of heat release in the cone calorimeter, at 40-kW/m² incident flux, at a thickness of 6 mm,[35] all under the same conditions.

[e] Pk RHR: Peak rate of heat release in the cone calorimeter, at 40-kW/m² incident flux, from sources othre than those in footnote *d*.

Behavior of Individual Polymers

The discussion, thus far, has been general, focusing on the essential aspects of thermal decomposition without the complications that inevitably arise in the treatment of a particular polymer. This approach may also tend to make the concepts abstract. Through the treatment of individual polymers by polymer class, this section provides an opportunity to apply the general concepts to real materials. In general, the section is restricted to polymers of commercial importance. More complete and detailed surveys of polymers and their thermal decomposition can be found in the literature.[2,30,43–52]

Polyolefins

Of the polyolefins, low-density polyethylene (LDPE), high-density polyethylene (HDPE), and polypropylene (PP) are of the greatest commercial importance because of their production volume. Upon thermal decomposition, very little monomer formation is observed for any of these polymers; they form a large number of different small molecules (up to 70), mostly hydrocarbons. Thermal stability of polyolefins is strongly affected by branching, with linear polyethylene most stable and polymers with branching less stable. The order of stability is illustrated as follows:

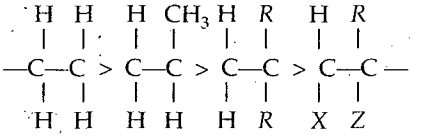

where *R* is any hydrocarbon group larger than a methyl group.

Polyethylene (PE): In an inert atmosphere, polyethylene begins to cross-link at 475 K and to decompose (reductions in molecular weight) at 565 K though extensive weight loss is not observed below 645 K. Piloted ignition of polyethylene due to radiative heating has been observed at a surface temperature of 640 K. The products of decomposition include a wide range of alkanes and alkenes. Branching of polyethylene causes enhanced intramolecular hydrogen transfer and results in lower thermal stability. The low-temperature molecular weight changes without volatilization are principally due to the scission of weak links, such as oxygen, incorporated into the main chain as impurities. Initiation reactions at higher temperatures involve scission of tertiary carbon bonds or ordinary carbon–carbon bonds in the beta position to tertiary carbons. The major products of decomposition are

propane, propene, ethane, ethene, butene, hexene-1, and butene-1. Propene is generated by intramolecular transfer to the second carbon and by scission of the bond beta to terminal $=CH_2$ groups.

The intramolecular transfer route is most important, with molecular coiling effects contributing to its significance. A broad range of activation energies has been reported, depending on the percent conversion, the initial molecular weight, and whether the remaining mass or its molecular weight were monitored. Decomposition is strongly enhanced by the presence of oxygen, with significant effects detectable at 423 K in air.

Polypropylene (PP): In polypropylene, every other carbon atom in the main chain is a tertiary carbon, which is thus prone to attack. This lowers the stability of polypropylene as compared to polyethylene. As with polyethylene, chain scission and chain transfer reactions are important during decomposition. By far, secondary radicals (i.e., radical sites on the secondary carbon) are more important than primary radicals. This is shown by the major products formed, i.e., pentane (24 percent), 2 methyl-1-pentene (15 percent), and 2–4 dimethyl-1-heptene (19 percent). These are more easily formed from intramolecular hydrogen transfer involving secondary radicals. Reductions in molecular weight are first observed at 500 to 520 K and volatilization becomes significant above 575 K. Piloted ignition of polypropylene due to radiative heating has been observed at a surface temperature of 610 K. Oxygen drastically affects both the mechanism and rate of decomposition. The decomposition temperature is reduced by about 200 K, and the products of oxidative decomposition include mainly ketones. Unless the polymer samples are very thin (less than 0.25–0.30 mm or 0.010–0.012 in. thick), oxidative pyrolysis can be limited by diffusion of oxygen into the material. At temperatures below the melting point, polypropylene is more resistant to oxidative pyrolysis as oxygen diffusion into the material is inhibited by the higher density and crystallinity of polypropylene. Most authors have assumed that the oxidation mechanism is based on hydrocarbon oxidation, but recent work suggests that it may actually be due to the decomposition of peracids resulting from the oxidation of primary decomposition products.[12]

Polyacrylics

Poly(methyl methacrylate) (PMMA): PMMA is a favorite material for use in fire research since it decomposes almost solely to monomer, and burns at a very steady rate. Methyl groups effectively block intramolecular H transfer as discussed in the General Chemical Mechanisms section, leading to a high monomer yield. The method of polymerization can markedly affect the temperatures at which decomposition begins. Free-radical polymerized PMMA decomposes around 545 K, with initiation occurring at double bonds at chain ends. A second peak between 625 and 675 K in dynamic TGA thermograms is the result of a second initiation reaction. At these temperatures, initiation is by both end-chain and random-chain initiation processes. An ionically produced PMMA decomposes at about 625 K because the end-chain initiation step does not occur due to the lack of double bonds at the chain end when PMMA is polymerized by this method. This may explain the range of observed piloted ignition temperatures (550 to 600 K). Decomposition of PMMA is first order with an activation energy of 120 to 200 kJ/mol, depending on the end group. The rate of decomposition is also dependent on the tacticity of the polymer and on its molecular weight. These effects can also have a profound effect on the flame spread rate.

It is interesting to note that a chemically cross-linked copolymer of PMMA was found to decompose by forming an extensive char, rather than undergoing end-chain scission which resulted in a polymer with greater thermal stability.[53]

Poly(methyl acrylate) (PMA): Poly(methyl acrylate) decomposes by random-chain scission rather than end-chain scission, with almost no monomer formation. This results because of the lack of a methyl group blocking intramolecular hydrogen transfer as occurs in PMMA. Initiation is followed by intra- and intermolecular hydrogen transfer.

Polyacrylonitrile (PAN): PAN begins to decompose exothermically between 525 K and 625 K with the evolution of small amounts of ammonia and hydrogen cyanide. These products accompany cyclization reactions involving the creation of linkages between nitrogen and carbon on adjacent side groups. (See Figure 1-7.8.) The gaseous products are not the result of the cyclization itself, but arise from the splitting off of side or end groups not involved in the cyclization. The ammonia is derived principally from terminal imine groups (NH) while HCN results from side groups that do not participate in the polymerization-like cyclization reactions. When the polymer is not isotactic, the cyclization process is terminated when hydrogen is abstracted by the nitrogen atom. The cyclization process is reinitiated as shown in Figure 1-7.9.

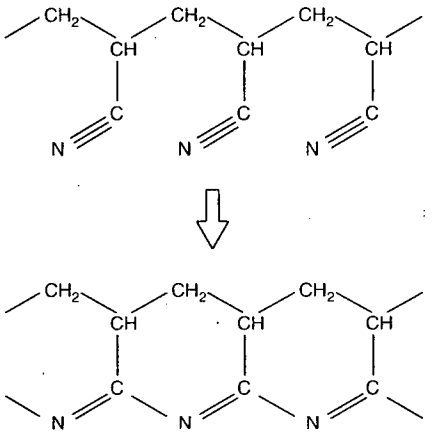

Figure 1-7.8. ***PAN cyclization.***

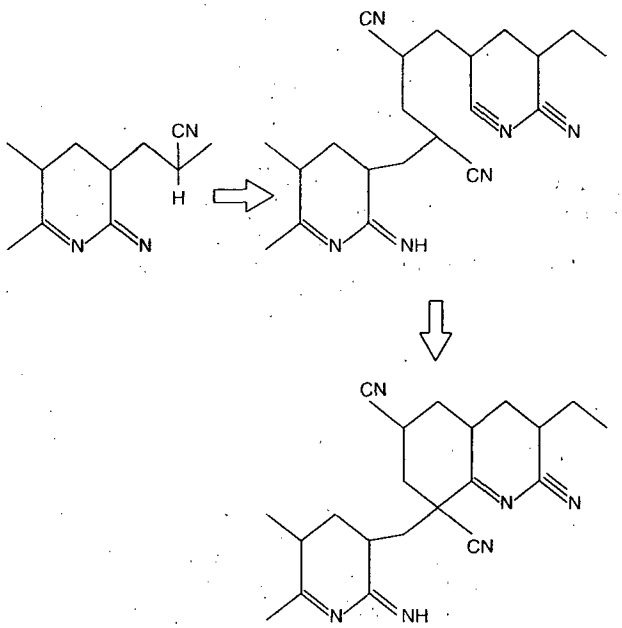

Figure 1-7.9. ***Reinitiation of PAN side-chain cyclization.***

This leaves CN groups not involved in the cyclization which are ultimately removed and appear among the products as HCN. Typically, there are between 0 and 5 chain polymerization steps between each hydrogen abstraction. At temperatures of 625 to 975 K, hydrogen is evolved as the cyclic structures carbonize. At higher temperatures, nitrogen is evolved as the char becomes nearly pure carbon. In fact, with adequate control of the process, this method can be used to produce carbon fibers. Oxygen stabilizes PAN, probably by reacting with initiation sites for the nitrile polymerization. The products of oxidative decomposition are highly conjugated and contain ketonic groups.

Halogenated Polymers

Poly(vinyl chloride) (PVC): The most common halogenated polymer is PVC; it is one of the three most widely used polymers in the world, with polyethylene and polypropylene. Between 500 and 550 K, hydrogen chloride gas is evolved nearly quantitatively, by a chain-stripping mechanism. It is very important to point out, however, that the temperature at which hydrogen chloride starts being evolved in any measurable way is heavily dependent on the stabilization package used. Thus, commercial PVC "compounds" have been shown, in recent work, not to evolve hydrogen chloride until temperatures are in excess of 520 K and to have a dehydrochlorination stage starting at 600 K.[54] Between 700 and 750 K, hydrogen is evolved during carbonization, following cyclization of the species evolved. At higher temperatures, cross-linking between chains results in a fully carbonized residue. The rate of dehydrochlorination depends on the molecular weight, crystallinity, presence of oxygen, hydrogen chloride gas, and stabilizers. The presence of oxygen accelerates the dehydrochlorination process, produces main-chain scissions, and reduces cross-linking. At temperatures above 700 K, the char (resulting from dehydrochlorination and further dehydrogenation) is oxidized, leaving no residue. Lower molecular weight increases the rate of dehydrochlorination. Dehydrochlorination stabilizers include zinc, cadmium, lead, calcium, and barium soaps and organotin derivatives. The stability of model compounds indicates that weak links are important in decomposition. The thermal decomposition of this polymer has been one of the most widely studied ones. It has been the matter of considerable controversy, particularly in terms of explaining the evolution of aromatics in the second decomposition stage. The most recent evidence seems to point to a simultaneous cross-linking and intramolecular decomposition of the polyene segments resulting from dehydrochlorination, via polyene free radicals.[54] Earlier evidence suggested a Diels-Alder cyclization process (which can only be intramolecular if the double bond ends up in a "cis" orientation).[55] Evidence for this was given by the fact that smoke formation (inevitable consequence of the emission of aromatic hydrocarbons) was decreased by introducing cross-linking additives into the polymer.[56] Thus, it has now become clear that formation of any aromatic hydrocarbon occurs intramolecularly. The chemical mechanism for the initiation of dehydrochlorination was also reviewed a few years ago.[57] More recently, a series of papers was published investigating the kinetics of chain stripping, based on PVC.[58]

Chlorinated poly(vinyl chloride) (CPVC): One interesting derivative of PVC is chlorinated PVC (CPVC), resulting from post-polymerization chlorination of PVC. It decomposes at a much higher temperature than PVC, but by the same chain-stripping mechanism. The resulting solid is a polyacetylene, which gives off much less smoke than PVC and is also more difficult to burn.[59]

Poly(tetrafluoroethylene) (PTFE): PTFE is a very stable polymer due to the strength of C–F bonds and shielding by the very electronegative fluorine atoms. Decomposition starts occurring between 750 and 800 K. The principal product of decomposition is the monomer, CF_4, with small amounts of hydrogen fluoride and hexafluoropropene. Decomposition is initiated by random-chain scission, followed by depolymerization. Termination is by disproportionation. It is possible that the actual product of decomposition is CF_2, which immediately forms in the gas phase. The stability of the polymer can be further enhanced by promoting chain transfer reactions that can effectively limit the zip length. Under conditions of oxidative pyrolysis, no monomer is formed. Oxygen reacts with the polymeric radical, releasing carbon monoxide, carbon dioxide, and other products.

Other fluorinated polymers are less stable than PTFE and are generally no more stable than their unfluorinated analogs. However, the fluorinated polymers are more stable in an oxidizing atmosphere. Hydrofluorinated polymers produce hydrogen fluoride directly by chain-stripping reactions, but the source of hydrogen fluoride by perfluorinated polymers, such as PTFE, is less clear. It is

related to the reaction of the decomposition products (including tetrafluoroethylene) with atmospheric humidity.

Other Vinyl Polymers

Several other vinyl polymers decompose by mechanisms similar to that of PVC: all those that have a single substituent other than a hydrogen atom on the basic repeating unit. These include poly(vinyl acetate), poly(vinyl alcohol), and poly(vinyl bromide), and result in gas evolution of acetic acid, water, and hydrogen bromide, respectively. While the chain-stripping reactions of each of these polymers occur at different temperatures, all of them aromatize by hydrogen evolution at roughly 720 K.

Styrenics: *Polystyrene (PS).* Polystyrene shows no appreciable weight loss below 575 K, though there is a decrease in molecular weight due to scission of "weak" links. Above this temperature, the products are primarily monomer with decreasing amounts of dimer, trimer, and tetramer. There is an initial sharp decrease in molecular weight followed by slower rates of molecular weight decrease. The mechanism is thought to be dominated by end-chain initiation, depolymerization, intramolecular hydrogen transfer, and bimolecular termination. The changes in molecular weight are principally due to intermolecular transfer reactions while volatilization is dominated by intramolecular transfer reactions. Depropagation is prevalent despite the lack of steric hindrance due to the stabilizing effect of the electron delocalization associated with the aromatic side group. The addition of an alpha methyl group to form poly(a-methylstyrene) provides additional steric hindrance such that only monomer is produced during decomposition while the thermal stability of the polymer is lessened. Free-radical polymerized polystyrene is less stable than an ionic polystyrene with the rate of decomposition dependent on the end group.

Other styrenics tend to be copolymers of polsytyrene with acrylonitrile (SAN), acrylonitrile and butadiene (ABS), or methyl methacrylate and butadiene (MBS), and their decomposition mechanisms are hybrids between those of the individual polymers.

Synthetic Carbon–Oxygen Chain Polymers

Poly(ethylene terephthalate) (PET): PET decomposition is initiated by scission of an alkyl–oxygen bond. The decomposition kinetics suggest a random-chain scission. Principal gaseous products observed are acetaldehyde, water, carbon monoxide, carbon dioxide, and compounds with acid and anhydride end groups. The decomposition is accelerated by the presence of oxygen. Recent evidence indicates that both PET and PBT [poly(butylene terephthalate)] decompose via the formation of cyclic or open-chain oligomers, with olefinic or carboxylic end groups.[60]

Polycarbonates (PC): Polycarbonates yield substantial amounts of char if products of decomposition can be removed (the normal situation). If volatile products are not removed, no cross-linking is observed due to competition between condensation and hydrolysis reactions. The decomposition is initiated by scission of the weak $O–CO_2$ bond, and the volatile products include 35 percent carbon dioxide. Other major products include bisphenol A and phenol. The decomposition mechanism seems to be a mixture of random-chain scission and cross-linking, initiated intramolecularly.[61] Decomposition begins at 650 to 735 K, depending on the exact structure of the polycarbonate in question.

Blends of polycarbonate and styrenics (such as ABS) make up a set of *engineered thermoplastics*. Their properties are intermediate between those of the forming individual polymers, both in terms of physical properties (and processability) and in terms of their modes of thermal breakdown.

Phenolic resins: Phenolic resin decomposition begins at 575 K and is initiated by the scission of the methylene–benzene ring bond. At 633 K, the major products are C_3 compounds. In continued heating (725 K and higher), char (carbonization), carbon oxides, and water are formed. Above 770 K, a range of aromatic, condensable products are evolved. Above 1075 K, ring breaking yields methane and carbon oxides. In TGA experiments at 3.3°C/min, the char yield is 50 to 60 percent. The weight loss at 700 K is 10 percent. All decomposition is oxidative in nature (oxygen provided by the polymer itself).

Polyoxymethylene (POM): Polyoxymethylene decomposition yields formaldehyde almost quantitatively. The decomposition results from end-chain initiation followed by depolymerization. The presence of oxygen in the chain prevents intramolecular hydrogen transfer quite effectively. With hydroxyl end groups, decomposition may begin at temperatures as low as 360 K while with ester end groups decomposition may be delayed to 525 K. Piloted ignition due to radiative heating has been observed at a surface temperature of 550 K. Acetylation of the chain end group also improves stability. Upon blocking the chain ends, decomposition is by random-chain initiation, followed by depolymerization with the zip length less than the degree of polymerization. Some chain transfer occurs. Amorphous polyoxymethylene decomposes faster than crystalline polyoxymethylene, presumably due to the lack of stabilizing intermolecular forces associated with the crystalline state (below the melting temperature). Incorporating oxyethylene in polyoxymethylene improves stability, presumably due to H transfer reactions that stop unzipping. Oxidative pyrolysis begins at 430 K and leads to formaldehyde, carbon monoxide, carbon dioxide, hydrogen, and water vapor.

Epoxy resins: Epoxy resins are less stable than phenolic resins, polycarbonate, polyphenylene sulphide, and polytetrafluoroethelyne. The decomposition mechanism is complex and varied and usually yields mainly phenolic compounds. A review of epoxy resin decomposition can be found in Lee.[43]

Polyamide Polymers

Nylons: The principal gaseous products of decomposition of nylons are carbon dioxide and water. Nylon 6

produces small amounts of various simple hydrocarbons while Nylon 6–10 produces notable amounts of hexadienes and hexene. As a class, nylons do not notably decompose below 615 K. Nylon 6–6 melts between 529 and 532 K, and decomposition begins at 615 K in air and 695 K in nitrogen. At temperatures in the range 625 to 650 K, random-chain scissions lead to oligomers. The C–N bonds are the weakest in the chain, but the $CO–CH_2$ bond is also quite weak, and both are involved in decomposition. At low temperatures, most of the decomposition products are nonvolatile, though above 660 K main chain scissions lead to monomer and some dimer and trimer production. Nylon 6–6 is less stable than nylon 6–10, due to the ring closure tendency of the adipic acid component. At 675 K, if products are removed, gelation and discoloration begin.

Aromatic polyamides have good thermal stability, as exemplified by Nomex, which is generally stable in air to 725 K. The major gaseous products of decomposition at low temperatures are water and carbon oxides. At higher temperatures, carbon monoxide, benzene, hydrogen cyanide (HCN), toluene, and benzonitrile are produced. Above 825 K, hydrogen and ammonia are formed. The remaining residue is highly cross-linked.

Wool: On decomposition of wool, a natural polyamide, approximately 30 percent is left as a residue. The first step in decomposition is the loss of water. Around 435 K, some cross-linking of amino acids occurs. Between 485 and 565 K, the disulphide bond in the amino acid cystine is cleaved with carbon disulphide and carbon dioxide being evolved. Pyrolysis at higher temperatures (873 to 1198 K) yields large amounts of hydrogen cyanide, benzene, toluene, and carbon oxides.

Polyurethanes As a class, polyurethanes do not break down below 475 K, and air tends to slow decomposition. The production of hydrogen cyanide and carbon monoxide increases with the pyrolysis temperature. Other toxic products formed include nitrogen oxides, nitriles, and tolylene diisocyanate (TDI) (and other isocyanates). A major breakdown mechanism in urethanes is the scission of the polyol–isocyanate bond formed during polymerization. The isocyanate vaporizes and recondenses as a smoke, and liquid polyol remains to further decompose.

Polydienes and Rubbers

Polyisoprene: Synthetic rubber or polyisoprene decomposes by random-chain scission with intramolecular hydrogen transfer. This, of course, gives small yields of monomer. Other polydienes appear to decompose similarly though the thermal stability can be considerably different. The average size of fragments collected from isoprene decomposition are 8 to 10 monomer units long. This supports the theory that random-chain scission and intermolecular transfer reactions are dominant in the decomposition mechanism. In nitrogen, decomposition begins at 475 K. At temperatures above 675 K, increases in monomer yield are attributable to secondary reaction of volatile products to form monomer. Between 475 and 575 K, low molecular weight material is formed, and the residual material is progressively more insoluble and intractable. Preheating at between 475 and 575 K lowers the monomer yield at higher temperatures. Decomposition at less than 575 K results in a viscous liquid and, ultimately, a dry solid. The monomer is prone to dimerize to dipentene as it cools. There seems to be little significant difference in the decomposition of natural rubber and synthetic polyisoprene.

Polybutadiene: Polybutadiene is more thermally stable than polyisoprene due to the lack of branching. Decomposition at 600 K can lead to monomer yields of up to 60 percent, with lower conversions at higher temperatures. Some cyclization occurs in the products. Decomposition in air at 525 K leads to a dark impermeable crust, which excludes further air. Continued heating hardens the elastomer.

Polychloroprene: Polychloroprene decomposes in a manner similar to PVC, with initial evolution of hydrogen chloride at around 615 K and subsequent breakdown of the residual polyene. The sequences of the polyene are typically around three (trienes), much shorter than PVC. Polychloroprene melts at around 50°C.

Cellulosics

The decomposition of cellulose involves at least four processes in addition to simple desorption of physically bound water. The first is the cross-linking of cellulose chains, with the evolution of water (dehydration). The second concurrent reaction is the unzipping of the cellulose chain. Laevoglucosan is formed from the monomer unit. (See Figure 1-7.10.) The third reaction is the decomposition of the dehydrated product (dehydrocellulose) to yield char and volatile products. Finally, the laevoglucosan can further decompose to yield smaller volatile products, including tars and, eventually, carbon monoxide. Some laevoglucosan may also repolymerize.

Below 550 K, the dehydration reaction and the unzipping reaction proceed at comparable rates, and the basic skeletal structure of the cellulose is retained. At higher temperatures, unzipping is faster, and the original structure of the cellulose begins to disappear. The cross-linked dehydrated cellulose and the repolymerized laevoglucosan begin to yield polynuclear aromatic structures, and graphite carbon structures form at around 770 K. It is well known that the char yield is quite dependent on the rate of heating of the sample. At very high rates of heating, no char is formed. On the other hand, preheating the sample at 520 K will lead to 30 percent char yields. This is due both to the importance of the low-temperature dehydration reactions for ultimate char formation and the increased opportunity for repolymerization of laevoglucosan that accompanies slower heating rates.

Wood is made up of 50 percent cellulose, 25 percent hemicellulose, and 25 percent lignin. The yields of gaseous products and kinetic data indicate that the decomposition may be regarded as the superposition of the individual constituent's decomposition mechanisms. On heating, the hemicellulose decomposes first (475 to 535

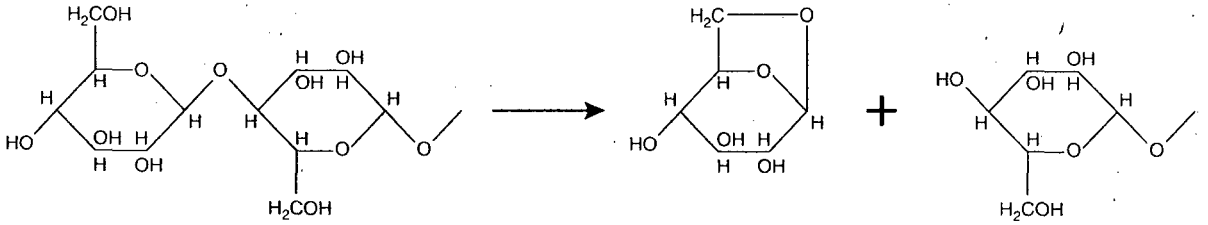

Figure 1-7.10. ***Formation of laevoglucosan from cellulose.***

K), followed by cellulose (525 to 625 K), and lignin (555 to 775 K). The decomposition of lignin contributes significantly to the overall char yield. Piloted ignition of woods due to radiative heating has been observed at a surface temperature of 620 to 650 K.

Polysulfides and Polysulphones

Polysulfides are generally stable to 675 K. Poly(1, 4 phenylene sulfide) decomposes at 775 K. Below this temperature, the principal volatile product is hydrogen sulfide. Above 775 K, hydrogen, evolved in the course of cross-linking, is the major volatile product. In air, the gaseous products include carbon oxides and sulfur dioxide.

The decomposition of polysulphones is analogous to polycarbonates. Below 575 K, decomposition is by heteroatom bridge cleavage, and above 575 K, sulfur dioxide is evolved from the polymer backbone.

Thermally Stable Polymers

The development of thermally stable polymers is an area of extensive ongoing interest. Relative to many other materials, polymers have fairly low use temperatures, which can reduce the utility of the product. This probable improvement in fire properties is, often, counterbalanced by a decrease in processability and in favorable physical properties. Of course, materials that are stable at high temperatures are likely to be better performers as far as fire properties are concerned. The high- temperature physical properties of polymers can be improved by increasing interactions between polymer chains or by chain-stiffening.

Chain interactions can be enhanced by several means. As noted previously, crystalline materials are more stable than their amorphous counterparts as a result of chain interactions. Of course, if a material melts before volatilization occurs, this difference will not affect chemical decomposition. Isotactic polymers are more likely to be crystalline due to increased regularity of structure. Polar side groups can also increase the interaction of polymer chains. The melting point of some crystalline polymers is shown in Table 1-7.1.

The softening temperature can also be increased by chain-stiffening. This is accomplished by the use of aromatic or heterocyclic structures in the polymer backbone. Some aromatic polymers are shown in Figure 1-7.11. Poly(p-phenylene) is quite thermally stable but is brittle, insoluble, and infusible. Thermal decomposition begins at 870 to 920 K; and up to 1170 K, only 20 to 30 percent of the original weight is lost. Introduction of the following groups:

$$-O-, -CO-, -NH-, -CH_2-, -O-CO-, -O-CO-O-$$

into the chain can improve workability though at the cost of some loss of oxidative resistance. Poly(p-xylene) melts at 675 K and has good mechanical properties though it is insoluble and cannot be thermoprocessed. Substitution of halogen, acetyl, alkyl, or ester groups on aromatic rings can help the solubility of these polymers at the expense of some stability. Several relatively thermostable polymers can be formed by condensation of bisphenol A with a second reagent. Some of these are shown in Figure 1–7.12. The stability of such polymers can be improved if aliphatic groups are not included in the backbone, as the $-C(CH_3)_2-$ groups are weak links.

Other thermostable polymers include ladder polymers and extensively cross-linked polymers. Cyclized PAN is an example of a ladder polymer where two chains are periodically interlinked. Other polymers, such as rigid polyurethanes, are sufficiently cross-linked so that it becomes impossible to speak of a molecular weight or

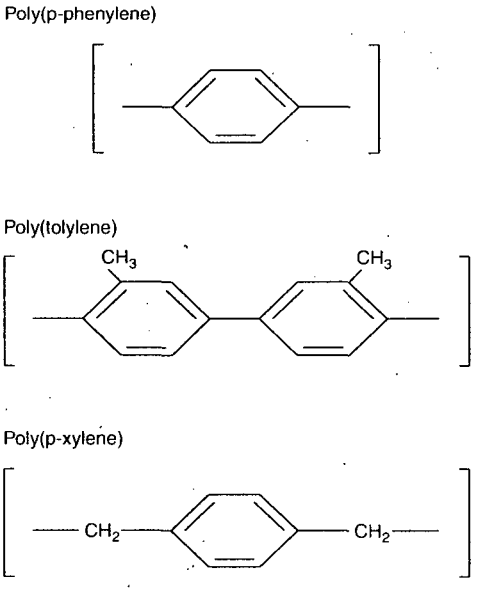

Figure 1-7.11. ***Thermostable aromatic polymers.***

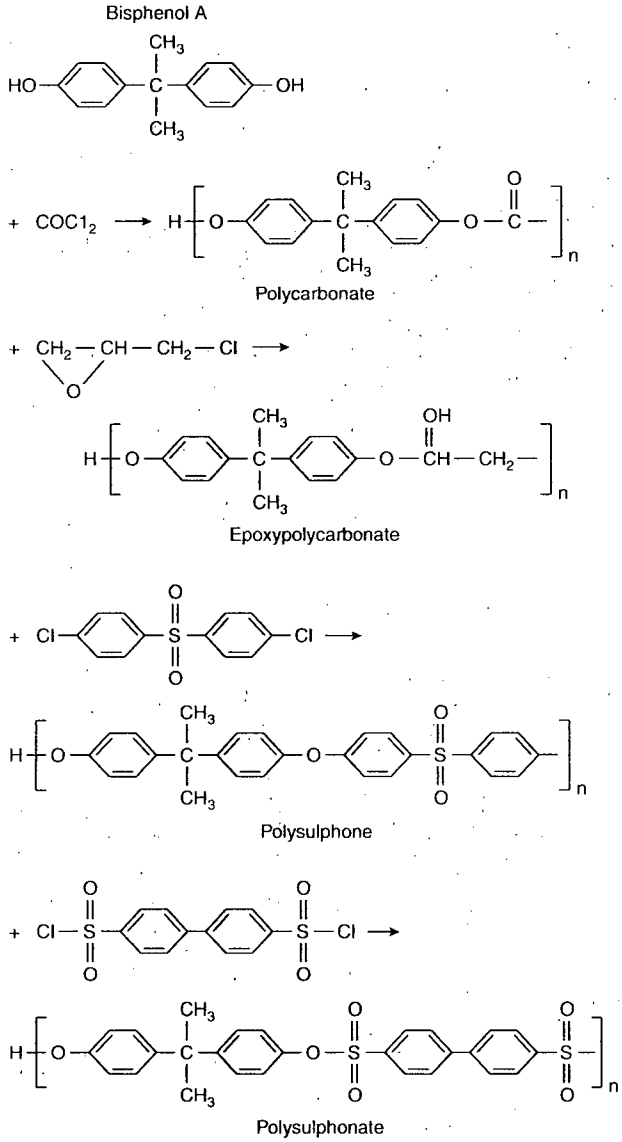

Figure 1-7.12. ***Bisphenol A polymers.***

definitive molecular repeating structure. As in polymers that gel or cross-link during decomposition, cross-linking of the original polymer yields a carbonized char residue upon decomposition, which can be oxidized at temperatures over 775 K.

References Cited

1. ASTM E 176, "Standard Terminology of Fire Standards," in *Annual Book of ASTM Standards*, Vol. 4.07, American Society for Testing and Materials, West Conshohocken, PA.
2. C.F. Cullis and M.M. Hirschler, *The Combustion of Organic Polymers*, Oxford University Press, Oxford, UK (1981).
3. E.D. Weil, R.N. Hansen, and N. Patel, "Prospective Approaches to More Efficient Flame-Retardant Systems," in *Fire and Polymers: Hazards Identification and Prevention* (G.L. Nelson, ed.), ACS Symposium Series 425, Developed from *Symp.* at 197th. ACS Mtg. Dallas, TX. April 1989, Chapter 8, p. 97–108, Amer. Chem. Soc., Washington, DC (1990).
4. M.M. Hirschler, "Recent Developments in Flame-Retardant Mechanisms," in *Developments in Polymer Stabilisation*, Vol. 5, (G. Scott, ed.), pp. 107–52, Applied Science Publ., London (1982).
5. D.E. Stuetz, A.H. DiEdwardo, F. Zitomer, and B.F. Barnes, "Polymer Flammability II," in *J. Polym. Sci., Polym. Chem. Ed.*, 18, pp. 987–1009 (1980).
6. T. Kashiwagi and T.J. Ohlemiller, "A Study of Oxygen Effects on Flaming Transient Gasification of PMMA and PE during Thermal Irradiation," in *Nineteenth Symp. (Int.) on Combustion*, The Combustion Institute, Pittsburgh, pp. 1647–54 (1982).
7. T. Kashiwagi, T. Hirata, and J.E. Brown, "Thermal and Oxidative Degradation of Poly(methyl methacrylate), Molecular Weight," *Macromolecules*, 18, pp. 131–138 (1985).
8. T. Hirata, T. Kashiwagi, and J.E. Brown, "Thermal and Oxidative Degradation of Poly(methyl methacrylate), Weight Loss," *Macromolecules*, 18, pp. 1410–1418 (1985).
9. T. Kashiwagi, A. Inabi, J.E. Brown, K. Hatada, T. Kitayama, and E. Masuda, "Effects of Weak Linkages on the Thermal and Oxidative Degradation of Poly(methyl methacrylates)," *Macromolecules*, 19, pp. 2160–2168 (1986).
10. T. Kashiwagi and A. Inabi, "Behavior of Primary Radicals during Thermal Degradation of Poly(methyl methacrylate)," *Polymer Degradation and Stability*, 26, pp. 161–184 (1989).
11. S.K. Brauman, "Polymer Degradation during Combustion," *J. Polymer Sci.*, B, 26, pp. 1159–71 (1988).
12. P. Gijsman, J. Hennekens, and J. Vincent, "The Mechanism of the Low-Temperature Oxidation of Polypropylene," *Polymer Degradation and Stability*, 42, pp. 95–105 (1993).
13. M.M. Hirschler, "Effect of Oxygen on the Thermal Decomposition of Poly(vinylidene fluoride)," *Europ. Polymer J.*, 18, pp. 463–67 (1982).
14. A. Inabi and T. Kashiwagi, "A Calculation of Thermal Degradation Initiated by Random Scission, Unsteady Radical Concentration," *Eur. Polym. J.*, 23, 11, pp. 871–881 (1987).
15. T. Kashiwagi and H. Nambu, "Global Kinetic Constants for Thermal Oxidative Degradation of a Cellulosic Paper," *Combust. Flame*, 88, pp. 345–68 (1992).
16. K.D. Steckler, T. Kashiwagi, H.R. Baum, and K. Kanemaru, "Analytical Model for Transient Gasification of Noncharring Thermoplastic Materials," in *Fire Safety Sci., Proc. Third Int. Symp.* (G. Cox and B. Langford, eds.) Elsevier, London (1991).
17. ASTM D 2859, "Standard Test Method for Flammability of Finished Textile Floor Covering Materials," in *Annual Book of ASTM Standards*, Vol. 7.01, American Society for Testing and Materials, West Conshohocken, PA.
18. CFR 1630, 16 CFR Part 1630, "Standard for the Surface Flammability of Carpets and Rugs (FF 1-70)," *Code of Federal Regulations, Commercial Practices, Subchapter D: Flammable Fabrics Act Regulations*, Vol. 16, Part 1602–1632, pp. 697–706 (2000).
19. CFR 1631, 16 CFR Part 1631, "Standard for the Surface Flammability of Small Carpets and Rugs (FF 2-70)," in *Code of Federal Regulations, Commercial Practices, Subchapter D: Flammable Fabrics Act Regulations*, Vol. 16, Parts 1602–1632, pp. 706–715 (2000).
20. L.A. Chandler, M.M. Hirschler, and G.F. Smith, "A Heated Tube Furnace Test for the Emission of Acid Gas from PVC Wire Coating Materials: Effects of Experimental Procedures and Mechanistic Considerations," *Europ. Polymer J.*, 23, pp. 51–61 (1987).

21. M.M. Hirschler, "Thermal Decomposition (STA and DSC) of Poly(vinyl chloride) Compounds under a Variety of Atmospheres and Heating Rates," *Europ. Polymer J.*, 22, pp. 153–60 (1986).
22. C.F. Cullis and M.M. Hirschler, "The Significance of Thermoanalytical Measurements in the Assessment of Polymer Flammability," *Polymer*, 24, pp. 834–40 (1983).
23. M.M. Hirschler, "Thermal Analysis and Flammability of Polymers: Effect of Halogen-Metal Additive Systems," *Europ. Polymer J.*, 19, pp. 121–9 (1983).
24. I.C. McNeill, "The Application of Thermal Volatilization Analysis to Studies of Polymer Degradation," in *Developments in Polymer Degradation*, Vol. 1 (N. Grassie, ed.), p. 43, Applied Science, London (1977).
25. C.F. Cullis, M.M. Hirschler, R.P. Townsend, and V. Visanuvimol, "The Pyrolysis of Cellulose under Conditions of Rapid Heating," *Combust. Flame*, 49, pp. 235–48 (1983).
26. C.F. Cullis, M.M. Hirschler, R.P. Townsend, and V. Visanuvimol, "The Combustion of Cellulose under Conditions of Rapid Heating," *Combust. Flame*, 49, pp. 249–54 (1983).
27. C.F. Cullis, D. Goring, and M.M. Hirschler, "Combustion of Cigarette Paper under Conditions Similar to Those during Smoking," Chichester, UK (1984). *Cellucon '84* (Macro Group U.K.), Wrexham (Wales), Chapter 35, pp. 401–10, Ellis Horwood, Chichester, UK (1984).
28. P.J. Baldry, C.F. Cullis, D. Goring, and M.M. Hirschler, "The Pyrolysis and Combustion of Cigarette Constituents," in *Proc. Int. Conf. on "Physical and Chemical Processes Occurring in a Burning Cigarette,"* R.J. Reynolds Tobacco Co., Winston-Salem, NC, pp. 280–301 (1987).
29. P.J. Baldry, C.F. Cullis, D. Goring, and M.M. Hirschler, "The Combustion of Cigarette Paper," *Fire and Materials*, 12, pp. 25–33 (1988).
30. L. Reich and S.S. Stivala, *Elements of Polymer Degradation*, McGraw-Hill, New York (1971).
31. A.A. Miroshnichenko, M.S. Platitsa, and T.P. Nikolayeva, "Technique for Calculating the Temperature at the Beginning and End of Polymer Thermal Degradation from Structural Data," in *Polymer Science* (USSR) 30, 12, pp. 2707–16 (1988).
32. O.F. Shlenskii and N.N. Lyasnikova, "Predicting the Temperature of Thermal Decomposition of Linear Polymers," *Intern. Polymer Sci. Technol.*, 16, 3, pp. T55–T56 (1989).
33. D.W. Van Krevelen, "Thermal Decomposition" and "Product Properties, Environmental Behavior and Failure," in *Properties of Polymers*, 3rd Edition, Elsevier, Amsterdam, pp. 641–653 and 725–743 (1990).
34. D.W. Van Krevelen, "Some Basic Aspects of Flame Resistance of Polymeric Materials," *Polymer*, 16, pp. 615–620 (1975).
35. ASTM D 2863, "Standard Method for Measuring the Minimum Oxygen Concentration to Support Candle-like Combustion of Plastics (Oxygen Index)," *Annual Book of ASTM Standards*, Vol. 8.02, American Society for Testing and Materials, West Conshohocken, PA.
36. E.D. Weil, M.M. Hirschler, N.G. Patel, M.M. Said, and S. Shakir, "Oxygen Index: Correlation to Other Tests," *Fire Materials*, 16, pp. 159–67 (1992).
37. ASTM E 1354, "Standard Test Method for Heat and Visible Smoke Release Rates for Materials and Products Using an Oxygen Consumption Calorimeter," in *Annual Book of ASTM Standards*, Volume 4.07, American Society for Testing and Materials, West Conshohocken, PA.
38. M.M. Hirschler, "Heat Release from Plastic Materials," Chapter 12a in *Heat Release in Fires* (V. Babrauskas and S.J. Grayson, eds.), Elsevier, London (1992).
39. R.E. Lyon, "Fire-Safe Aircraft Materials" in Fire and Materials, Proceeding 3rd Int. Conference and Exhibition, Crystal City, VA, Interscience Communications, pp. 167–177 (1994).
40. N. Grassie, "Polymer Degradation and Fire Hazard," *Polymer Degradation and Stability*, 30, pp. 3–12 (1990).
41. G. Camino and L. Costa, "Performance and Mechanisms of Fire Retardants in Polymers—A Review," *Polymer Degradation and Stability*, 20, pp. 271–294 (1988).
42. G. Bertelli, L. Costa, S. Fenza, F.E. Marchetti, G. Camino, and R. Locatelli, "Thermal Behaviour of Bromine-Metal Fire Retardant Systems," *Polymer Degradation and Stability*, 20, pp. 295–314 (1988).
43. L.H. Lee, *J. Polymer Sci.*, 3, p. 859 (1965).
44. R.T. Conley, ed., *Thermal Stability of Polymers*, Marcel Dekker, New York (1970).
45. W.J. Roff and J.R. Scott, *Fibres, Films, Plastics, and Rubbers*, Butterworths, London (1971).
46. F.A. Williams, in *Heat Transfer in Fires*, Scripta, Washington, DC (1974).
47. C. David, in *Comprehensive Chemical Kinetics*, Elsevier, Amsterdam (1975).
48. S.L. Madorsky, *Thermal Degradation of Polymers*, reprinted by Robert E. Kreiger, New York (1975).
49. D.W. Van Krevelen, *Properties of Polymers*, Elsevier, Amsterdam (1976).
50. T. Kelen, *Polymer Degradation*, Van Nostrand Reinhold, New York (1983).
51. W.L. Hawkins, *Polymer Degradation and Stabilization*, Springer Verlag, Berlin (1984).
52. N. Grassie and G. Scott, *Polymer Degradation and Stabilisation*, Cambridge University Press, Cambridge, UK (1985).
53. S.M. Lomakin, J.E. Brown, R.S. Breese, and M.R. Nyden, "An Investigation of the Thermal Stability and Char-Forming Tendency of Cross-Linked Poly(methyl methacrylate)," *Polymer Degradation Stability*, 41, pp. 229–43 (1993).
54. G. Montaudo and C. Puglisi, "Evolution of Aromatics in the Thermal Degradation of Poly(vinyl chloride): A Mechanistic Study," *Polymer Degradation Stability*, 33, pp. 229–62 (1991).
55. W.H. Starnes, Jr., and D. Edelson, *Macromolecules*, 12, p. 797 (1979).
56. D. Edelson, R.M. Lum, W.D. Reents, Jr., W.H. Starnes, Jr., and L.D. Westcott, Jr., "New Insights into the Flame Retardance Chemistry of Poly(vinyl chloride)," in *Proc. Nineteenth (Int.) Symp. on Combustion*, The Combustion Institute, Pittsburgh, pp. 807–814 (1982).
57. K.S. Minsker, S.V. Klesov, V.M. Yanborisov, A.A. Berlin, and G.E. Zaikov, "The Reason for the Low Stability of Poly(vinyl chloride)—A Review," *Polymer Degradation Stability*, 16, pp. 99–133 (1986).
58. P. Simon et al., "Kinetics of Polymer Degradation Involving the Splitting off of Small Molecules, Parts 1–7," *Polymer Degradation Stability*, 29, pp. 155; 253; 263 (1990); pp. 35, 45; 157; 249 (1992); pp. 36, 85 (1992).
59. L.A. Chandler and M.M. Hirschler, "Further Chlorination of Poly(vinyl chloride): Effects on Flammability and Smoke Production Tendency," *Europ. Polymer J.*, 23, pp. 677–83 (1987).
60. G. Montaudo, C. Puglisi, and F. Samperi, "Primary Thermal Degradation Mechanisms of PET and PBT," *Polymer Degradation Stability*, 42, pp. 13–28 (1993).
61. G. Montaudo, C. Puglisi, R. Rapisardi, and F. Samperi, "Further Studies on the Thermal Decomposition Processes in Polycarbonates," *Polymer Degradation Stability*, 31, pp. 229–46 (1991).

SIGNATURE PAGE

Document Name : CHG-CAL-0002.docx

Document Title : Self-shielding Surrogate Material Evaluation for TRUPACT-II ar

Date (GMT)	Signed by
2012/09/27 15:04:13	dayb
For Department	
Justification	Author

2012/09/27 15:13:48	porters
For Department	
Justification	Independent Reviewer

2012/09/27 18:54:40	reddd
For Department	
Justification	Quality Assurance

2012/09/27 19:23:25	lastram
For Department	
Justification	Independent Reviewer

2012/09/27 20:41:49	dayb
For Department	
Justification	Project Representative

For Department	
Justification	

For Department	
Justification	

1. Document Title: Self-shielding Surrogate Material Evaluation for TRUPACT-II and HalfPACT		
2. Document Number: CHG-CAL-0002	3. Document Revision: 0	4. Page: 1 of 26

5. Summary Description

This calculation evaluates the comparable efficacy of common waste payload materials in providing self-shielding of distributed ^{137}Cs and ^{60}Co gamma sources. The study is applied to the general payload case of 55-gallon, 85-gallon, and 100-gallon drums, Standard Waste Boxes (SWB), and the Ten Drum Overpack (TDOP) in a TRUPACT-II, but the comparison is also applicable to other authorized payload containers in the TRUPACT-II and HalfPACT packagings. The evaluations consider only normal conditions of transport (NCT) geometries as NCT is the only configuration where self-shielding in distributed waste forms is credited in meeting the regulatory dose rate limits under exclusive use requirements. Particularly, the study evaluates the relative efficacy of zirconium as the waste material surrogate for other common waste material constituents (i.e., aluminum, brick, concrete, leaded glass, lead, nylon, polyethylene, carbon steel, and wood) and demonstrates that zirconium is a reasonable surrogate material to represent the dose rate attenuation due to self-shielding in contact-handled transuranic waste.

6. Software Usage

	Software Name	Version
1.	MNCP5	1.60
2.		
3.		
4.		
5.		

7. Preparer

Name	Signature	Date
Brad Day		

8. Independent Reviewer(s)

Name	Signature	Date
Steve Porter		
Michael Lastra		

9. Project Representative

Name	Signature	Date
Brad Day		

10. QA Representative

Name	Signature	Date
Dale Hood		

TABLE OF CONTENTS

LIST OF TABLES

LIST OF FIGURES

TABLE OF REVISIONS

Revision Number	Pages Affected	Revision Description
0	All	New Issue

1.0 INTRODUCTION

The TRUPACT-II and HalfPACT packages are used to transport contact-handled (CH) transuranic (TRU) waste. By definition, CH-TRU waste is restricted to require the dose rate at the surface of each payload container to be less than 200 mrem/hr. Two sets of activity limits for the packagings are established for each of the authorized payload container configurations; one set for concentrated sources and one set for distributed sources. For distributed sources, the limits are provided as a function of the limiting bulk density of the payload materials from 0.5 to 8 g/cc. Zirconium is utilized as the surrogate waste material to conservatively represent the myriad of materials that are transported in TRU waste. This calculation compares the self-shielding efficacy of the zirconium surrogate with common materials present in TRU waste for two common gamma radionuclides; namely, ^{137}Cs and ^{60}Co.

This calculation demonstrates that zirconium is a reasonable and appropriate surrogate to represent the self-shielding property of common TRU waste materials, as a function of the waste bulk density, when used in shielding models to predict the dose rate attenuation of gamma energies in distributed source configurations.

2.0 ANALYSIS MODEL

All model parameters used to compare the efficacy of zirconium to common waste materials (i.e., aluminum, brick, concrete, leaded glass, lead, nylon, polyethylene, carbon steel, and wood) were taken directly from CHG-CAL-0001[1] for the Generic payload case with a distributed waste assumption using the TRUPACT-II geometry. All calculational methodologies, with the exception of the source material specification, are identical to the shielding model that is also documented in the TRUPACT-II Safety Analysis Report[2] (SAR). MCNP5 v1.60 is used for the shielding analysis.[3] MCNP5 is a standard, well-accepted shielding program utilized to compute dose rates for shielding licenses.

2.1 Self-Shielding Materials and Source Specification

The elemental composition of each of the evaluated self-shielding materials listed in Table 2-1 was obtained from PNNL-15870[4]. The evaluated materials were each analyzed at multiple fractional densities up to the theoretical density, with zirconium being evaluated from 0.5 to 8 g/cc as in the TRUPACT-II SAR shielding analysis.

Based on the assumed bulk density of the waste contents, the height of the source in the TRUPACT-II was adjusted to retain the inside diameter of the payload cavity and satisfy the authorized maximum gross weight of the payload contents. This approach ensures that the primary factor influencing the dose rate is material attenuation for a source that is axially shrinking as density is increased rather than distance attenuation for a source that is radially shrinking as density is increased. Figure 2-1 shows the shielding model with a 0.5 g/cc source and Figure 2-2 shows the shielding model with an 8 g/cc source. Two radionuclides, ^{137}Cs and ^{60}Co, were chosen for evaluation with unit source strength of 1 gamma/second (γ/s). The source energies and intensities are provided in Table 2-2.[5]

---

[1] B. A. Day, *TRUPACT-II and HalfPACT Shielding Analysis*, CHG-CAL-0001, Rev. 2, Washington TRU Solutions LLC, Carlsbad, NM, September 2012.

[2] U.S. Department of Energy (DOE), *TRUPACT-II Safety Analysis Report*, USNRC Certificate of Compliance 71-9218, U.S. Department of Energy, Carlsbad Area Office, Carlsbad, New Mexico.

[3] LA-CP-03-0245, *MCNP – A General Monte Carlo N-Particle Transport Code, Version 5, Vol. 2: User's Guide*, Los Alamos National Laboratory, February 2008.

[4] R.G. Williams III, et. al., *Compendium of Material Composition Data for Radiation Transport Modeling*, PNNL-15870, Pacific Northwest National Laboratory, April 2006.

[5] R.R. Kinsey, et al., *The NUDAT/PCNUDAT Program for Nuclear Data*, paper submitted to the 9th International Symposium of Capture Gamma-Ray Spectroscopy and Related Topics, Budapest, Hungary, October 1996; data extracted from the NUDAT database, version September 7, 2000, CD-ROM.

Table 2-1 – Evaluated Self-Shielding Materials

Material	Theoretical Density (g/cc)	MCNP Material Card
Aluminum	2.6989	13000 -1.000000
Brick (Silica)	1.80	8000 -0.524858 13000 -0.005227 14000 -0.449011 20000 -0.014419 26000 -0.007213
Concrete (Ordinary)	2.30	1000 -0.022100 6000 -0.002484 8000 -0.574930 11000 -0.015208 12000 -0.001266 13000 -0.019953 14000 -0.304627 19000 -0.010045 20000 -0.042951 26000 -0.006435
Glass (Lead)	6.22	8000 -0.156453 14000 -0.080866 22000 -0.008092 33000 -0.002651 82000 -0.751938
Lead	11.35	82000 -1.000000
Nylon (Type 6)	1.14	1000 -0.097976 6000 -0.636856 7000 -0.123779 8000 -0.141389
Polyethylene (Normal)	0.93	1000 -0.143716 6000 -0.856284
Steel (Carbon)	7.82	6000 -0.005 26000 -0.995
Wood (Southern Pine)	0.650	1000 -0.057889 6000 -0.482667 8000 -0.459444
Zirconium	6.506	40000 -1.000000

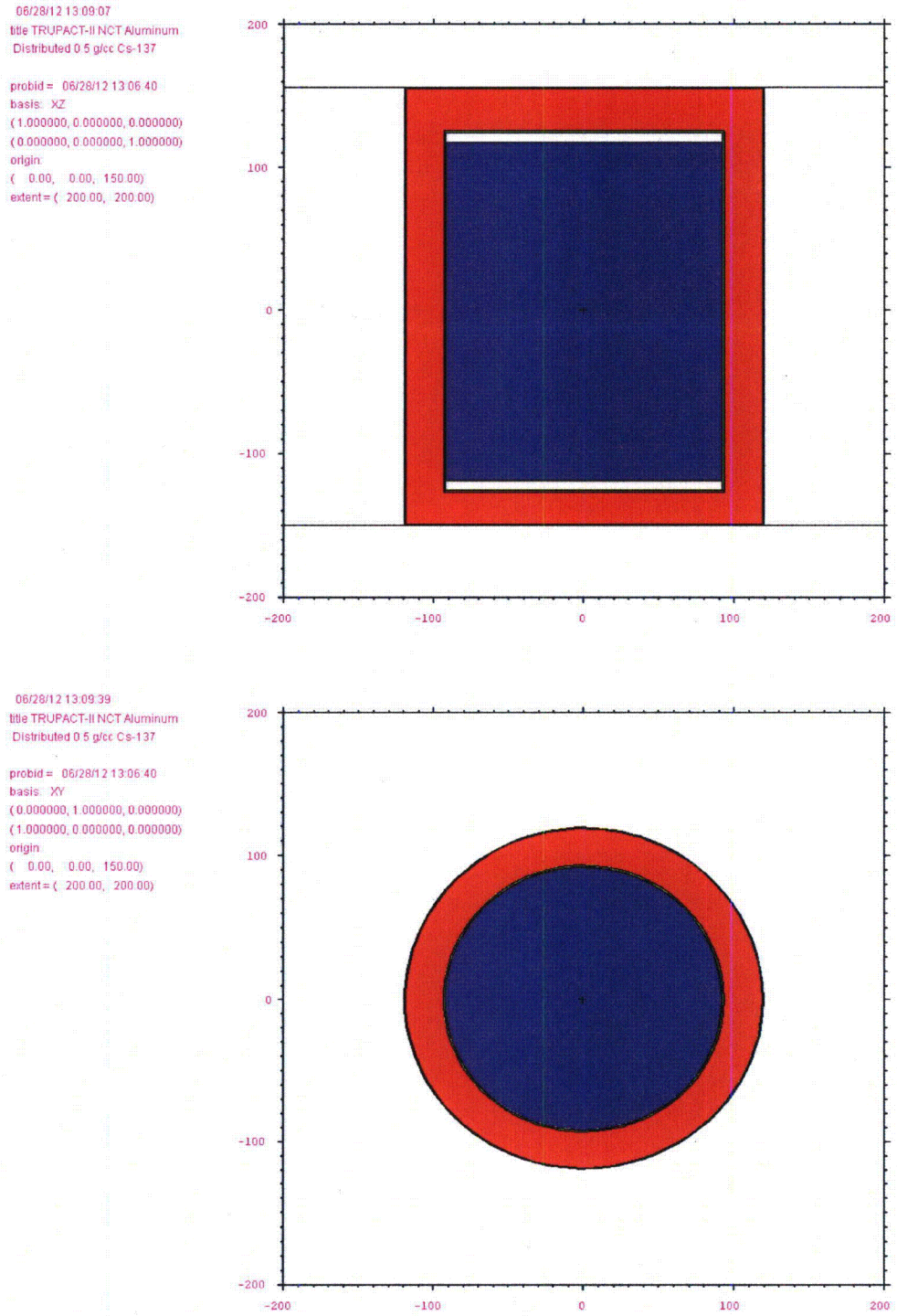

Figure 2-1 – TRUPACT-II with 0.5 g/cc Distributed Source

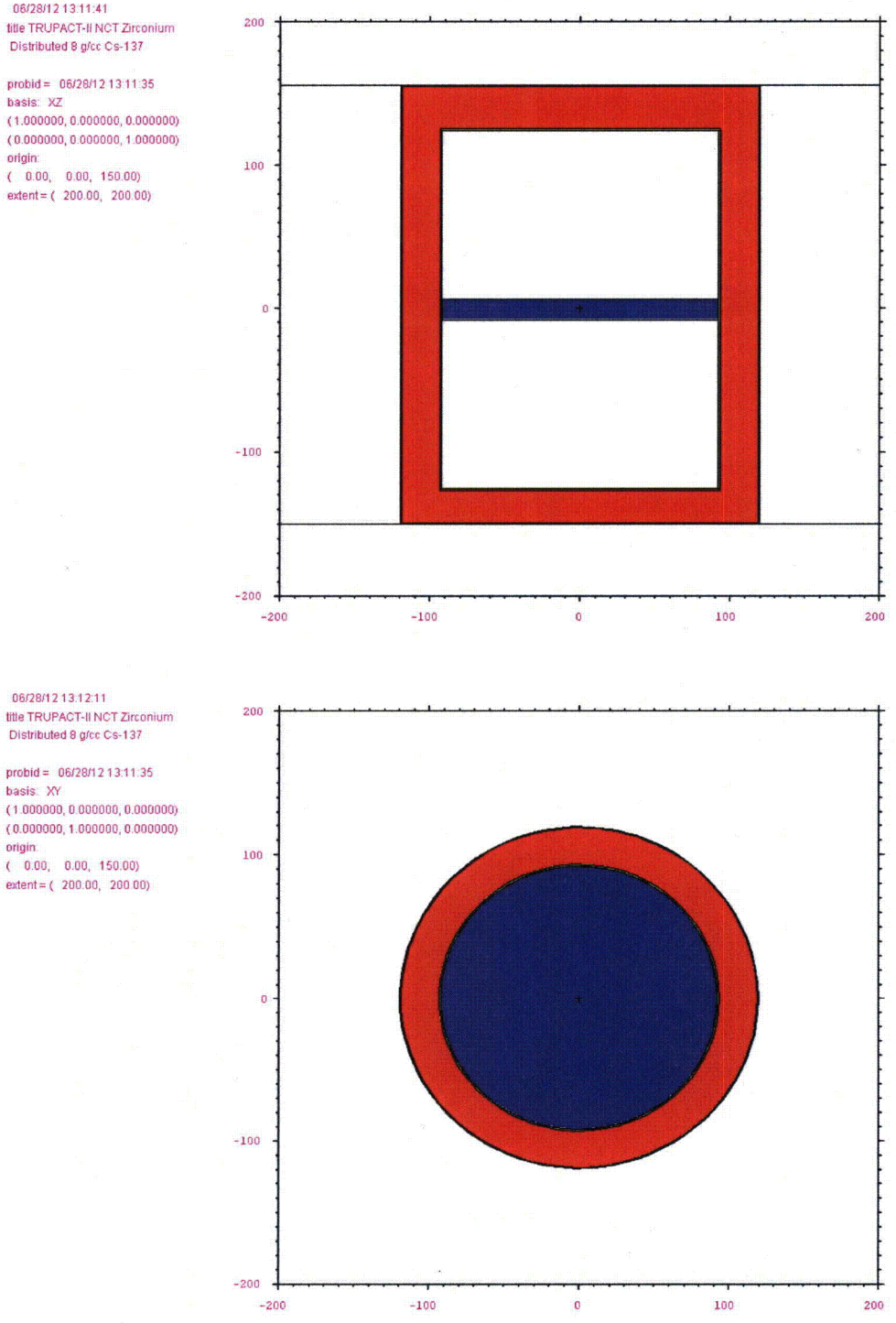

Figure 2-2 – TRUPACT-II with 8 g/cc Distributed Source

Table 2-2 – Gamma Source Data

Radionuclide	Photon Energy (MeV)	Intensity (%)
^{137}Cs	2.835000E-01	5.800000E-04
	6.616570E-01	8.510000E+01
^{60}Co	3.469300E-01	7.600000E-03
	8.262800E-01	7.600000E-03
	1.173237E+00	9.997360E+01
	1.332501E+00	9.998560E+01
	2.158770E+00	1.110000E-03
	2.505000E+00	2.000000E-06

3.0 RESULTS

The dose rates due to ^{60}Co and ^{137}Cs distributed sources at the surface and at 2-meters from the surface of the TRUPACT-II were determined for all of the self-shielding materials at a range of fractional densities up to the theoretical density for each material. All results passed the MCNP statistical checks with a tally error less than 0.4%. As the 2-meter dose rate is limiting by a large margin for both NCT and Hypothetical Accident Condition (HAC) dose rate compliance, the 2-meter results are of primary importance in comparing the relative efficacy of the waste materials analyzed to the zirconium surrogate.

As shown in Figure 3-1 and Figure 3-2, the highest dose rates are associated with the self-shielding materials with the least efficacy. Zirconium is seen to be a conservative surrogate to represent the self-shielding properties of TRU waste with a high-energy, ^{60}Co, gamma source term as it results in the highest dose rates and provides the least amount of gamma dose rate attenuation at 2-meters in comparison to the other common TRU waste materials. For the ^{137}Cs source term, the dose rates at 2-meters are all reasonably within 6% of the highest calculated values determined for aluminum and/or steel. The numerical results for all evaluations are summarized in Table 3-1 and Table 3-2.

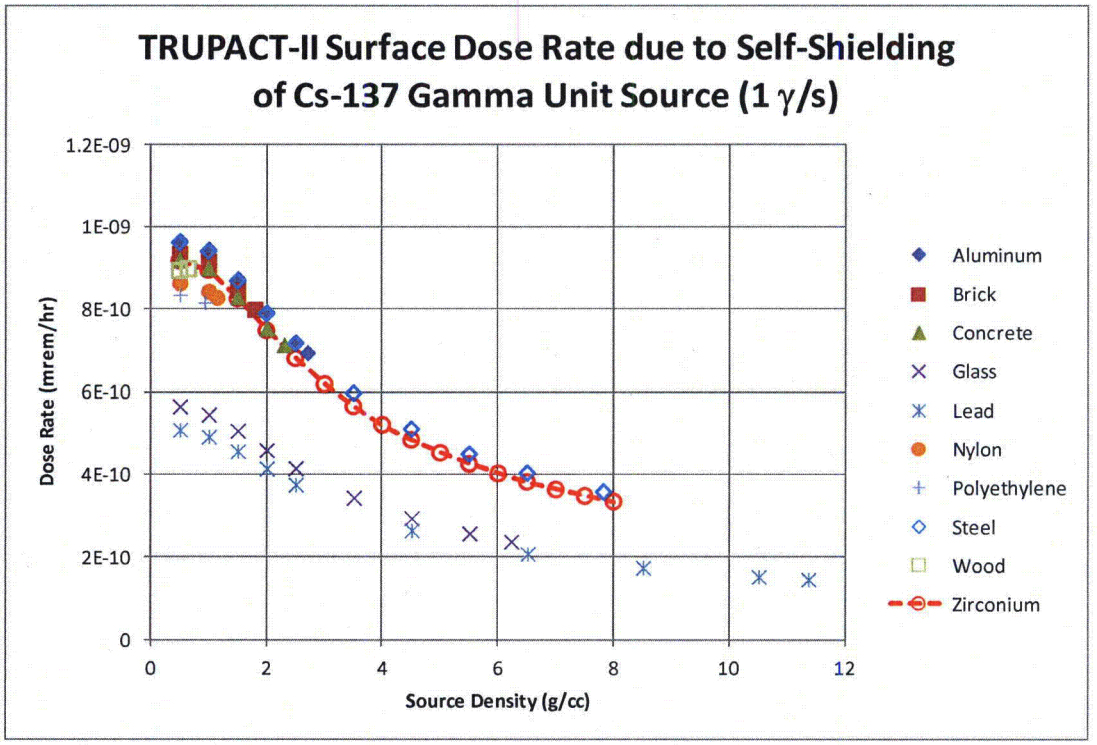

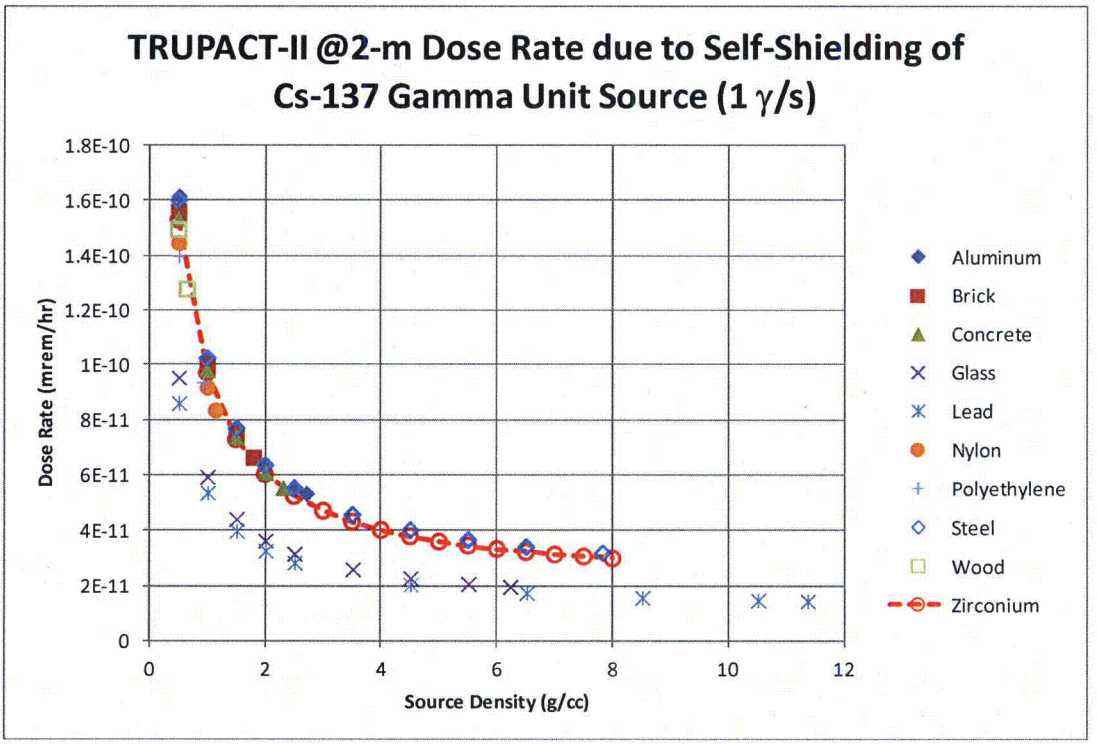

Figure 3-1 – ^{137}Cs Dose Rate Comparison

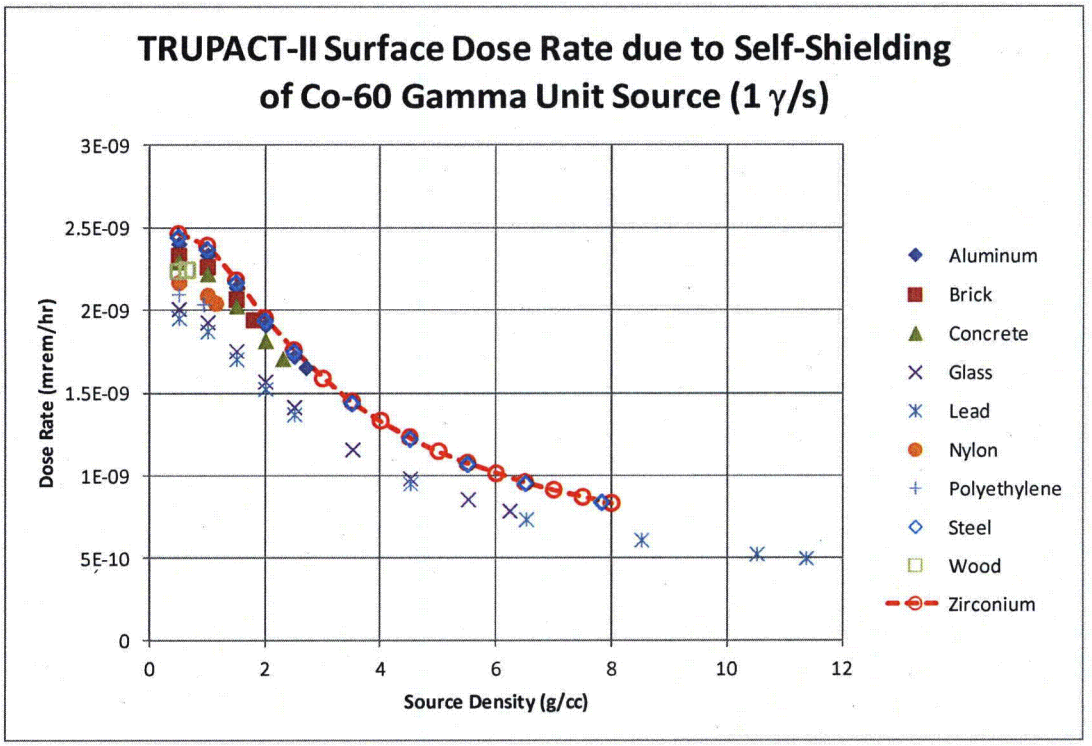

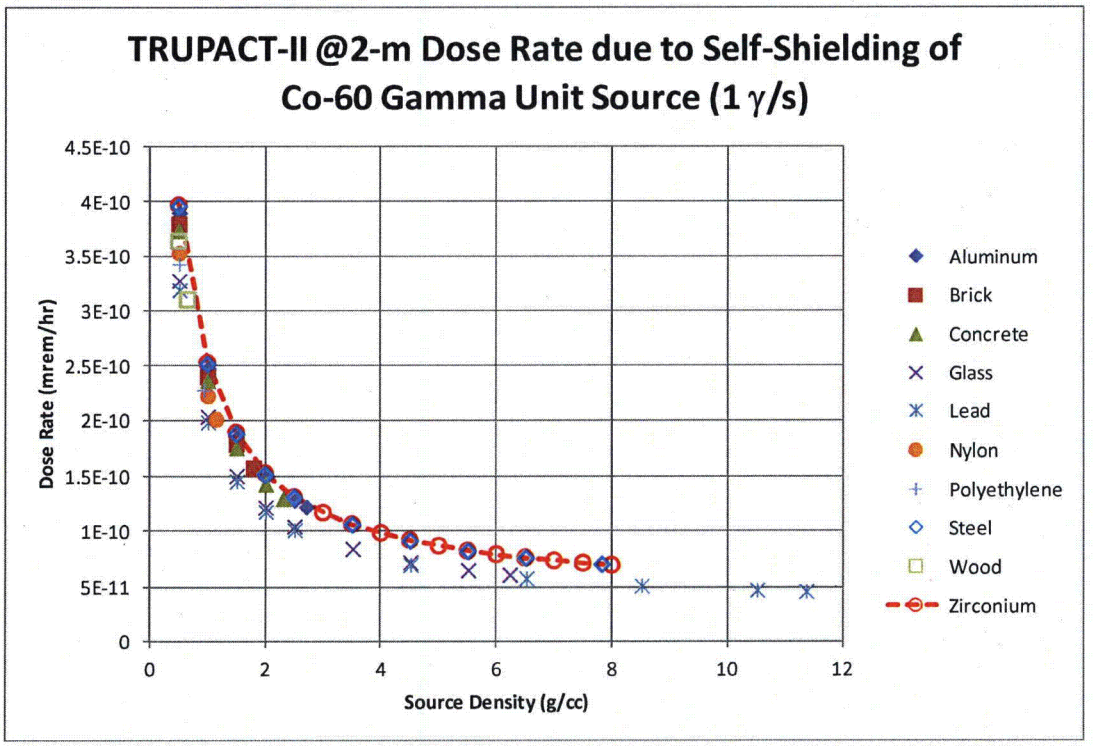

Figure 3-2 – ^{60}Co Dose Rate Comparison

Table 3-1 – TRUPACT-II – Distributed ^{137}Cs Source Dose Rates

Case	Material	Source Density (g/cc)	Dose Rate at Surface (mrem/hr)	Dose Rate at 2-meters (mrem/hr)
csa100.i	Aluminum	0.5	9.66E-10	1.62E-10
csa101.i	Aluminum	1	9.45E-10	1.03E-10
csa102.i	Aluminum	1.5	8.74E-10	7.75E-11
csa103.i	Aluminum	2	7.93E-10	6.41E-11
csa104.i	Aluminum	2.5	7.20E-10	5.57E-11
csa105.i	Aluminum	2.6989	6.94E-10	5.34E-11
csb100.i	Brick	0.5	9.35E-10	1.56E-10
csb101.i	Brick	1	9.17E-10	1.00E-10
csb102.i	Brick	1.5	8.46E-10	7.50E-11
csb103.i	Brick	1.8	8.00E-10	6.66E-11
csc100.i	Concrete	0.5	9.19E-10	1.54E-10
csc101.i	Concrete	1	9.00E-10	9.83E-11
csc102.i	Concrete	1.5	8.30E-10	7.39E-11
csc103.i	Concrete	2	7.53E-10	6.11E-11
csc104.i	Concrete	2.3	7.13E-10	5.55E-11
csg100.i	Glass	0.5	5.65E-10	9.55E-11
csg101.i	Glass	1	5.46E-10	5.94E-11
csg102.i	Glass	1.5	5.07E-10	4.42E-11
csg103.i	Glass	2	4.60E-10	3.64E-11
csg104.i	Glass	2.5	4.15E-10	3.17E-11
csg105.i	Glass	3.5	3.45E-10	2.61E-11
csg106.i	Glass	4.5	2.96E-10	2.29E-11
csg107.i	Glass	5.5	2.59E-10	2.08E-11
csg108.i	Glass	6.22	2.39E-10	1.97E-11
csl100.i	Lead	0.5	5.09E-10	8.62E-11
csl101.i	Lead	1	4.93E-10	5.37E-11
csl102.i	Lead	1.5	4.57E-10	4.00E-11
csl103.i	Lead	2	4.14E-10	3.29E-11
csl104.i	Lead	2.5	3.75E-10	2.85E-11

Case	Material	Source Density (g/cc)	Dose Rate at Surface (mrem/hr)	Dose Rate at 2-meters (mrem/hr)
csl105.i	Lead	4.5	2.67E-10	2.05E-11
csl106.i	Lead	6.5	2.09E-10	1.74E-11
csl107.i	Lead	8.5	1.75E-10	1.58E-11
csl108.i	Lead	10.5	1.53E-10	1.47E-11
csl109.i	Lead	11.35	1.46E-10	1.44E-11
csn100.i	Nylon	0.5	8.64E-10	1.45E-10
csn101.i	Nylon	1	8.44E-10	9.20E-11
csn102.i	Nylon	1.14	8.29E-10	8.37E-11
csp100.i	Polyethylene	0.5	8.35E-10	1.40E-10
csp101.i	Polyethylene	0.93	8.16E-10	9.38E-11
css100.i	Steel	0.5	9.61E-10	1.60E-10
css101.i	Steel	1	9.40E-10	1.02E-10
css102.i	Steel	1.5	8.68E-10	7.68E-11
css103.i	Steel	2	7.88E-10	6.36E-11
css104.i	Steel	2.5	7.16E-10	5.53E-11
css105.i	Steel	3.5	5.97E-10	4.56E-11
css106.i	Steel	4.5	5.11E-10	4.02E-11
css107.i	Steel	5.5	4.49E-10	3.66E-11
css108.i	Steel	6.5	4.03E-10	3.41E-11
css109.i	Steel	7.82	3.57E-10	3.19E-11
csw100.i	Wood	0.5	8.93E-10	1.49E-10
csw101.i	Wood	0.65	8.98E-10	1.28E-10
csz100.i	Zirconium	0.5	9.17E-10	1.53E-10
csz101.i	Zirconium	1	8.94E-10	9.72E-11
csz102.i	Zirconium	1.5	8.26E-10	7.29E-11
csz103.i	Zirconium	2	7.48E-10	6.03E-11
csz104.i	Zirconium	2.5	6.80E-10	5.24E-11
csz105.i	Zirconium	3	6.18E-10	4.71E-11
csz106.i	Zirconium	3.5	5.65E-10	4.31E-11
csz107.i	Zirconium	4	5.21E-10	4.02E-11

Case	Material	Source Density (g/cc)	Dose Rate at Surface (mrem/hr)	Dose Rate at 2-meters (mrem/hr)
csz108.i	Zirconium	4.5	4.84E-10	3.79E-11
csz109.i	Zirconium	5	4.52E-10	3.60E-11
csz110.i	Zirconium	5.5	4.25E-10	3.46E-11
csz111.i	Zirconium	6	4.02E-10	3.33E-11
csz112.i	Zirconium	6.5	3.82E-10	3.23E-11
csz113.i	Zirconium	7	3.63E-10	3.14E-11
csz114.i	Zirconium	7.5	3.48E-10	3.07E-11
csz115.i	Zirconium	8	3.35E-10	3.00E-11

Table 3-2 – TRUPACT-II – Distributed ^{60}Co Source Dose Rates

Case	Material	Source Density (g/cc)	Dose Rate at Surface (mrem/hr)	Dose Rate at 2-meters (mrem/hr)
coa100.i	Aluminum	0.5	2.40E-09	3.90E-10
coa101.i	Aluminum	1	2.34E-09	2.48E-10
coa102.i	Aluminum	1.5	2.14E-09	1.85E-10
coa103.i	Aluminum	2	1.91E-09	1.50E-10
coa104.i	Aluminum	2.5	1.72E-09	1.29E-10
coa105.i	Aluminum	2.6989	1.66E-09	1.23E-10
cob100.i	Brick	0.5	2.33E-09	3.80E-10
cob101.i	Brick	1	2.26E-09	2.40E-10
cob102.i	Brick	1.5	2.07E-09	1.79E-10
cob103.i	Brick	1.8	1.94E-09	1.58E-10
coc100.i	Concrete	0.5	2.30E-09	3.74E-10
coc101.i	Concrete	1	2.22E-09	2.37E-10
coc102.i	Concrete	1.5	2.03E-09	1.76E-10
coc103.i	Concrete	2	1.82E-09	1.43E-10
coc104.i	Concrete	2.3	1.71E-09	1.30E-10
cog100.i	Glass	0.5	2.01E-09	3.27E-10
cog101.i	Glass	1	1.93E-09	2.04E-10
cog102.i	Glass	1.5	1.76E-09	1.51E-10
cog103.i	Glass	2	1.57E-09	1.22E-10
cog104.i	Glass	2.5	1.42E-09	1.05E-10
cog105.i	Glass	3.5	1.16E-09	8.42E-11
cog106.i	Glass	4.5	9.87E-10	7.23E-11
cog107.i	Glass	5.5	8.60E-10	6.49E-11
cog108.i	Glass	6.22	7.90E-10	6.11E-11
col100.i	Lead	0.5	1.96E-09	3.19E-10
col101.i	Lead	1	1.88E-09	1.98E-10
col102.i	Lead	1.5	1.71E-09	1.46E-10
col103.i	Lead	2	1.53E-09	1.18E-10

Case	Material	Source Density (g/cc)	Dose Rate at Surface (mrem/hr)	Dose Rate at 2-meters (mrem/hr)
col104.i	Lead	2.5	1.37E-09	1.01E-10
col105.i	Lead	4.5	9.55E-10	7.00E-11
col106.i	Lead	6.5	7.40E-10	5.77E-11
col107.i	Lead	8.5	6.15E-10	5.12E-11
col108.i	Lead	10.5	5.31E-10	4.75E-11
col109.i	Lead	11.35	5.03E-10	4.62E-11
con100.i	Nylon	0.5	2.17E-09	3.53E-10
con101.i	Nylon	1	2.09E-09	2.23E-10
con102.i	Nylon	1.14	2.04E-09	2.01E-10
cop100.i	Polyethylene	0.5	2.10E-09	3.43E-10
cop101.i	Polyethylene	0.93	2.04E-09	2.28E-10
cos100.i	Steel	0.5	2.44E-09	3.96E-10
cos101.i	Steel	1	2.37E-09	2.52E-10
cos102.i	Steel	1.5	2.16E-09	1.88E-10
cos103.i	Steel	2	1.94E-09	1.52E-10
cos104.i	Steel	2.5	1.75E-09	1.31E-10
cos105.i	Steel	3.5	1.44E-09	1.06E-10
cos106.i	Steel	4.5	1.22E-09	9.11E-11
cos107.i	Steel	5.5	1.07E-09	8.17E-11
cos108.i	Steel	6.5	9.53E-10	7.58E-11
cos109.i	Steel	7.82	8.39E-10	7.00E-11
cow100.i	Wood	0.5	2.23E-09	3.64E-10
cow101.i	Wood	0.65	2.24E-09	3.10E-10
coz100.i	Zirconium	0.5	2.46E-09	3.97E-10
coz101.i	Zirconium	1	2.39E-09	2.53E-10
coz102.i	Zirconium	1.5	2.18E-09	1.89E-10
coz103.i	Zirconium	2	1.95E-09	1.53E-10
coz104.i	Zirconium	2.5	1.76E-09	1.32E-10
coz105.i	Zirconium	3	1.59E-09	1.17E-10
coz106.i	Zirconium	3.5	1.45E-09	1.07E-10

Case	Material	Source Density (g/cc)	Dose Rate at Surface (mrem/hr)	Dose Rate at 2-meters (mrem/hr)
coz107.i	Zirconium	4	1.33E-09	9.85E-11
coz108.i	Zirconium	4.5	1.23E-09	9.20E-11
coz109.i	Zirconium	5	1.15E-09	8.68E-11
coz110.i	Zirconium	5.5	1.08E-09	8.23E-11
coz111.i	Zirconium	6	1.01E-09	7.91E-11
coz112.i	Zirconium	6.5	9.61E-10	7.61E-11
coz113.i	Zirconium	7	9.15E-10	7.36E-11
coz114.i	Zirconium	7.5	8.71E-10	7.14E-11
coz115.i	Zirconium	8	8.35E-10	6.96E-11

4.0 CONCLUSIONS

Although it is generally understood from an evaluation of mass attenuation coefficients that the amount of material attenuation typically (note: hydrogen is a notable exception) increases with increasing atomic (Z) number, the calculational results presented herein demonstrate that zirconium (Z=40) reasonably represents the common materials present in TRU waste by producing a relatively low amount of material self-attenuation for moderate to high energy gamma source terms. Other potential elemental surrogates such as lithium (Z=3) and argon (Z=18) have relatively low mass attenuation coefficients in comparison to zirconium, but are not present in dominant quantities (by mass) in TRU waste.

In comparison with the common TRU waste materials, zirconium produces the least amount of material attenuation for the ^{60}Co source term and produces very close to (within 6%) the least amount of material attenuation for the ^{137}Cs source term. Lower energy gamma source terms are not of primary importance due to the fact that the approximately 11/16-inch thickness of stainless steel in the packaging shells, along with the contact-handled dose rate requirements (≤200 mrem/hr) imposed on each payload container surface, limit the ability of lower energy gammas to significantly affect the package dose rate at 2-meters.

Due to the increasing penetration of gammas with increasing energy, it is preferential to have the surrogate material represent a conservative bound for material attenuation subject to higher gamma energies while still reasonably representing the self-shielding effects of common TRU waste materials subject to lower gamma energies. As such, zirconium is an appropriate and reasonable surrogate to represent the self-shielding properties of the common and predominant (by mass) materials present in TRU waste as it is the most conservative choice for gamma energies in excess of 1.0 MeV and it is insignificantly different from other common TRU waste materials for moderate gamma energies.

Based on a comparison of the Density Correction Factors (DCFs) reported for both the TRUPACT-II and HalfPACT in CHG-CAL-0001, which are within a few percent of one another, it is concluded that the self-shielding surrogate material evaluation results produced herein for the TRUPACT-II package apply equally to the HalfPACT package.

5.0 APPENDICES

5.1 Sample MCNP Input Files

5.1.1 TRUPACT-II – Generic

5.1.1.1 Distributed 137Cs Gamma Source with 0.5 g/cc Aluminum – csa100.i

```
title TRUPACT-II NCT Aluminum Distributed 0.5 g/cc Cs-137
C
C Cell Cards
C
1   1 -0.5        10  -20  -30                  imp:p=1  $ Source
10  0           210 -250 -230 (-10:20:30)     imp:p=2  $ ICV cavity
20  2 -8.01280  200 -210 -220                  imp:p=1  $ ICV/OCV bottom
30  2 -8.01280  250 -240 -220                  imp:p=1  $ ICV/OCV top
40  2 -8.01280  210 -250  230 -220             imp:p=4  $ ICV/OCV shell
50  3 -0.13215  110 -150 -130 (-200:220:240)  imp:p=8  $ OCA annulus
60  2 -8.01280  100 -110 -120                  imp:p=1  $ OCA bottom
70  2 -8.01280  150 -140 -120                  imp:p=1  $ OCA top
80  2 -8.01280  110 -150  130 -120             imp:p=16 $ OCA shell
777 0           120 -160  100 -140             imp:p=32 $ Outside to tally
888 0          -999 (-100:160:140)             imp:p=8  $ Outside pkg
999 0           999                            imp:p=0  $ Outside world

C
C Geometry Cards
C
10  pz 31.051                                          $ Source bottom
20  pz 267.399                                          $ Source top
30  c/z 0 0 91.916                                        $ Source radius
C
100 pz 0                                                $ OCA bottom (outside)
110 pz 0.635                                            $ OCA bottom (inside)
120 cz 119.38                                           $ OCA shell (outside)
130 cz 118.745                                          $ OCA shell (inside)
140 pz 306.07                                           $ OCA top (outside)
150 pz 305.435                                          $ OCA top (inside)
160 cz 319.38                                           $ 2-meter from OCA
C
200 pz 22.86                                            $ ICV/OCV bottom (outside)
210 pz 24.13                                            $ ICV/OCV bottom (inside)
220 cz 93.345                                           $ ICV/OCV shell (outside)
230 cz 92.234                                           $ ICV/OCV shell (inside)
240 pz 275.59                                           $ ICV/OCV top (outside)
250 pz 274.32                                           $ ICV/OCV top (inside)
C
777 pz 146.685                                          $ Ring tally (lower)
888 pz 151.765                                          $ Ring tally (upper)
999 sz 149.225 382.88                                   $ Outside world

C
C Physics Cards
C
mode p
C
C Source Cards
C
C Cylindrical Source
sdef pos 0 0 149.225 erg=d1 par=2 axs=0 0 1 rad=d2 ext=d3
sc1 Cs-137 MeV
C Source Energy (MeV) and Intensity (%)
si1 L 0.2835 0.661657
```

```
sp1 5.8000E-04 8.5100E+01
si2 0 91.916                                          $ Source radius
sp2 -21 1
si3 -118.174 118.174                                  $ Source extent
sp3 -21 0
C
C Tally Cards
C
f2:p 120
fc2 Surface Dose (mrem/hr)                            $ Surface detector
fs2 888 777 t
sd2 1.0 3810.44 1.0 1.0                               $ Surface tally area
f22:p 160
fc22 2-meter Dose (mrem/hr)                           $ 2-m detector
fs22 888 777 t
sd22 1.0 10194.144 1.0 1.0                            $ Surface tally area
C
C ANSI/ANS-6.1.1-1977 Gamma Flux to Dose Factors (mrem/hr)
de0 1.0e-02 3.0e-02 5.0e-02 7.0e-02 1.0e-01           $ Energy (Mev)
     1.5e-01 2.0e-01 2.5e-01 3.0e-01 3.5e-01
     4.0e-01 4.5e-01 5.0e-01 5.5e-01 6.0e-01
     6.5e-01 7.0e-01 8.0e-01 1.00 1.40
     1.80 2.20 2.60 2.80 3.25
     3.75 4.25 4.75 5.00 5.25
     5.75 6.25 6.75 7.50 9.00
     11.00 13.00 15.0000
df0 3.96e-03 5.82e-04 2.90e-04 2.58e-04 2.83e-04      $ Conversion (mrem/hr)
     3.79e-04 5.01e-04 6.31e-04 7.59e-04 8.78e-04
     9.85e-04 1.08e-03 1.17e-03 1.27e-03 1.36e-03
     1.44e-03 1.52e-03 1.68e-03 1.98e-03 2.51e-03
     2.99e-03 3.42e-03 3.82e-03 4.01e-03 4.41e-03
     4.83e-03 5.23e-03 5.60e-03 5.80e-03 6.01e-03
     6.37e-03 6.74e-03 7.11e-03 7.66e-03 8.77e-03
     1.03e-02 1.18e-02 1.33e-02
C
C Material Cards
C
m1   13000 -1.00                                       $ Aluminum
m2   14000 -0.01                                       $ Stainless Steel
     24000 -0.19
     25000 -0.02
     26000 -0.68
     28000 -0.10
m3   6000  -0.60                                       $ Urethane Foam
     7000  -0.08
     8000  -0.24
     1000  -0.07
     14000 -0.01
C
C Runtime and Print Cards
C
prdmp j j 1 2
ctme 20
```

5.1.1.2 Distributed 137Cs Gamma Source with 8.0 g/cc Zirconium – csa100.i

```
title TRUPACT-II NCT Zirconium Distributed 8 g/cc Cs-137
C
C Cell Cards
C
1   1 -8        10  -20  -30                 imp:p=1  $ Source
10  0           210 -250 -230 (-10:20:30)    imp:p=2  $ ICV cavity
20  2 -8.01280  200 -210 -220                imp:p=1  $ ICV/OCV bottom
30  2 -8.01280  250 -240 -220                imp:p=1  $ ICV/OCV top
40  2 -8.01280  210 -250  230 -220           imp:p=4  $ ICV/OCV shell
```

```
50  3 -0.13215  110 -150 -130 (-200:220:240) imp:p=8  $ OCA annulus
60  2 -8.01280  100 -110 -120               imp:p=1  $ OCA bottom
70  2 -8.01280  150 -140 -120               imp:p=1  $ OCA top
80  2 -8.01280  110 -150  130 -120          imp:p=16 $ OCA shell
777 0           120 -160  100 -140          imp:p=32 $ Outside to tally
888 0          -999 (-100:160:140)          imp:p=8  $ Outside pkg
999 0           999                         imp:p=0  $ Outside world

C
C Geometry Cards
C
10  pz 141.839                                       $ Source bottom
20  pz 156.611                                       $ Source top
30  c/z 0 0 91.916                                     $ Source radius
C
100 pz 0                                             $ OCA bottom (outside)
110 pz 0.635                                         $ OCA bottom (inside)
120 cz 119.38                                        $ OCA shell (outside)
130 cz 118.745                                       $ OCA shell (inside)
140 pz 306.07                                        $ OCA top (outside)
150 pz 305.435                                       $ OCA top (inside)
160 cz 319.38                                        $ 2-meter from OCA
C
200 pz 22.86                                         $ ICV/OCV bottom (outside)
210 pz 24.13                                         $ ICV/OCV bottom (inside)
220 cz 93.345                                        $ ICV/OCV shell (outside)
230 cz 92.234                                        $ ICV/OCV shell (inside)
240 pz 275.59                                        $ ICV/OCV top (outside)
250 pz 274.32                                        $ ICV/OCV top (inside)
C
777 pz 146.685                                       $ Ring tally (lower)
888 pz 151.765                                       $ Ring tally (upper)
999 sz 149.225 382.88                                $ Outside world

C
C Physics Cards
C
mode p
C
C Source Cards
C
C Cylindrical Source
sdef pos 0 0 149.225 erg=d1 par=2 axs=0 0 1 rad=d2 ext=d3
sc1 Cs-137 MeV
C Source Energy (MeV) and Intensity (%)
si1 L 0.2835 0.661657
sp1 5.8000E-04 8.5100E+01
si2 0 91.916                                           $ Source radius
sp2 -21 1
si3 -7.386 7.386                                       $ Source extent
sp3 -21 0
C
C Tally Cards
C
f2:p 120
fc2 Surface Dose (mrem/hr)                           $ Surface detector
fs2 888 777 t
sd2 1.0 3810.44 1.0 1.0                              $ Surface tally area
f22:p 160
fc22 2-meter Dose (mrem/hr)                          $ 2-m detector
fs22 888 777 t
sd22 1.0 10194.144 1.0 1.0                           $ Surface tally area
C
C ANSI/ANS-6.1.1-1977 Gamma Flux to Dose Factors (mrem/hr)
de0 1.0e-02 3.0e-02 5.0e-02 7.0e-02 1.0e-01          $ Energy (Mev)
     1.5e-01 2.0e-01 2.5e-01 3.0e-01 3.5e-01
     4.0e-01 4.5e-01 5.0e-01 5.5e-01 6.0e-01
```

```
          6.5e-01 7.0e-01 8.0e-01 1.00 1.40
          1.80 2.20 2.60 2.80 3.25
          3.75 4.25 4.75 5.00 5.25
          5.75 6.25 6.75 7.50 9.00
          11.00 13.00 15.0000
     df0 3.96e-03 5.82e-04 2.90e-04 2.58e-04 2.83e-04      $ Conversion (mrem/hr)
          3.79e-04 5.01e-04 6.31e-04 7.59e-04 8.78e-04
          9.85e-04 1.08e-03 1.17e-03 1.27e-03 1.36e-03
          1.44e-03 1.52e-03 1.68e-03 1.98e-03 2.51e-03
          2.99e-03 3.42e-03 3.82e-03 4.01e-03 4.41e-03
          4.83e-03 5.23e-03 5.60e-03 5.80e-03 6.01e-03
          6.37e-03 6.74e-03 7.11e-03 7.66e-03 8.77e-03
          1.03e-02 1.18e-02 1.33e-02
     C
     C Material Cards
     C
     m1   40000 -1.00                                      $ Zirconium
     m2   14000 -0.01                                      $ Stainless Steel
          24000 -0.19
          25000 -0.02
          26000 -0.68
          28000 -0.10
     m3   6000  -0.60                                      $ Urethane Foam
          7000  -0.08
          8000  -0.24
          1000  -0.07
          14000 -0.01
     C
     C Runtime and Print Cards
     C
     prdmp j j 1 2
     ctme 20
```

5.1.1.3 Distributed 60C0 Gamma Source with 0.5 g/cc Steel – cos100.i

```
     title TRUPACT-II NCT Steel Distributed 0.5 g/cc Co-60
     C
     C Cell Cards
     C
     1   1 -0.5        10  -20  -30                imp:p=1  $ Source
     10  0           210 -250 -230 (-10:20:30)    imp:p=2  $ ICV cavity
     20  2 -8.01280  200 -210 -220                imp:p=1  $ ICV/OCV bottom
     30  2 -8.01280  250 -240 -220                imp:p=1  $ ICV/OCV top
     40  2 -8.01280  210 -250  230 -220           imp:p=4  $ ICV/OCV shell
     50  3 -0.13215  110 -150 -130 (-200:220:240) imp:p=8  $ OCA annulus
     60  2 -8.01280  100 -110 -120                imp:p=1  $ OCA bottom
     70  2 -8.01280  150 -140 -120                imp:p=1  $ OCA top
     80  2 -8.01280  110 -150  130 -120           imp:p=16 $ OCA shell
     777 0           120 -160  100 -140           imp:p=32 $ Outside to tally
     888 0          -999 (-100:160:140)           imp:p=8  $ Outside pkg
     999 0           999                          imp:p=0  $ Outside world

     C
     C Geometry Cards
     C
     10  pz 31.051                                      $ Source bottom
     20  pz 267.399                                      $ Source top
     30  c/z 0 0 91.916                                    $ Source radius
     C
     100 pz 0                                           $ OCA bottom (outside)
     110 pz 0.635                                       $ OCA bottom (inside)
     120 cz 119.38                                      $ OCA shell (outside)
     130 cz 118.745                                     $ OCA shell (inside)
     140 pz 306.07                                      $ OCA top (outside)
     150 pz 305.435                                     $ OCA top (inside)
```

```
160 cz 319.38                                          $ 2-meter from OCA
C
200 pz 22.86                                           $ ICV/OCV bottom (outside)
210 pz 24.13                                           $ ICV/OCV bottom (inside)
220 cz 93.345                                          $ ICV/OCV shell (outside)
230 cz 92.234                                          $ ICV/OCV shell (inside)
240 pz 275.59                                          $ ICV/OCV top (outside)
250 pz 274.32                                          $ ICV/OCV top (inside)
C
777 pz 146.685                                         $ Ring tally (lower)
888 pz 151.765                                         $ Ring tally (upper)
999 sz 149.225 382.88                                  $ Outside world

C
C Physics Cards
C
mode p
C
C Source Cards
C
C Cylindrical Source
sdef pos 0 0 149.225 erg=d1 par=2 axs=0 0 1 rad=d2 ext=d3
sc1 Co-60 MeV
C Source Energy (MeV) and Intensity (%)
si1 L 3.469300E-01 8.262800E-01 1.173237E+00 1.332501E+00
     2.158770E+00 2.505000E+00
sp1 7.600000E-03 7.600000E-03 9.997360E+01 9.998560E+01
     1.110000E-03 2.000000E-06
si2 0 91.916                                             $ Source radius
sp2 -21 1
si3 -118.174 118.174                                         $ Source extent
sp3 -21 0
C
C Tally Cards
C
f2:p 120
fc2 Surface Dose (mrem/hr)                             $ Surface detector
fs2 888 777 t
sd2 1.0 3810.44 1.0 1.0                                $ Surface tally area
f22:p 160
fc22 2-meter Dose (mrem/hr)                            $ 2-m detector
fs22 888 777 t
sd22 1.0 10194.144 1.0 1.0                             $ Surface tally area
C
C ANSI/ANS-6.1.1-1977 Gamma Flux to Dose Factors (mrem/hr)
de0 1.0e-02 3.0e-02 5.0e-02 7.0e-02 1.0e-01            $ Energy (Mev)
     1.5e-01 2.0e-01 2.5e-01 3.0e-01 3.5e-01
     4.0e-01 4.5e-01 5.0e-01 5.5e-01 6.0e-01
     6.5e-01 7.0e-01 8.0e-01 1.00 1.40
     1.80 2.20 2.60 2.80 3.25
     3.75 4.25 4.75 5.00 5.25
     5.75 6.25 6.75 7.50 9.00
     11.00 13.00 15.0000
df0 3.96e-03 5.82e-04 2.90e-04 2.58e-04 2.83e-04       $ Conversion (mrem/hr)
     3.79e-04 5.01e-04 6.31e-04 7.59e-04 8.78e-04
     9.85e-04 1.08e-03 1.17e-03 1.27e-03 1.36e-03
     1.44e-03 1.52e-03 1.68e-03 1.98e-03 2.51e-03
     2.99e-03 3.42e-03 3.82e-03 4.01e-03 4.41e-03
     4.83e-03 5.23e-03 5.60e-03 5.80e-03 6.01e-03
     6.37e-03 6.74e-03 7.11e-03 7.66e-03 8.77e-03
     1.03e-02 1.18e-02 1.33e-02
C
C Material Cards
C
m1   6000  -0.005                                       $ Steel (Carbon)
     26000 -0.995
m2   14000 -0.01                                        $ Stainless Steel
```

```
      24000 -0.19
      25000 -0.02
      26000 -0.68
      28000 -0.10
m3    6000  -0.60                                  $ Urethane Foam
      7000  -0.08
      8000  -0.24
      1000  -0.07
      14000 -0.01
C
C Runtime and Print Cards
C
prdmp j j 1 2
ctme 20
```

5.1.1.4 Distributed 60C0 Gamma Source with 8.0 g/cc Zirconium – coz115.i

```
title TRUPACT-II NCT Zirconium Distributed 8 g/cc Co-60
C
C Cell Cards
C
1   1 -8         10  -20  -30                  imp:p=1  $ Source
10  0            210 -250 -230 (-10:20:30)    imp:p=2  $ ICV cavity
20  2 -8.01280   200 -210 -220                 imp:p=1  $ ICV/OCV bottom
30  2 -8.01280   250 -240 -220                 imp:p=1  $ ICV/OCV top
40  2 -8.01280   210 -250  230 -220            imp:p=4  $ ICV/OCV shell
50  3 -0.13215   110 -150 -130 (-200:220:240) imp:p=8  $ OCA annulus
60  2 -8.01280   100 -110 -120                 imp:p=1  $ OCA bottom
70  2 -8.01280   150 -140 -120                 imp:p=1  $ OCA top
80  2 -8.01280   110 -150  130 -120            imp:p=16 $ OCA shell
777 0            120 -160  100 -140            imp:p=32 $ Outside to tally
888 0           -999 (-100:160:140)            imp:p=8  $ Outside pkg
999 0            999                           imp:p=0  $ Outside world

C
C Geometry Cards
C
10  pz 141.839                                 $ Source bottom
20  pz 156.611                                 $ Source top
30  c/z 0 0 91.916                               $ Source radius
C
100 pz 0                                       $ OCA bottom (outside)
110 pz 0.635                                   $ OCA bottom (inside)
120 cz 119.38                                  $ OCA shell (outside)
130 cz 118.745                                 $ OCA shell (inside)
140 pz 306.07                                  $ OCA top (outside)
150 pz 305.435                                 $ OCA top (inside)
160 cz 319.38                                  $ 2-meter from OCA
C
200 pz 22.86                                   $ ICV/OCV bottom (outside)
210 pz 24.13                                   $ ICV/OCV bottom (inside)
220 cz 93.345                                  $ ICV/OCV shell (outside)
230 cz 92.234                                  $ ICV/OCV shell (inside)
240 pz 275.59                                  $ ICV/OCV top (outside)
250 pz 274.32                                  $ ICV/OCV top (inside)
C
777 pz 146.685                                 $ Ring tally (lower)
888 pz 151.765                                 $ Ring tally (upper)
999 sz 149.225 382.88                          $ Outside world

C
C Physics Cards
C
mode p
C
```

```
C Source Cards
C
C Cylindrical Source
sdef pos 0 0 149.225 erg=d1 par=2 axs=0 0 1 rad=d2 ext=d3
sc1 Co-60 MeV
C Source Energy (MeV) and Intensity (%)
si1 L 3.469300E-01 8.262800E-01 1.173237E+00 1.332501E+00
     2.158770E+00 2.505000E+00
sp1 7.600000E-03 7.600000E-03 9.997360E+01 9.998560E+01
     1.110000E-03 2.000000E-06
si2 0 91.916                                          $ Source radius
sp2 -21 1
si3 -7.386 7.386                                      $ Source extent
sp3 -21 0
C
C Tally Cards
C
f2:p 120
fc2 Surface Dose (mrem/hr)                            $ Surface detector
fs2 888 777 t
sd2 1.0 3810.44 1.0 1.0                               $ Surface tally area
f22:p 160
fc22 2-meter Dose (mrem/hr)                           $ 2-m detector
fs22 888 777 t
sd22 1.0 10194.144 1.0 1.0                            $ Surface tally area
C
C ANSI/ANS-6.1.1-1977 Gamma Flux to Dose Factors (mrem/hr)
de0 1.0e-02 3.0e-02 5.0e-02 7.0e-02 1.0e-01           $ Energy (Mev)
     1.5e-01 2.0e-01 2.5e-01 3.0e-01 3.5e-01
     4.0e-01 4.5e-01 5.0e-01 5.5e-01 6.0e-01
     6.5e-01 7.0e-01 8.0e-01 1.00 1.40
     1.80 2.20 2.60 2.80 3.25
     3.75 4.25 4.75 5.00 5.25
     5.75 6.25 6.75 7.50 9.00
     11.00 13.00 15.0000
df0 3.96e-03 5.82e-04 2.90e-04 2.58e-04 2.83e-04      $ Conversion (mrem/hr)
     3.79e-04 5.01e-04 6.31e-04 7.59e-04 8.78e-04
     9.85e-04 1.08e-03 1.17e-03 1.27e-03 1.36e-03
     1.44e-03 1.52e-03 1.68e-03 1.98e-03 2.51e-03
     2.99e-03 3.42e-03 3.82e-03 4.01e-03 4.41e-03
     4.83e-03 5.23e-03 5.60e-03 5.80e-03 6.01e-03
     6.37e-03 6.74e-03 7.11e-03 7.66e-03 8.77e-03
     1.03e-02 1.18e-02 1.33e-02
C
C Material Cards
C
m1   40000 -1.00                                       $ Zirconium
m2   14000 -0.01                                       $ Stainless Steel
     24000 -0.19
     25000 -0.02
     26000 -0.68
     28000 -0.10
m3   6000  -0.60                                       $ Urethane Foam
     7000  -0.08
     8000  -0.24
     1000  -0.07
     14000 -0.01
C
C Runtime and Print Cards
C
prdmp j j 1 2
ctme 20
```